UNIVERSIDADE DE SÃO PAULO
INSTITUTO DE QUÍMICA
Programa de Pós-Graduação em Ciências Biológicas (Bioquímica)

HELLEN PAULA VALERIO

Proteomic analysis of human keratinocytes under UVA radiation-induced stress

Versão corrigida da Tese conforme Resolução CoPGr 5890
O original se encontra disponível na Secretaria de Pós-Graduação do IQ-USP

São Paulo

Data do Depósito na SPG:
08/11/2021

HELLEN PAULA VALERIO

Análise proteômica de queratinócitos humanos sob estresse induzido por radiação UVA

Tese apresentada ao Instituto de Química da Universidade de São Paulo para obtenção do Título de Doutora em Ciências (Bioquímica)

Orientador: Prof. Dr. Paolo Di Mascio

São Paulo
2021

Hellen Paula Valerio

Análise proteômica de queratinócitos humanos sob estresse induzido por radiação UVA

Tese apresentada ao Instituto de Química da Universidade de São Paulo para obtenção do Título de Doutora em Ciências (Bioquímica)

Aprovado em: _____

Banca Examinadora

Prof. Dr. _____

Instituição: _____

Assinatura:_____

Prof. Dr. _____

Instituição: _____

Assinatura:_____

Prof. Dr. _____

Instituição: _____

Assinatura:_____

Prof. Dr. _____

Instituição: _____

Assinatura:_____

Aos meus pais,
com todo o meu amor

AGRADECIMENTOS

A todos que foram gentis e generosos comigo nos últimos anos. Especialmente:

– ao meu pai, porque sem o apoio incondicional dele nada disso seria possível

– à minha mãe, por estar sempre junto comigo

– ao professor Paolo, pelas oportunidades, pela paciência, amizade e por me inspirar como pesquisador

– à professora Graziella, uma das cientistas mais inteligentes que eu conheço, pelo apoio, amizade e por ter contribuído imensamente para o desenvolvimento deste trabalho

– à Mariane, pela amizade essencial na minha vida

– aos meus gatos e ao Nick, por me fazerem mais feliz

– à Kátia, que me orientou com muita delicadeza durante a iniciação científica e me inspirou a seguir essa profissão

– à Bruna, pela amizade e pelo apoio no ano em que nós trabalhamos juntas

– ao Felipe e à Angela, pela competência, pela ajuda em vários experimentos que compõem essa tese e pelo companheirismo nesse fim de doutorado

– à professora Marisa, em especial pela generosidade de ter me recebido em seu laboratório para conversar sobre iniciação científica no começo de tudo

– a todos dos laboratórios do professor Paolo, da professora Graziella e da professora Marisa, que compartilham o dia a dia maluco da bancada

– a todos do IQ que me ajudaram de formas variadas com experimentos, sempre com muita generosidade

– a Agda, Mariana, Izaura, Fernanda e Dóris, pelas ajudas variadas no laboratório e no Lumos e pela gentileza constante

APOIO FINANCEIRO

"Nature is a harmonious mechanism where all parts,
including those appearing to play a secondary role,
cooperate in the functional whole."

Santiago Ramón y Cajal

RESUMO

Valerio, H. P. **Análise proteômica de queratinócitos humanos sob estresse induzido por radiação UVA**. 2021. 159p. Tese (Doutorado) - Programa de Pós-Graduação em Ciências Biológicas (Bioquímica). Instituto de Química, Universidade de São Paulo, São Paulo.

A radiação ultravioleta (UV) solar que atinge a superfície terrestre é composta por 95% de radiação UVA (320 a 400 nm) e 5% de radiação UVB (280 a 320 nm). A radiação UVB é carcinogênica e gera lesões potencialmente mutagênicas no DNA. A radiação UVA solar também gera danos no DNA, mas a genotoxicidade dessa radiação não explica inteiramente o seu impacto biológico. Atualmente, sabe-se que a radiação UVA é absorvida por cromóforos celulares, gerando espécies reativas de oxigênio, como o oxigênio singlete. Sabendo que o proteoma é um mediador de respostas ao estresse celular, nós investigamos os efeitos celulares de uma dose não-citotóxica de radiação UVA, equivalente a cerca de 20 minutos de exposição ao sol, no proteoma de queratinócitos humanos. Utilizando espectrometria de massas, bioinformática e ensaios bioquímicos convencionais, nós analisamos dois aspectos do estresse induzido por radiação UVA: o remodelamento espacial do proteoma 30 minutos depois do estresse e alterações nos níveis e na secreção de proteínas no longo prazo (24 horas e 7 dias depois da irradiação). Na primeira parte desta tese, nós quantificamos e atribuímos classificações de localização subcelular a mais de 3000 proteínas. Dentre essas proteínas, 600 tem potencialmente a sua distribuição subcelular alterada em resposta à radiação. As redistribuições subcelulares são acompanhadas de modulações redox, fragmentação mitocondrial e danos no DNA. Na segunda parte da tese, os nossos resultados mostraram que queratinócitos humanos primários entram em senescência sob exposição a uma única dose de radiação UVA, montando respostas antioxidantes e pró-inflamatórias. Células sob senescência induzida por UVA, por sua vez, desencadeiam respostas parácrinas em queratinócitos pré-tumorais (células HaCaT) por meio de mediadores inflamatórios. Em conjunto, esses resultados reiteram o papel da radiação UVA como um potente estressor metabólico em células da pele.

Palavras-chave: radiação UVA, pele, queratinóticos, proteômica espacial, resposta ao estresse, senescência

ABSTRACT

Valerio, H. P. **Proteomic analysis of human keratinocytes under UVA-induced stress.** 2021. 159p. PhD Thesis - Graduate Program in Biochemistry. Instituto de Química, Universidade de São Paulo, São Paulo.

The solar ultraviolet (UV) radiation that reaches the Earth is composed of 95% of UVA (320 to 400 nm) and 5% of UVB (280 to 320 nm) radiation. UVB is carcinogenic, generating potentially mutagenic DNA lesions. The solar UVA radiation also causes DNA damage, but this fact does not fully account for its biological impact. UVA is absorbed by non-DNA cellular chromophores, generating reactive oxygen species such as singlet oxygen. Knowing the proteome mediates stress responses in cells, here we investigated the cellular effects of a non-cytotoxic dose of UVA radiation, equivalent to about 20 minutes of midday sun exposure, on the proteome of human keratinocytes. Using a combination of mass spectrometry-based proteomics, bioinformatics, and conventional biochemical assays, we analyzed two aspects of UVA-induced stress: spatial remodeling of the proteome in subcellular compartments 30 minutes after stress and long-term changes in protein levels and secretion (24 hours and 7 days post-irradiation). In the first part of this thesis, we quantified and assigned subcellular localization for over 3000 proteins, of which about 600 potentially redistribute upon UVA exposure. Protein redistributions were accompanied by redox modulations, mitochondrial fragmentation and DNA damage. In the second part of the work, our results showed that primary human keratinocytes enter senescence upon exposure to a single dose of UVA, mounting antioxidant and inflammatory responses. Cells under UVA-induced senescence further elicit paracrine responses in neighboring pre-malignant HaCaT epithelial cells via inflammatory mediators. Altogether, these results reiterate the role of UVA radiation as a potent metabolic stressor in the skin.

Keywords: UVA radiation; keratinocytes; skin; stress response, spatial proteomics, senescence

Summary

CHAPTER 1 – Literature review

1. 1. Photochemistry and photobiology

Sunlight triggers numerous biochemical responses in organisms. Bioluminescence, photosynthesis, phototaxis, phototropism, perception of the environment and the circadian rhythm are examples of the interplay between light and biological systems (Kochevar, 1983).

As described in detail by Brash et al. (2018), photon absorption by a biological chromophore is the initial event in a photobiological response. A photon of light excites a single electron in a chromophore to a higher-energy orbital. When an electron is excited, the other unpaired electron is left behind. This change in the electronic structure of the chromophore leads to altered orbital shapes and reactivity, favoring reactions that would not happen in the ground state. Remarkably, the newly occupied orbital has an energy up to 10-fold higher than that of the hydrolysis of one molecule of ATP. Thus, light absorption may result in photochemical changes in the absorbing chromophore and vicinal biomolecules. The energy of electron excitation can also be given off as heat or as a lower energy light (i.e., fluorescence or phosphorescence) so that the chromophore can return to the ground state. A photosensitizer is a chromophore that absorbs a photon, and initiates chemical or physical reactions, generating reactive intermediates and photoproducts, instead of returning to the ground state by mechanisms of energy dissipation (Wondrak et al., 2006). The magnitude of a given biological response to light is defined by the nature of the chromophore and quantum mechanics of the excited electron (Slominski et al., 2018).

1. 2. Ultraviolet radiation

The electromagnetic energy of solar radiation reaching the Earth's surface is composed of about 55% of infrared radiation (700 nm to 1 mm), 45% of visible light (400 to 700 nm) and 5% of UV radiation (200 to 400 nm), considering the ground level spectrum radiation of the sun in zenith (Slominski et al., 2018). UV radiation, which constitutes the major skin stressor, is composed of UVC (200 to 280 nm), UVB (280 to 320 nm) and UVA (320 to 400 nm). The oxygen and ozone in the atmosphere completely absorb

UVC radiation and absorb approximately 95% of UVB. Thus, UVA and UVB are the most relevant UV wavelengths to human health, comprising 95% and 5% of the solar UV radiation reaching the Earth, respectively (Schuch et al., 2017).

Sunlight is necessary for human health (An et al., 2016; Holick, 2001). Besides converting 7-dehydrocholesterol to pre-vitamin D3, UV radiation also impacts the central nervous system and endocrine functions through interactions with the skin (Slominski et al., 2018). However, UV radiation also has several detrimental consequences for human health, such as tumorigenesis and photoaging (Brash, 1997). Both UVA and UVB are implicated in the etiology of basal cell carcinoma (BCC), squamous cell carcinoma (SCC) and cutaneous malignant melanoma (CMM) (El Ghissassi et al., 2009). Skin cancer is the most prevalent form of cancer in the world (Leiter et al., 2014). The risk of skin cancer can be significantly attenuated by changes in behavioral patterns, such as avoiding harmful UV intensities and wavelengths and wearing sunscreen (Brash, 1997). Therefore, understanding the molecular mechanisms underlying the carcinogenicity of different UV bands is relevant for skin protection and cancer prevention.

1.2.1. UVB-induced DNA damage and mutagenesis

While the molecular mechanisms underlying UVB's carcinogenicity have been well-described for at least 60 years (Cadet and Douki, 2018), UVA has only been classified as "probably carcinogenic to humans" by the World Health Organization's International Agency for Research on Cancer in 2009 (El Ghissassi et al., 2009). This stems from the fact that DNA is the primary chromophore for UVB radiation, but not for UVA. UVB photons are efficiently absorbed by DNA, leading to excitation of pyrimidine nucleobases and inducing the formation of cyclobutane pyrimidine dimers (CPD) and pyrimidine (6-4) pyrimidone photoproducts (6-4PP) (Schuch et al., 2017) (**Fig. 1A**).

CPD forms in a photochemically allowed [2 + 2] cycloaddition reaction between the C5 and C6 double bounds of two adjacent pyrimidine rings (Friedel et al., 2009). Theoretical and spectroscopy-based approaches indicate that, after absorption of a UVB photon by the DNA, excitation energy can be delocalized over a few bases (Cadet & Douki, 2018). Formation of CPDs is documented for all possible doublets of pyrimidines: 5'-TT-3', 5'-

TC-3', 5'-CT-3', 5'-CC-3', as well as for 5-methylcytosine (Cadet & Douki, 2018), but they are predominantly formed between neighboring thymines (Friedel et al., 2009).

DNA sequence influences CPD formation. At high percentages of GC, the yield of TT photoproducts decrease, while the levels of C-containing photoproducts increase (Douki, 2013). DNA condensation also affects the formation of pyrimidine dimers. In this sense, CPDs are formed both in hetero and euchromatin regions, while 6-4PPs are uniquely formed in euchromatin (Han et al., 2016). It has also been demonstrated that telomeric regions, G-Quadruplex loops and methylcytosine-rich sequences are more prone to CPD formation (Lee & Pfeifer, 2003; Rochette & Brash, 2010; Su et al., 2009; Tommasi et al., 1997).

UVB-mutation signature is characterized mainly by C → T transitions and CC → TT tandem base substitutions in daughter cells (Cadet et al., 2015) (**Fig. 1B**). One of the most accepted mechanisms that explains UVB-induced mutations involve deamination of cytosine to uracil or of methylcytosine to thymine within a pyrimidine dimer (Pfeifer, 2020). When a CPD is not repaired by the nucleotide excision repair (NER) pathway, translesion synthesis DNA polymerase η can synthetize a DNA strand opposite to the lesion, following the base pairing rule faithfully. Thus, DNA polymerase η can bypass CPDs error-free. However, cytosines in CPDs are unstable and easily deaminate to produce uracil, or thymine if cytosine is methylated at position 5. Thus, deamination converts a cytosine or 5-methylcytosine-containing CPD to an uracil or thymine-containing CPD, which results in a C → T transition. Importantly, sunlight-induced C to T mutation hotspots in skin cancers occur primarily at methylated CpG sites (Song et al., 2014). Furthermore, genetic deficiencies in the gene encoding DNA polymerase η produce considerable changes in the UV-induced mutation frequency, supporting this mechanism (Ikehata & Ono, 2011). Other mechanisms involving error-prone DNA polymerases probably also contribute to UVB-induced C → T transitions (Pfeifer, 2020).

UVB-induced mutations are relevant to skin tumorigenesis since an overwhelming majority of mutations at bipyrimidine sites occur in specific genes of skin tumors, both in non-melanoma (Brash et al., 1991) and melanoma skin cancers (T. Zhang et al., 2016). In UVB-induced mouse skin tumors, CPDs have been reported to be formed preferentially at the major p53 mutational hotspot (You et al., 2000). More than 80% of

p53 mutations in UVB-induced mouse skin tumors are C → T transitions at dipyrimidine sequences (You et al., 2000) (**Fig. 1**).
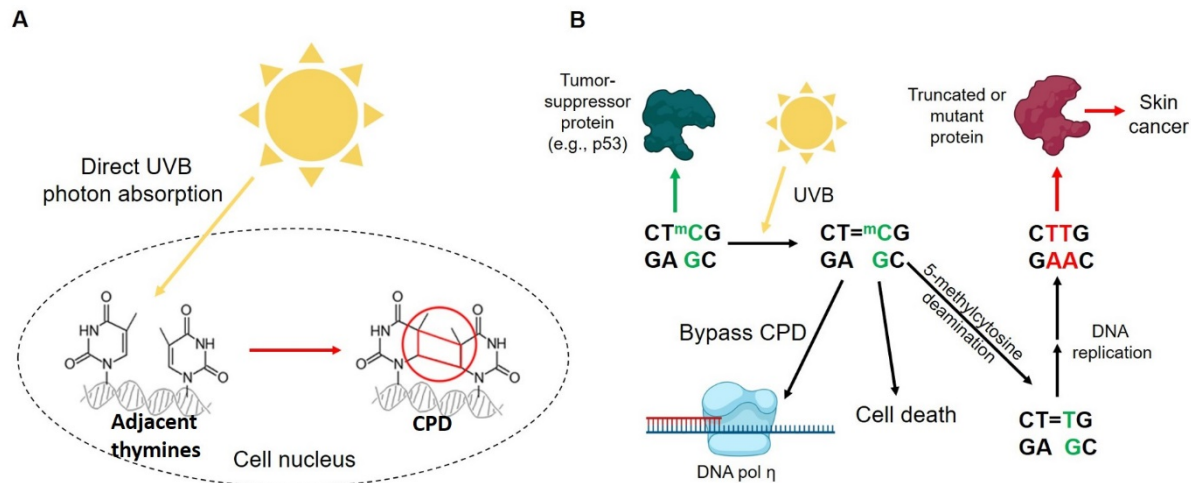
Fig. 1. Scheme representing UVB's mutagenic and carcinogenic effects on the skin. (A) A UVB photon is directly absorbed by pyrimidines in the DNA, leading to CPD formation. **(B)** CPD formation (represented by the = sign) may lead to C → T transitions in tumor-suppressor genes, giving rise to skin cancer.

Importantly, the contribution of photoproducts to solar carcinogenesis is not only given by their mutagenic properties, but also by how these lesions are repaired. In this sense, CPDs are acknowledged to be more relevant to UV-induced carcinogenesis than 6-4PPs since 6-4PPs are efficiently repaired by cells (Courdavault et al., 2005; Mitchell et al., 1985). This is explained by the larger impact of 6-4PPs on DNA structure, which makes them more easily detected by the DNA repair machinery (Cadet & Douki, 2018). On the other hand, CPDs are slowly repaired by the transcription-coupled repair branch of the NER pathway and rarely by the global genome repair (Courdavault et al., 2005). Research has shown that at least 80% of all mutations induced by UVB in keratinocytes are derived from CPDs (Courdavault et al., 2005).

UVB also induces other types of DNA damage, such as adenine dimers and adenine-thymine dimers, but these lesions are minor products (Asgatay et al., 2010; Banyasz et al., 2016; Koning et al., 1990; Zhao et al., 1996). For example, it has been estimated that UVB-induced guanine oxidation in human DNA accounts for less than 0.1% of the total formation of UVB-induced DNA lesions, while CPDs represent 90% (Cadet & Douki, 2018; Douki et al., 1999).

Dewar isomers are also detected at bipyrimidine sites in isolated DNA exposed to UVB (Douki & Cadet, 2001). However, the combination of UVB and UVA leads to higher ratios of Dewar isomers to 6-4PPs than UVB alone, which indicates that UVA is possibly involved in this isomerization (Douki, 2016). Formation of Dewar isomers requires a first UVB photon absorption, which gives rise to 6-4PP, followed by a second photon absorption required for the isomerization of the 6-4PP lesion into Dewar isomers. The second photon is more likely to come from the UVA range, which is efficiently absorbed by 6-4PPs (Schuch et al., 2017). Importantly, up to 20% of 6-4PPs are converted into Dewar isomers and these photoproducts seem to be more mutagenic than CPDs (Douki and Sage, 2016).

1.2.2. UVA photosensitization

UVA is poorly absorbed by canonical nucleotides, causing much less direct DNA damage than UVB. UVA is absorbed 1000 times less efficiently by DNA than UVB (Kuluncsics et al., 1999). Most of the DNA damage generated by UVA can be explained by photodynamic effects involving the participation of singlet oxygen ($^1O_2$) and, to a lesser extent, of other reactive oxygen species (ROS) (Cadet et al., 2015).

Photosensitization reactions induced by the absorption of UVA photons are mostly initiated by non-DNA chromophores (Wondrak et al., 2006). The identity and roles of UVA photosensitizers in skin biology remain elusive, but molecules such as flavins, heme, urocanic acid, quinones, porphyrins, bilirubin, melanin and NADH/NADPH are likely the predominant cellular chromophores mediating UVA's biological action (Wondrak et al., 2006). Importantly, UVA can also exert its biological effects through exogenous photosensitizers, such as antibacterial agents (i. e. fluoroquinolone and nalidixic acid) (Karran & Brem, 2016; Klecak et al., 1997, 1997; Moore, 2002), the immunosuppressive drug azathioprine (O'Donovan et al., 2005) and 8-methoxypsoralen, used in combination with UVA for photochemotherapy (de Mol et al., 1981).

Usually, the endogenous photosensitizer absorbs an UVA photon and it is excited to a singlet state, undergoing intersystem crossing to a triplet state. Triplet states have lower energy relative to singlet states but have longer lifetimes. Thus, triplet states provide time for the photosensitizer to collide with other biomolecules, initiating reactions. The

photoexcited state intermediate of the UVA photosensitizer, most often its long-lived triplet state, can transfer energy to other biomolecules, resulting in the formation of free radicals and $^1O_2$ via type I and II photosensitization reactions, respectively (Baptista et al., 2021).

As revised in detail by Cadet et al. (2015), in type I reactions the triplet state of the photosensitizer may be involved in charge-transfer reactions with a given biomolecule. In most cases, this leads to electron abstraction and formation of a pair of charged radicals. The radical cation undergoes deprotonation or hydration reactions, generating neutral radicals. The later transient species generated by these reactions reacts with molecular oxygen or eventually with superoxide ($O_2^{\bullet-}$). The resulting peroxyl radicals and/or hydroperoxides trigger other oxidative reactions, modifying DNA, lipids and proteins. The anion radical, on the other hand, is usually oxidized back to the starting molecule by oxygen, giving rise to $O_2^{\bullet-}$. Type II photosensitization reactions involve energy transfer from the triplet state of the photosensitizer to molecular oxygen. This reaction generates singlet oxygen, which then reacts with electron-rich biomolecules in cells, forming oxidized products, as described in detail by (Di Mascio et al., 2019). Type I and type II reactions are summarized in **Fig. 2**.
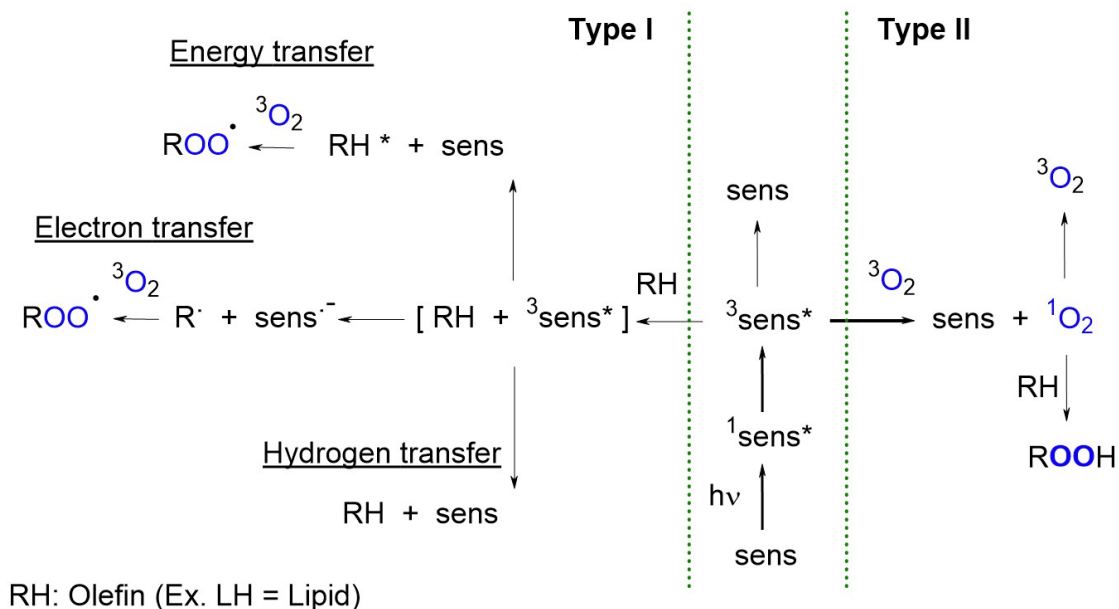
Fig. 2. Generation of reactive oxygen species through type I and II photosensitization reactions (sens = sensitizer). (Di Mascio et al., 2019)

Singlet oxygen is considered the predominant mediator of UVA-induced oxidative effects in skin cells. Early studies implicated $^1O_2$ in UVA-induced damage by showing enhanced UVA response in cells kept in deuterated water (D_2O) (Grether-Beck et al., 1996; Tyrrell, 2000). D_2O prolongs the lifetime of $^1O_2$, but not of other ROS. Similarly, UVA effects are attenuated by singlet oxygen quenchers and mimicked in unirradiated cells exposed to chemical sources of singlet oxygen (Grether-Beck et al., 1996; Tyrrell, 2000). Furthermore, singlet oxygen has been directly detected in keratinocytes and human skin exposed to UVA radiation (Baier et al., 2007), based on chemiluminescence measurements at 1270 nm.

While $^1O_2$ is involved in an immediate response of cells to UVA, other potential sources of ROS (e. g., NADPH oxidase, the mitochondrial electron transport and oxidation products derived from the reaction of $^1O_2$ with unsaturated lipids and proteins) account for UVA damage over time (Ouédraogo & Redmond, 2003). For example, it has been demonstrated that UVA stimulates ROS production via a NADPH oxidase (Nox1)-dependent mechanism and subsequently modulates pro-inflammatory responses (Valencia and Kochevar, 2008). Mitochondria is also possibly involved in UVA-induced damage, since blocking complex I of the electron transport chain partially inhibits ROS formation upon UVA exposure (Gniadecki et al., 2001).

Additionally, UVA-mediated oxidative effects are exacerbated by immediate and delayed release of iron and heme. In this sense, UVA-induced lysosomal damage has been shown to lead to ferritin proteolysis and release of labile iron into the cytosol (Basu-Modak et al., 2006; Pourzand et al., 1999). The increase in the cytosolic levels of the labile iron pool seems to be correlated with cellular susceptibility to necrosis, since modulations in the labile iron pool by desferal and/or hemin treatment significantly increased the extent of UVA-induced necrosis in mammalian cell lines (Zhong et al., 2004). Furthermore, UVA can induce the release of free heme by microsomal hemeproteins (Kvam et al., 1999). Heme is thought to be a major UVA photosensitizer and its release could amplify the oxidative stress generated by UVA (Tyrrell, 2011). Altogether, these evidences indicate the possibility of prolonged cellular effects after exposure to a single dose of UVA radiation.

1.2.3. UVA-induced DNA damage and mutagenesis

Even though UVA generates lower levels of CPDs than UVB, this type of lesion still accounts for most of UVA-induced DNA damage (Mouret et al., 2006a). In early studies, electrophoretic analysis combined with the use of specific DNA repair enzymes showed that CPDs are more frequently formed by UVA than oxidized purines, oxidized pyrimidines and single strand breaks in Chinese hamster ovary cells (Douki et al., 2003). LC-MS/MS analysis confirmed the predominance of CPD formation over base oxidation by UVA in keratinocytes, fibroblasts and skin explants (Courdavault et al., 2004; Mouret et al., 2006b). Contrarily to UVB, there is no strong evidence to date that UVA induces formation of 6-4PPs (Schuch et al., 2017).

The distribution in bipyrimidine composition is different for UVA and UVB radiation. While UVB generates TT > TC > CT > CC, UVA generates TT >>> TC > CT with undetectable levels of CC (Douki et al., 2003). This difference in bipyrimidine composition strongly suggests that UVA-induced CPDs are formed by photosensitized triplet energy transfer from yet unidentified chromophores to thymine instead of direct photon absorption (Douki et al., 2003), even though many authors discuss that direct photon absorption may also occur to some extent (Jiang et al., 2009; Mouret et al., 2010). Because UVA and UVB induce predominantly CPD formation, both UV bands induce mostly C → T transitions (Sage et al., 2011). However, CC → TT tandem base substitutions occur in UVB-exposed cells and hardly occur under UVA exposure (Ikehata, 2018). This variation in the sequence-dependent mutational spectrum of different UV wavelengths could be also explained by different photochemical mechanisms of CPD formation upon UVA or UVB exposure (Ikehata, 2018). **Fig. 3** represents the main mechanisms involved in UVA-induced DNA damage and the main mutations associated with these lesions.
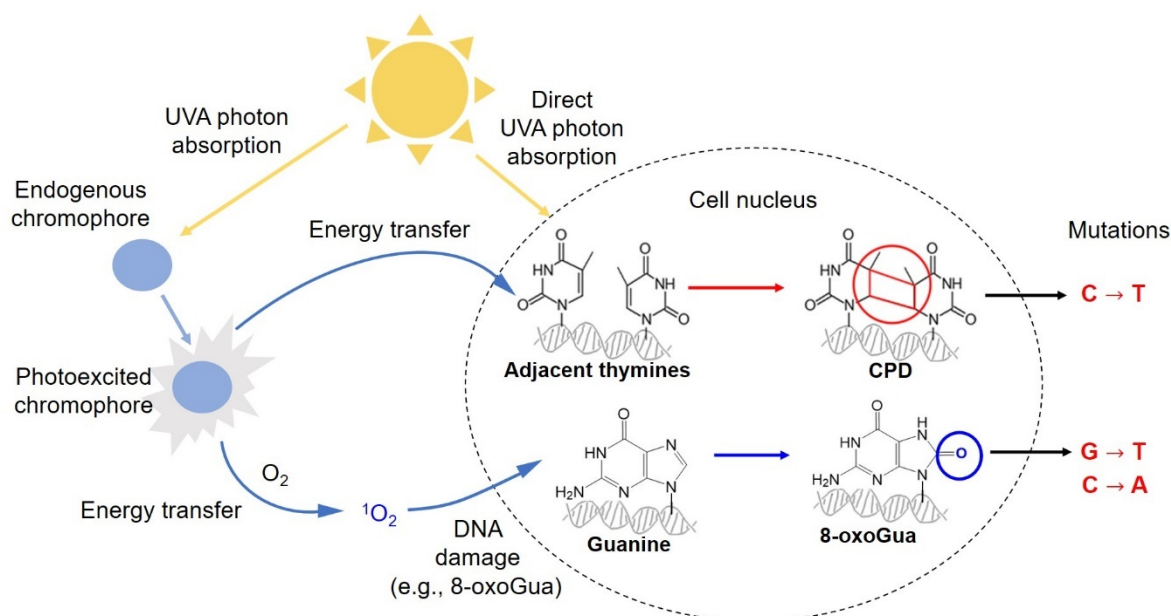
Fig. 3. Scheme representing UVA's genotoxic effects on the skin. (A) A UVA photon may be absorbed by endogenous chromophores, and through energy transfer processes generate CPD and singlet oxygen. Direct UVA photon absorption by pyrimidines may also occur to some extent.

Even though oxidative DNA lesions are not the predominant lesions induced by UVA in human cells, UVA induces higher levels of oxidized purines in DNA than UVB (Kvam and Tyrrell, 1997; Rosen et al., 1996; Warner and Wei, 1997; Zhang et al., 1997). In this sense, 8-oxoGua has been the predominant DNA oxidation product detected on UVA-irradiated cells (Cadet et al., 2015). Early research showed, based on measurements of HPLC coupled with an electrochemical detector, that 8-oxoGua was generated by UVA in the DNA of mammalian cells (Kvam and Tyrrell, 1997; Rosen et al., 1996; Warner and Wei, 1997; Zhang et al., 1997). The preferential oxidation of guanine was confirmed by LC-MS/MS measurements of DNA extracted from UVA-irradiated fibroblasts (Besaratinia et al., 2004, 2005).

While 8-oxoGua is a ubiquitous DNA product that has been shown to be generated by the hydroxyl radical ($\cdot$OH) and one-electron oxidants (Cadet et al., 2008), UVA-induced 8-oxoGua formation has been mainly attributed to singlet oxygen (Cadet et al., 2015). The oxidation of guanine entails the introduction of a carbonyl group in C8 in response to $^1O_2$ attack (type II reaction) and/or in smaller amounts by one electron (or hydrogen atom) abstraction (type I reaction) (Pouget et al., 2000) (**Fig. 4**). This chemical

9

modification leads to a base twist from an anti to a syn position, resulting in erroneous pairing with adenine and potentially in a G →T transversion (Schuch et al., 2017). Importantly, 8-oxoGua is not cytotoxic because it does not completely block DNA or RNA polymerases (Batista et al., 2009).

Oxidatively generated DNA damage likely contributes to UVA mutagenicity. Even though UVA and UVB induce mostly C → T transitions (Cadet et al., 2015), G → T transversions derived from 8-oxoGua formation have been detected in UVA-exposed cells and have been proposed as a possible "UVA fingerprint mutation" (Besaratinia et al., 2004). Moreno et al., 2020, observed a strong contribution of C → A transversions in UVA-exposed DNA polymerase η-deficient cells, potentially due to nucleobase oxidation by UVA photons. *In vitro* experiments indicate that the translesion DNA polymerase η can replicate 8-oxoGua and insert an A or C opposite the lesion, whether it is in syn or anti configuration, resulting in C → A transversions (McCulloch et al., 2009; Silverstein et al., 2010).

dR = 2-deoxyribose
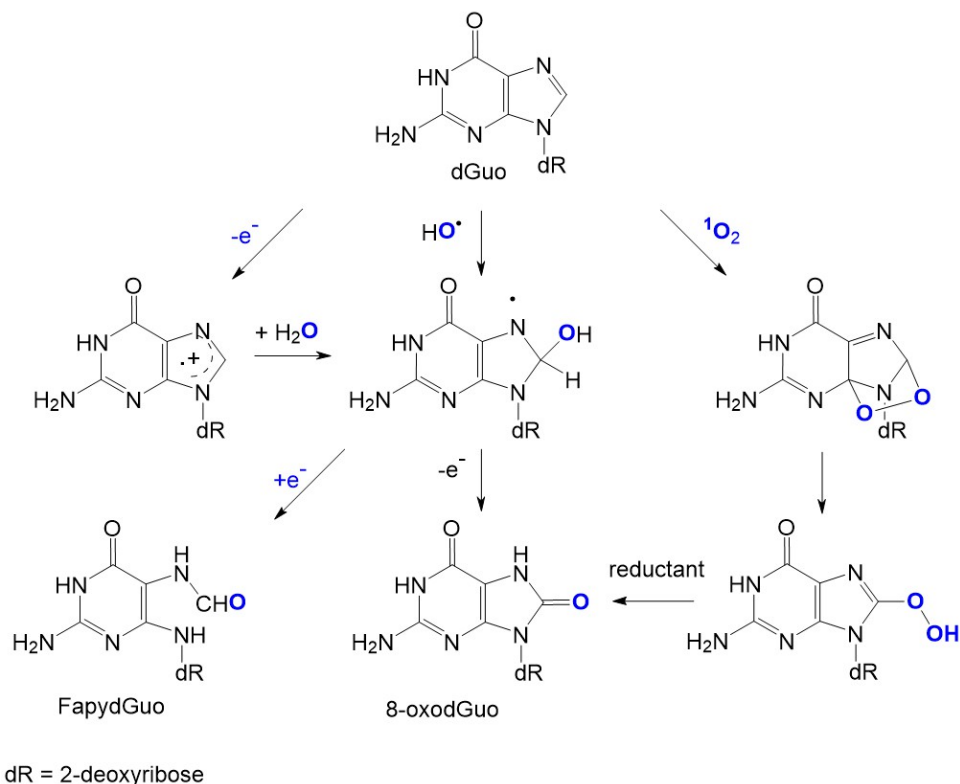
Fig. 4. Major oxidative pathways involved in the degradation of 2'-deoxyguanosine (dGuo). (Di Mascio et al., 2019)

The involvement of $^1O_2$ in UVA-induced 8-oxoGua formation has been demonstrated on the basis of a comparison of the spectrum of UVA generated oxidative DNA damage with the well-characterized DNA degradation pattern of ionizing radiation, which is dominated by $^{\cdot}OH$ (Pouget et al., 2000). Combining the comet assay with the use of specific DNA repair enzymes, strand breaks, oxidized pyrimidines and purines were measured on the DNA of human monocytes. While UVA generated a 6-fold higher level of oxidized purines relative to oxidized pyrimidines and single strand breaks, ionizing radiation generated predominantly strand breaks over oxidized bases. This difference may be due to the fact that singlet oxygen reacts exclusively with the guanine moiety of cellular DNA, while $^{\cdot}OH$ is able to oxidize all DNA components (Pouget et al., 2000). Furthermore, 2,6-diamino-4-hydroxy-5-formamidopyrimidine (FapyGua), a product of guanine oxidation by $^{\cdot}OH$, has not been detected in DNA of UVA-irradiated cells, suggesting lack of or low involvement of $\bullet OH$ in 8-oxoGua formation by UVA (Cadet et al., 2009) (the reaction that gives rise to FapyGua is shown in **Fig. 4**).

The ratio of CPD to 8-oxoGua has been estimated to be 9:1 in keratinocytes and fibroblasts (Courdavault et al., 2004; Mouret et al., 2006b). However, different cell types seem to be differentially susceptible to DNA damage formation by UVA. Thus, in melanocytes, for example, UVA has been shown to produce a ratio of CPDs to 8-oxoGua of 1.4:1, based on quantitative LC-MS/MS measurements (Ikehata et al., 2008; Kappes et al., 2006). In a more recent study, melanocytes were shown to produce 4-fold higher levels of 8-oxoGua compared to keratinocytes, based on LC-MS/MS measurements (Mouret et al., 2012). Mounting evidences indicate that this difference is likely due to photo-oxidation of DNA by melanin. The first evidence for oxidative effects of UVA-excited melanin was provided by measurements of single strand breaks in melanocytes derived from individuals of different skin phototypes (Wenczl et al., 1998). In this study, it has been demonstrated that susceptibility to single strand break formation correlated with melanin cellular content. Spectroscopic measurements have shown that UVA irradiation of synthetic eumelanins and pheomelanins generates singlet oxygen and $O_2^{\bullet-}$ (Szewczyk et al., 2016). Furthermore, UVA induces formation of CPDs in the dark in melanocytes and this has been proposed to happen through chemiexcitation of melanin as a result of peroxynitrite oxidation (Premi et al., 2015).

Finally, single strand breaks have been detected on cellular DNA exposed to UVA (Cadet et al., 2012; Melnikova & Ananthaswamy, 2005). Singlet oxygen on its own does not cleave DNA backbone, however the presence of 8-oxoGua may lead to DNA strand breaks under oxidative conditions, since 8-oxoGua is 100-fold more reactive with singlet oxygen than guanine (Dumont et al., 2016). The secondary oxidation of guanine may lead to single strand break formation (Cadet et al., 2015; Di Mascio et al., 1989). UVA-mediated formation of $^{\bullet}$OH also likely plays a role in single strand breaks formation, even though this radical is not the primary oxidizing species generated by UVA (Cadet et al., 2015).

A general scheme of the DNA lesions generated by UVA and UVB in DNA is represented below (**Fig. 5**).
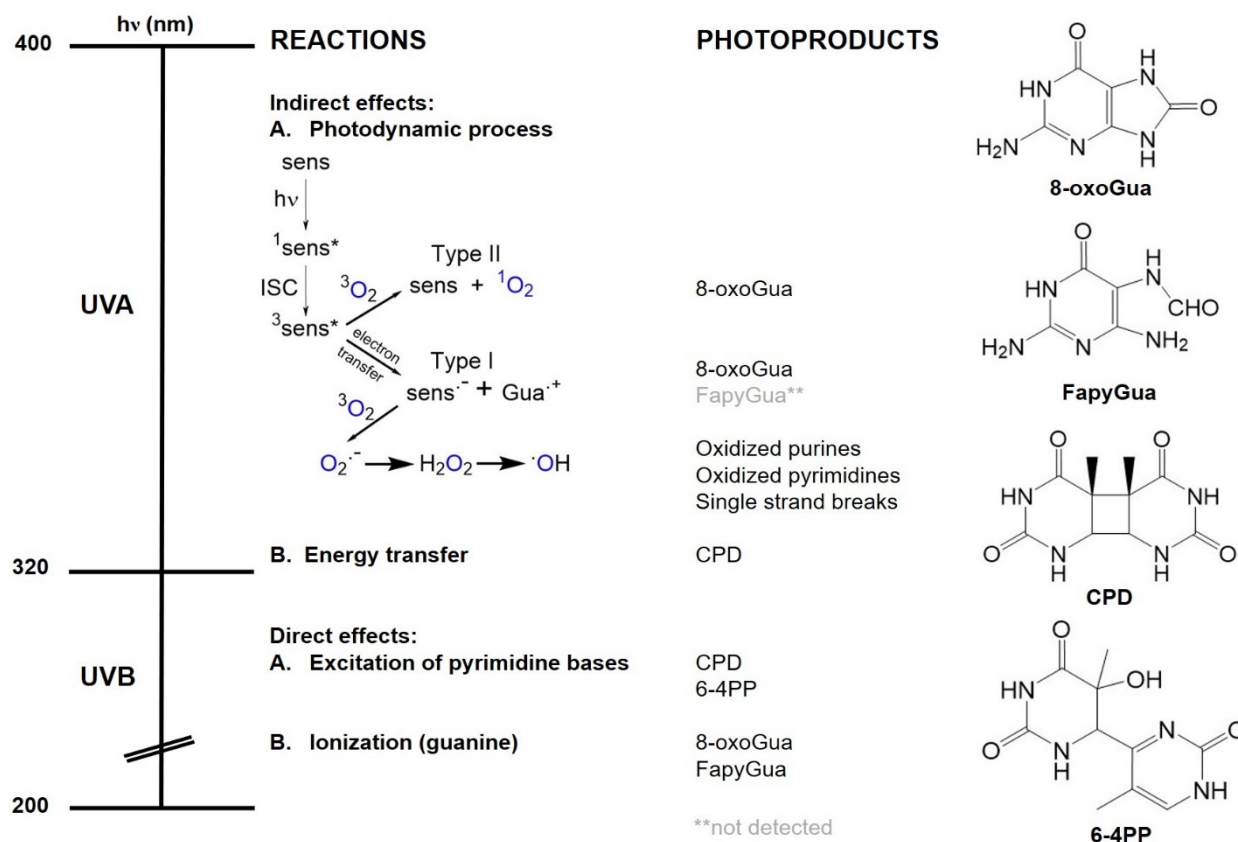
Fig. 5. Major DNA lesions generated by UVA and UVB in human DNA (Cadet et al., 2015).

Of note, UVA penetrates the skin more deeply than UVB. Agar et al. (2004) showed that in human samples of SCC and pre-malignant solar keratosis UVA-induced fingerprint

mutations were located mostly in the basal, germinative layer of the skin, while UVB fingerprint mutations were found mostly in the suprabasal layer. This observation indicates that UVA is an important carcinogen in the stem cell compartment of the skin, where most skin cancers occur (Agar et al., 2004; Pincelli & Marconi, 2010). This may also bear consequences for photoaging since stem cell exhaustion is a hallmark of aging (López-Otín et al., 2013). UVA has been shown to cause more protein carbonylation than UVB, affecting DNA repair proteins (i.e. NER components) and making cells more vulnerable to other mutagenic agents, such as UVB (Karran and Brem, 2016). Because of these characteristics, UVA seems to play a predominant role in skin photoaging and tumor promotion, while UVB wavelengths seem to be more relevant during tumor initiation since UVB is more mutagenic (Battie et al., 2014).

1.2.4. UVA-induced changes in gene expression, protein levels and cellular physiology

Early studies investigating the effects of UVA exposure on gene and protein expression focused mainly on redox-responsive genes (specially NFR2, HO-1, AP-1 and AP-2), antioxidant enzymes, stress-signaling kinases (JNK, MAPK and p38) and pro-inflammatory proteins (ICAM-1 and COX-2). In general, these UVA-induced gene expression modulations have been shown to depend on singlet oxygen formation, as inferred by indirect methods involving the use of $^1O_2$ quenchers, D_2O and chemical sources of $^1O_2$. Additionally, UVA-induced alterations in the levels of cell membrane lipids seem to be critically involved in signaling cascades that lead to altered gene expression (Grether-Beck et al., 2008).

In this sense, it has been proposed that $^1O_2$ and ceramide formation would underlie UVA-induced activation of AP-2/ICAM-1 and Ser/Thr stress kinases, such as MAPK/ERK, SAPK/JNK and p38 (Mazière et al., 2001), contributing to the stabilization and increased levels of COX-2 (Schuch et al., 2017). Additionally, increases in the levels of a lipid peroxidation product, 4-hydroxynonenal (4-HNE), has been shown to correlate with increased levels of JNK upon UVA exposure (Yang et al., 2003). UVA-mediated increases in AP-1 and COX-2 have been proposed to play a role in tumor promotion through increases in interleukin-8 (IL-8) and vascular endothelial growth factor (VEGF) (Bachelor & Bowden, 2004). Promotion of angiogenesis by up-regulation of VEGF has

been observed in skin after UV (UVA + UVB) exposure (Chung & Eun, 2007; Zhu et al., 2013).

An early study suggested that $^1O_2$ would be able to trigger a non-enzymatic mechanism of ceramide formation upon UVA exposure (Grether-Beck et al., 2000), but there is controversy about this mechanism in the literature (Mazière et al., 2001). Further analysis revealed that UVA leads to a biphasic formation of ceramide in keratinocytes, which co-occurs with biphasic increases in ICAM-1 expression and AP-2 activation (Grether-Beck et al., 2005). While the first peak of formation (0.5 – 1h post-exposure) would involve a non-enzymatic step, the second peak (16 – 48h) would involve increase expression and activity of serine palmitoyltransferase, a key enzyme in ceramide synthesis (Grether-Beck et al., 2005). A recent study based on lipidomic measurements confirmed the increase in intracellular ceramide post-UVA exposure and showed that antioxidants (i.e. ascorbic acid and rutin) prevented the increase in ceramide levels in 3D-cultured fibroblasts (Gęgotek et al., 2021).

Furthermore, UVA has been used as an oxidizing agent to demonstrate the oxidant inducibility of heme-oxygenase 1 (HO-1), a gene that codifies for an enzyme involved in heme metabolism, in skin fibroblasts (Keyse & Tyrrell, 1987). The UVA-induced increase in HO-1 levels is believed to be mediated by the generation of an oxidized phospholipid derived from 1-palmitoyl-2-arachidonoyl-sn-glycero-3-phosphorylcholine and seems to occur in a $^1O_2$-dependent manner (Gruber et al., 2007). Additionally, 4-HNE, is generated upon UVA exposure and is a strong inducer of HO-1 expression (Basu-Modak et al., 1996). Since UVA induces the release of free heme by microsomal hemeproteins (Kvam et al., 1999), HO-1 up-regulation by UVA has been proposed to play a role in maintaining low levels of free heme and preventing cellular damage (Tyrrell, 2011).

Microarray analysis has shown that fibroblasts exposed to UVA or UVA-oxidized 1-palmitoyl-2-arachidonoyl-sn-glycero-3-phosphorylcholine up-regulate the expression of antioxidant genes (HO-1, glutamate-cysteine ligase modifier subunit, aldo-keto reductases-1-C1 and -C2, and IL-8) (Gruber et al., 2010). Up-regulation of these genes by UVA is correlated with nuclear accumulation of the redox-regulated transcription factor NRF2 (Gruber et al., 2010). In terms of modulating antioxidant enzymes, work in cultured fibroblasts and in rodent skin has demonstrated that UVA leads to catalase and

glutathione depletion (Lautier et al., 1992; Okada et al., 1994; Shindo & Hashimoto, 1997). Conversely, UVA up-regulates manganese-dependent superoxide dismutase and selenium-dependent glutathione peroxidases and these modulations are protective against repeated UVA exposure (Meewes et al., 2001; Poswig et al., 1999). There is also a considerable literature showing that topically applied antioxidants counteract some of the effects of UVA on the skin, providing photoprotection (e.g., quercetin, β-carotene, rutin, vitamin E, vitamin C) (Delinasios et al., 2018; Fernández-García, 2014; Kimura et al., 2009; Matsui et al., 2009; Wertz et al., 2005).

Additionally, UVA has been shown to induce up-regulation of matrix metalloproteinase 1 (MMP-1) in fibroblasts (Wlaschek et al., 1995). Up-regulation and increased secretion of MMPs by skin fibroblasts play a role in remodeling of damaged skin, since MMPs break down collagen and other matrix proteins (Fisher et al., 1996, 2009). MMP-1 was shown to be increased by UVA exposure in human fibroblasts, but not in keratinocytes (Petersen et al., 1992; Scharffetter et al., 1991), with the exception of pre-malignant HaCaT cells and tumoral keratinocytes (Ramos et al., 2004; Wertz et al., 2004). MMP-1 up-regulation by UVA seems to be dependent on $^1O_2$ (Wlaschek et al., 1995). Inflammatory mediators (IL1, IL6, MIF), phospholipid hydroperoxides and cholesterol hydroperoxides have also been shown to be necessary for induction of MMP-1 by UVA (Minami et al., 2009; Watanabe et al., 2004; Wenk et al., 2004; Wlaschek et al., 1994).

Recent, omics-based studies have evaluated the effects of UVA radiation on skin cells, and confirmed many of the trends observed in early studies. For example, exposure of hairless mice to 15 J/cm² of UVA radiation lead to fibroblast senescent patterns characterized by accumulation of HNE adducts, DNA damage and ubiquitinated proteins (Swiader et al., 2021), reinforcing the role of lipid peroxidation in UVA's biological action. Topical application of carnosine, a free radical scavenger, prevented adduct formation, DNA damage and senescence induction (Swiader et al., 2021). Carnosine protection against UVA effects was further validated by a proteomics-based approach that evaluated regulation of protein levels in the dermis of hairless mice exposed to an acute UVA dose of 20 J/cm² (Radrezza et al., 2021). The main processes affected by UVA in the dermis involved mitochondrial function, calcium metabolism and cytoskeleton signaling. Another study (Narzt et al., 2019) based on a multi-omics approach revealed that 40 J/cm² of UVA lead to the generation of phospholipid hydroperoxides, with

consequent up-regulation of antioxidant enzymes (peroxiredoxin 6 and glutathione peroxidase) in primary keratinocytes, also reiterating the role of lipid peroxidation in UVA-induced damage and gene expression modulation. Importantly, both UVA exposure and administration of in-vitro UVA-oxidized phospholipids to keratinocytes lead to modulations in lipid metabolism and antioxidant mechanisms (Narzt et al., 2019).

Finally, three recent proteomics-based studies restated the role of redox imbalance, pro-inflammatory reactions and apoptosis in the response of skin cells to UVA radiation (Atalay et al., 2021; Gęgotek et al., 2018, 2019). Changes in the levels of redox-responsive proteins (e.g., NRF2, glutathione S-transferase, peroxiredoxin-1 and 2, superoxide dismutase, thioredoxin reductase 1, thioredoxin-dependent peroxide reductase, protein disulfide-isomerase and glutathione S-transferase) were observed in rat skin, as well as in fibroblasts and 3D cultured keratinocytes. Importantly, the scope of protein identification in these three studies was limited (< 700 identified proteins across all samples) and in-gel digestion was performed before MS analysis.

1.2.5. UVA radiation and tumorigenesis

Chronic exposure to UVA leads to malignant transformation of HaCaT cells in culture (He et al., 2006) and induces tumorigenesis in hairless mouse (de Laat et al., 1997; Kranen et al., 1997, p. 53) and fish (Setlow et al., 1993) models.

Epidemiological evidence also shows that repeated exposure of human to UVA radiation from tanning beds constitute a major risk for melanoma induction (Buckel et al., 2006; Ting et al., 2007). The drug thiopurine azathioprine provides an additional evidence of increased skin cancer risk associated with UVA exposure (Karran & Brem, 2016; O'Donovan et al., 2005). Azathioprine is a UVA photosensitizer, and it is used as an immunosuppressant prescribed to prevent rejection after organ transplant, and for inflammatory bowel diseases. In both treatment contexts, azathioprine is associated with a significantly increased risk of non-melanoma skin cancer. Importantly, tumorigenesis occurs almost exclusively on sunlight-exposed areas of the body (Karran & Brem, 2016; O'Donovan et al., 2005). There is also epidemiological evidence of increased skin cancer risk following phototherapy with 8-methoxypsoralen and UVA radiation (PUVA) for psoriasis (Archier et al., 2012).

1.3. Skin structure

The skin is the largest organ in the human body, preventing water evaporation and protecting internal organs from biological, physical and chemical stresses. The skin is subdivided into three layers: epidermis, dermis and subcutaneous tissue (Rudan et al., 2020) (Fig. 6).

The epidermis, the outermost layer of the skin, is a stratified squamous epithelium. At least 80% of epidermal cells are keratinocytes, but the epidermis also harbors other cell populations, such as melanocytes, Langerhans cells, Merkel cells and dendritic cells (Kolarsick et al., 2011). The basal layer of the epidermis is composed of stem cells attached to a basement membrane (Blanpain & Fuchs, 2006). The basement membrane consists of a collagen and laminin-rich sheet produced by both keratinocytes and fibroblasts (Plikus et al., 2021). Differentiating keratinocytes are pushed towards suprabasal layers of the epidermis by the proliferation of stem cells within the basal layer (Cursons et al., 2015). As migration occurs, keratinocytes undergo terminal differentiation, establishing a spatiotemporal differentiation gradient across the depth of the epidermis (Cursons et al., 2015). This process is tightly regulated by calcium, which forms a gradient that parallels keratinocyte differentiation (Bikle et al., 2012). After terminal differentiation, keratinocytes may undergo a unique process of cell death termed cornification (Lippens et al., 2005). This process involves the breakdown of the nucleus and other cytoplasmic organelles, as well as crosslinking of proteins (e.g. loricrin and involucrin) by transglutaminases into an impermeable cornified envelope (Lippens et al., 2005). **Fig. 6** summarizes the skin structure and epidermis organization.

In the dermis, fibroblasts produce a mechanically resilient, adhesive and elastic structural foundation that supports epidermal keratinocytes and epidermal appendages (e.g., hair follicles and sweat glands). As described in detail by Plikus et al., (2021), fibroblasts and other mesenchymal lineages establish three anatomically distinct layers in the dermis: papillary and reticular dermis and dermal white adipose tissue. Papillary fibroblasts underlie and secrete components of the basement membrane. Reticular fibroblasts produce densely packed extracellular matrix (ECM), which is responsible for the skin's mechanical strength. On the dermal white adipose tissue, fibroblast

progenitors produce a fine ECM that encases clusters of adipocytes. The secretory capacity of fibroblasts is necessary for ECM remodeling and is modulated by a variety of stimuli (e.g., cell-to-cell interactions, matrix stiffness, tensile forces, oxygen levels, epigenetic changes, aging and telomere length) (Winkler et al., 2020). The dermis still contains other complex networks of cellular communities and structures, including immune cells, epidermal appendages, sensory neurons, blood and lymphatic vessels (Plikus et al., 2021).
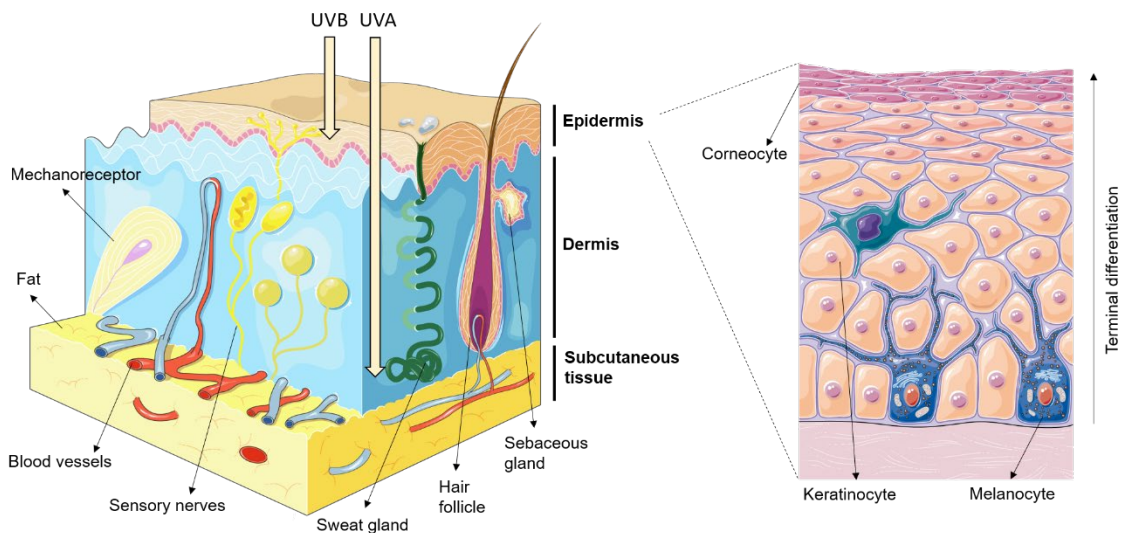
Fig. 6. Structure of the skin and detailed composition of the epidermis. We acknowledge Servier Medical Art (https://smart.servier.com) for providing the images.

1.4. Aging

1.4.1. UVA radiation and photoaging

Skin aging can be subdivided into chronological aging and photoaging. Chronological aging is mainly presented in photoprotected areas, whereas photoaging is usually observed in sun-exposed areas, and it is characterized by epidermal thickening, dryness, deep wrinkles, loss of elasticity, delayed wound healing and susceptibility to cancer (Fitsiou et al., 2020). In this sense, cellular aging is thought to be driven by intrinsic and extrinsic damage to biomolecules. Cells burdened with accumulated damage may die and not be replaced, contributing to the functional decline of tissues.

Alternatively, cells may undergo phenotypic reprogramming and lose their proliferative capacity, a process that has been termed senescence (Campisi, 1998).

UVA's impact on dermal photoaging has been widely studied, likely because UVA is much more efficient in reaching this skin layer than UVB. Dermal changes in photoaging reflect senescence (Fitsiou et al., 2020), as well as apoptosis of fibroblasts (Bernerd & Asselineau, 1998). In this context, UVA has been described to induce apoptosis in dermal fibroblasts, leading to dermal alterations usually observed during photoaging (Battie et al., 2014; Bernerd & Asselineau, 1998). Furthermore, in four recent studies, human fibroblasts have been shown to acquire a senescent phenotype after UVA exposure, up-regulating well-known senescence markers, such as p16INK4a, p21, p53 and senescence-associated β-galactosidase levels (Bai et al., 2021; Leontieva & Blagosklonny, 2017; Swiader et al., 2021; Yi et al., 2018). Swiader et al., 2021, described UVA-induced senescence in fibroblasts to be dependent on HNE, a lipid peroxidation product. Topical application of carnosine, which adducts with HNE (Liu et al., 2003), prevented senescence induction. Another study demonstrated that singlet oxygen likely induces the most frequent mtDNA deletion found in photoaged skin (Berneburg et al., 1999).

Similarly, photoaging also impacts the ultrastructure and function of the epidermis, interfering with skin thickness, barrier capacity, prevention of water loss, hydration maintenance and reepithelization post wound healing (Gilhar et al., 2004). While UVB's action on the epidermis is well-characterized, UVA-induced cellular mechanisms underlying epidermal alterations during aging are not as well understood (Fitsiou et al., 2020). Lethal UVA doses have been shown to induce apoptosis in epidermal keratinocytes and melanocytes, but less is known about the impact of low doses of UVA on epidermal health (Assefa et al., 2005; Bivik et al., 2006). The only evidence to date suggesting senescence induction by UVA on keratinocytes relies on the fact that UVA modulates the levels of p63, ki67, and activated caspase-3 in the germinative layer of the epidermis (Casale et al., 2018).

1.4.2. Senescence

Senescence was first characterized as a limitation in the proliferative potential of primary cells in culture by Hayflick and Moorhead in the 1960s (Hayflick & Moorhead, 1961).

Currently, senescence is also recognized as a cellular stress response (Kuilman et al., 2010) and may be triggered by DNA damage (d'Adda di Fagagna, 2008), epigenetic (Sen et al., 2016), mitochondrial (Wiley et al., 2016) and oxidative stresses (Dumont et al., 2000; Höhn et al., 2017; Vono et al., 2017), as well as by oncogene activation (Liu et al., 2018).

The DNA damage response, p53 and p21 play causal roles in the induction of cellular senescence by DNA damage (d'Adda di Fagagna, 2008). The DNA damage response induces p53, leading to its stabilization and increasing this protein's ability to induce the transcription of p21, a cyclin-dependent kinase inhibitor involved in stable cell-cycle arrest (Deng et al., 1995). Gene deletion of TP53 (which encodes p53) and CDKN1A (which encodes p21) extends the proliferation of fibroblasts in culture beyond their senescence limit (Bond et al., 1994; Brown et al., 1997). Triggering of the DNA damage response has also been linked to replicative senescence (d'Adda di Fagagna, 2008). In this case, progressive telomere shortening causes chromosome ends to be recognized by the DNA damage response machinery, eventually leading to senescence (d'Adda di Fagagna, 2008).

Besides p53 and p21, the tumor suppressor p16[INK4a], another cyclin-dependent kinase inhibitor, also plays a critical role in senescence (d'Adda di Fagagna, 2008). For example, p16[INK4a] is increased in stem cells of different mouse organs during aging (Janzen et al., 2006). Furthermore, p16[INK4a] inactivation has been shown to rescue the cellular proliferative impairment associated with aging (Berent-Maoz et al., 2012). In mice, accumulation of p16[INK4a] leads to age-related phenotype and loss of replicative capacity (Baker et al., 2016). Finally, the clearance of p16[INK4a]-expressing cells attenuates aging phenotypes and improves lifespan in mice (Baker et al., 2011; Cosgrove et al., 2014). It has been shown that p16[INK4a] responds to DNA damage, but also to other types of stresses, such as oxidative stress (Ben-Porath & Weinberg, 2005).

Oxidative stress is a trigger of senescence. It has been demonstrated that, when exogenous hydrogen peroxide is added to cell culture, cells exhibit a strong senescent-phenotype (Du et al., 2019; Kiyoshima et al., 2012). Similarly, inhibition of ROS scavenging enzymes, such as superoxide dismutase, causes premature senescence (Blander et al., 2003). As previously described, ROS can damage DNA, protein and

lipids, besides acting as messengers to regulate signaling pathways. There is evidence that some types of oxidative stresses may act through p53 and p21 activation to induce senescence, similarly to telomere dysfunction (Itahana et al., 2003). Another study indicates that cells under oxidative stress can activate p16^{INK4a}, possibly through the p38-MAPK signaling pathway (Iwasa et al., 2003).

Besides provoking permanent cell cycle arrest, senescence induces other changes in the cellular phenotype (Marusyk et al., 2007), such as metabolic reprogramming (Aird et al., 2015; Nacarelli et al., 2019), alterations in organellar morphology and a specific pro-inflammatory senescence-associated secretory phenotype (SASP) (Basisty et al., 2020). For example, senescent cells display a flat and large appearance, with enlarged nuclei, altered plasma membrane composition and accumulation of both lysosomes and mitochondria (Lee & Schmitt, 2019). Additionally, proteostasis is altered during senescence, leading to accumulation of protein aggregates and increases in post-translational modifications of proteins, as well as altered functionality of the proteasomal and autophagic systems (Höhn et al., 2017). Cellular senescence is driven by dynamic changes in gene expression, varying between cell types and depending on the stressor that triggered the senescence program (Basisty et al., 2020; Lee & Schmitt, 2019). However, some markers have been proposed to be present in most senescent cells. For example, the discovery of increased levels of lysosomal β-galactosidase due to increased lysosomal content in senescent cells provided the first marker for their detection *in vivo* (Campisi, 1998). In this sense, the amount of senescence-associated (SA) β-galactosidase positive cells has been shown to increase with age in human skin (Campisi, 1998).

Stress-triggered and replicative senescence have been largely associated to the development of an aging phenotype in multiple mammalian tissues, including the skin (Hernandez-Segura et al., 2018). Accumulation of senescent stem cells in tissues, presumably following replicate exhaustion, is thought to impair tissue homeostasis over time (Vono et al., 2017). Various sources of evidence support the connection between senescence and aging. For example, clearance of senescent cells by the immune system or reversal of the senescent phenotype by senolytic agents is associated to tissue rejuvenation in various organs (Baker et al., 2011; Jaskelioff et al., 2011). On the

other hand, inhibition of cell proliferation has been shown to cause aged phenotypes (Boquoi et al., 2015; Pruitt et al., 2013) and senescent cells accumulate *in vivo* in aged organisms (Bahar et al., 2006; Herbig et al., 2006).

Besides being associated with aging, senescence is also though to act as an antitumorigenic mechanism. For example, cellular senescence can be induced by oncogenic stress. Oncogenic mutations in Ras and hyper-expression of Ras has been shown to induce senescence in fibroblasts (Sarkisian et al., 2007; Serrano et al., 1997). Overexpression of other oncogenes, such as BRAF and AKT, is also able to induce senescence (Courtois-Cox et al., 2008). However, there is also mounting evidence that senescent cells can guide the progression of hyperplasic pathologies, a process that has been termed antagonistic pleiotropy (Campisi, 2013).Therefore, for example, senescent fibroblasts can induce epithelial-to-mesenchymal transition in premalignant immortalized epithelial cells through secretion of specific SASP factors (Coppé et al., 2008; Parrinello et al., 2005). On the other hand, non-immortalized, normal cells exposed to the SASP of senescent cells enter paracrine senescence (Acosta et al., 2013). For a more detailed view of the relationship between senescence and cancer, we refer the reader to Lee & Schmitt, 2019.

Even though senescence has been regarded as an irreversible condition, it depends primarily on gene expression modulation, therefore in principle it could be reversible. In this sense, it has been demonstrated that senescence escape may happen in certain contexts, when senescence maintenance genes are not expressed. Thus, for example, senescent cells under chemotherapy may develop stemness and latter escape from senescence (Milanovic et al., 2018). When these cells escape from senescence, bearing markers of stemness, they present an enhanced tumorigenic potential in comparison with cells that never entered senescence under the same conditions (Milanovic et al., 2018). Senescence escape seem to be modulated by specific components of the senescence machinery. In this sense, senescence arrest caused by telomere dysfunction is reversible, being maintained primarily by p53 and reversed by p53 inactivation (Beauséjour et al., 2003). On the other hand, p16^{INK4a} is apparently linked to an irreversible cell cycle arrest, since cells presenting high levels of p16^{INK4a} cannot be rescued from senescence by p53 inactivation (Beauséjour et al., 2003).

Overall, characterizing which stressors cause senescence in different tissues and the molecular patterns that senescence assumes when triggered by different types of stressors has been proven to be detrimental to the understanding of the interplay between senescence, aging and tumorigenesis.

1.5. Proteomics

Proteomics encompasses efforts to identify and quantify all proteoforms of a proteome (Y. Zhang et al., 2013). Each molecular form of a protein is called a proteoform. Variability in the molecular form of a protein can result from variability in DNA sequence (i.e., polymorphisms), RNA splicing and post-translational modifications (Ponomarenko et al., 2016). It has been estimated that approximately 20000 genes of the human genome can codify about 6 million proteoforms (Ponomarenko et al., 2016), even though this number is far below the theoretical number of possible combinations (Aebersold et al., 2018). Altogether, these characteristics make proteomics more challenging than sequencing a genome. Technological advances mainly in peptide separation, mass spectrometry and bioinformatics have been driving the development of this research area (Senko et al., 2013).

1.5.1. Shotgun proteomics

In analogy to shotgun DNA sequencing, which involves reconstructing DNA sequences from short sequencing reads, the term "shotgun proteomics" has been coined to describe the methodology by which proteins are identified on the basis of mass spectra obtained from sequencing of peptides (Y. Zhang et al., 2013). Shotgun proteomics is a discovery-driven technique that does not focus on specific sites or proteins of interest, offering a hypothesis-free and systems-wide analysis that complements antibody-based and other targeted approaches (Meissner & Mann, 2014). Quantitative changes in protein levels within space or time may reflect modulation in expression, localization, post-translational modifications, turnover and interactions, for example (Lundberg & Borner, 2019).

In a typical shotgun proteomics workflow, proteins extracted from a biological sample are enzymatically digested to peptides and the peptides are characterized by LC-MS/MS

(Aebersold & Mann, 2016) (**Fig. 7**). Proteins are usually cleaved into peptides by sequence-specific proteases (Y. Zhang et al., 2013). Proteolytic enzymes differ based on their specificity for cleaving amide bonds between residues of amino acids in a protein. Trypsin, which cleaves at the carboxyl side of arginine and lysine, has become a standard for protein digestion in shotgun proteomics, even though combinations of proteolytic enzymes are also used to deepen protein coverage (Dau et al., 2020). After digestion, the resulting peptide mixtures are desalted for mass spectrometry analysis, commonly in pipette-based devices (Rappsilber et al., 2007). Liquid chromatography separates the peptides, reducing sample complexity and enabling better proteome coverage. Eluting peptides are aerosolized and ionized, commonly by electrospray ionization, at the tip of the column and injected into the vacuum of a mass spectrometer for direct analysis (Aebersold & Mann, 2016).
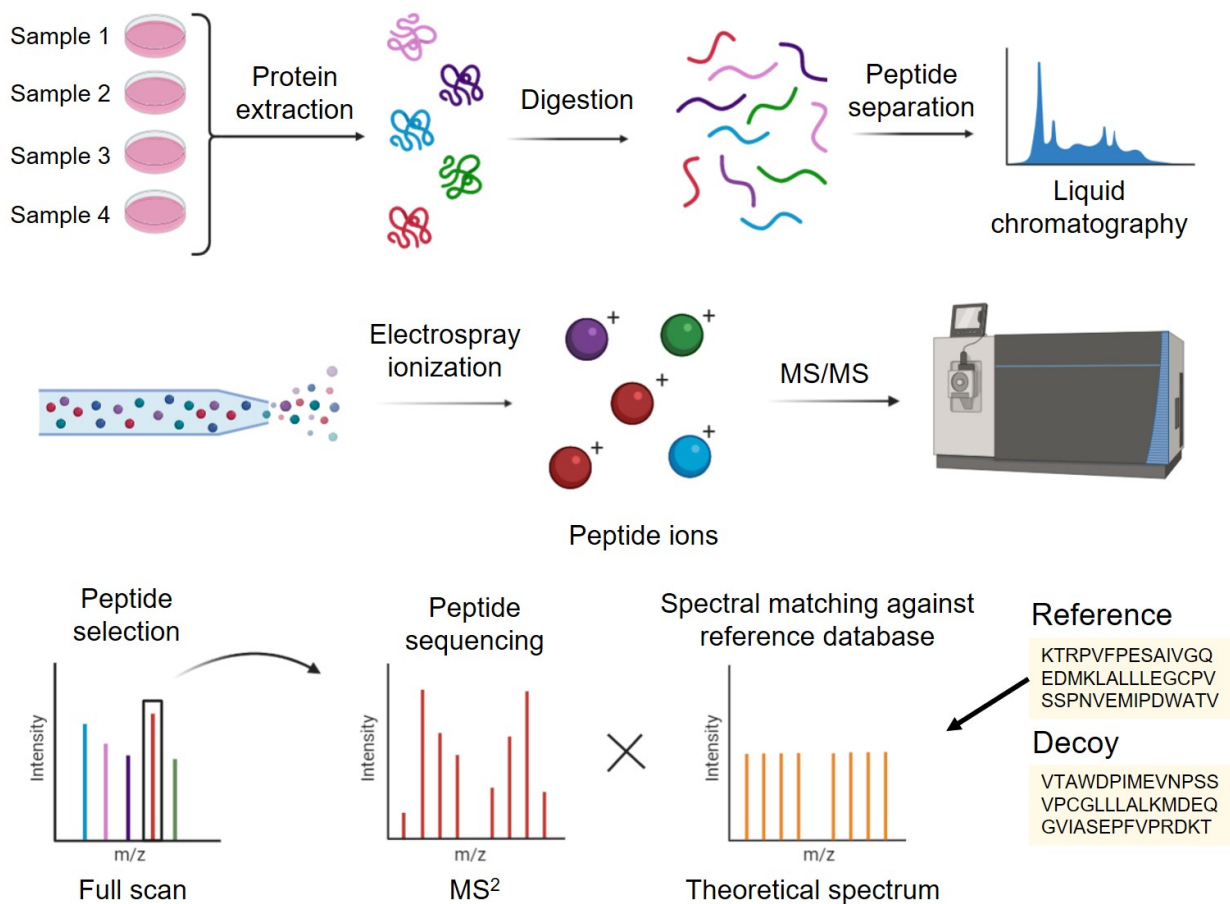
Fig. 7. Generic data-dependent acquisitions workflow. (Image created with BioRender.com.)

As described in detail by Aebersold & Mann (2016) and Y. Zhang et al. (2013), in commonly used data-dependent acquisition (DDA) approaches, mass spectra of peptide ions that co-elute at a specific point in the gradient elution (precursor ions) are recorded at the MS^1 level (full scan). The most abundant peptides are isolated and fragmentated in a collision cell before a subsequent MS^2 (or MS/MS) scan (**Fig. 8**). Before fragmentation, the ions are translationally excited and upon collisions with gas molecules they convert the translational energy to internal (vibrational) energy, fragmenting (Diedrich et al., 2013). MS^2 is used to determine the specific amino acid sequence of peptides, since this type of spectrum presents their fragmentation profiles. The mass spectrometer alternates between MS^1 and MS^2 acquisitions, and as many precursor ions as possible are isolated and fragmented in-between full scans, within cycle times of about 1 to 3 seconds (Aebersold & Mann, 2016). In intruments equipped with ion trap or orbitrap technologies, sequential trapping and isolation of precursor ions is achieved by filling the trap and ejecting all ions except for a population of peptides within a mass window containing the precursor peptide mass-to-charge ratio (m/z) into the mass analyzer (**Fig. 8**). Then, the mass analyzer separates the ions based on their m/z and outputs them to a detector, where they are detected and converted to a digital output (Perry et al., 2008). This process is sequentially repeated until the highest number possible of the peptides have been sampled.

There are many different mass analyzers, such as the quadrupole, ion trap, orbitrap, Fourier transform ion cyclotron resonance and time-of-flight (TOF). A review of these analyzers is out of the scope of this introduction. For detailed descriptions of these technologies please refer to Marshall and Hendrickson (2008). The main mass analyzer we used in this study is the orbitrap, which determines the m/z of peptides by the oscillation frequency of the peptide around a central spindle-shaped electrode (Zubarev & Makarov, 2013). In the last decade, Orbitrap analyzers have gained substantially in mass spectrometric resolution, accuracy and speed (Senko et al., 2013). For complex peptide mixtures, such as those derived from cell lysates, high resolution enables accurate identification and quantification of thousands of peptides (Meissner & Mann, 2014; Senko et al., 2013).

As proteomic analysis has been driving technological advances in mass spectrometry in recent years, different instrumentations have been created to fragment peptides and

measure their m/z. In particular, hybrid instruments, involving different mass analyzers, ion optics and fragmentation sources, have been developed to enhance accuracy of mass measurements and to create more informative fragmentation patterns (**Fig. 8**) (Senko et al., 2013; Y. Zhang et al., 2013).
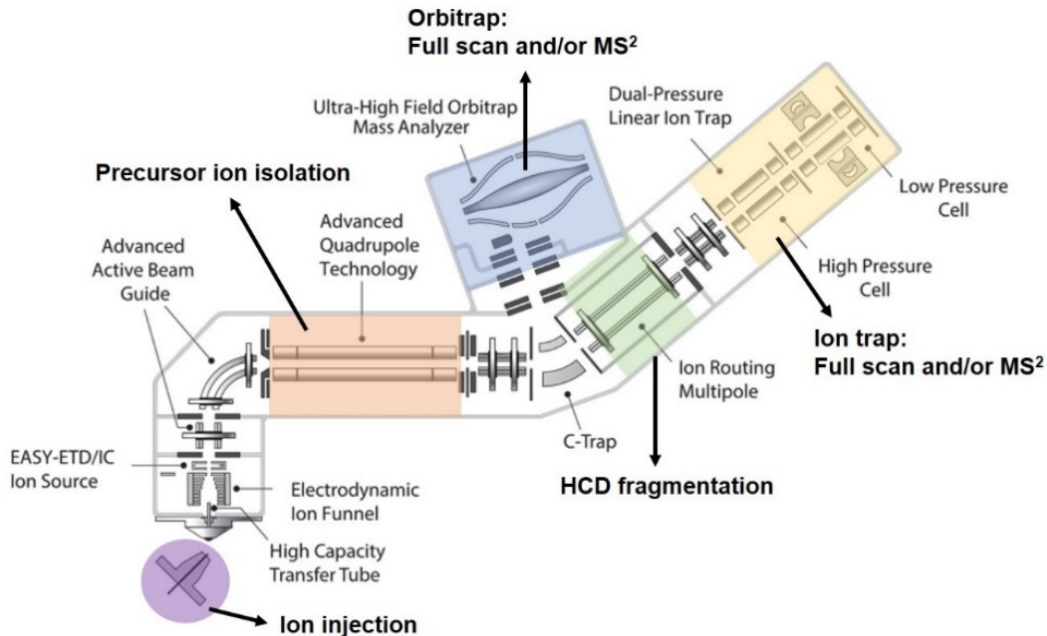
Fig. 8. Diagram summary of the hybrid mass spectrometer Orbitrap Fusion Lumos, used for data acquisition in this thesis. (Scheme from Thermo Scientific™)

In terms of data analysis, mass spectra are compared against a reference database of canonical sequences for inference of peptide identity (Eng et al., 2011). The comparison of experimental peptide spectra with theoretical spectra generated from *in silico* digestion of a protein database allows calculation of peptide spectral match scores, which reflect the likelihood that the corresponding peptide is present in a given sample (Christopher et al., 2021). To assess the reliability of peptide identification, experimental spectra are searched against both the target species peptide database and a decoy database. The decoy database consists of a reversed or randomized version of the target database. Comparison of the experimental spectra with the decoy database enables calculation of the percentage of peptide spectral match hits that are false positives, allowing for estimation of false discovery rates (Moosa et al., 2020). Inference of protein identity is accomplished by assigning peptide sequences to proteins. As peptides can be either uniquely assigned to a single protein or shared between multiple

proteins, the identified proteins can be scored and grouped based on their peptides (Y. Zhang et al., 2013). Complex algorithms for database searching have been developed for DDA, including Andromeda, Sequest and Mascot, for example (Cox et al., 2011; Eng et al., 1994; Perkins et al., 1999). Importantly, database searching tools are packaged into softwares such as MaxQuant and Proteome Discoverer, which allow customizable pipelines for different types of experimental designs, as well as protein quantification (Cox & Mann, 2008).

Quantification of protein levels by label-free methods is accomplished either by spectral counting or ion intensity. In spectral counting, the frequency of peptide spectral matches can be correlated with the amount of a protein, whereas ion intensity is based on integration of the chromatographic peak areas of peptides. The area under the curve (AUC) correlates to peptide concentration and peptide quantification is used as a proxy for protein abundance. Quantification of proteins based on AUC by measurement of ion abundance at specific retention times for given ionized peptides is useful for quantification within the given detection limits of the instrument (Y. Zhang et al., 2013). Different softwares and statistical packages implement different label-free quantification approaches. In MaxQuant, for example, sum of normalized peptide intensities are used as a proxy for protein abundance (Cox et al., 2014), whereas MSstats performs protein quantification by summarizing peptide intensities of a given protein via Tukey's median polish (Choi et al., 2014).

Several limitations impact the accuracy and reproducibility of protein quantification, such as co-elution of peptides, particularly when peptide signals are spread over a large retention time window, multiple signals from the same peptide due to technical or biological variation in retention time and background noise due to chemical interference (Y. Zhang et al., 2013). Computational methods have been developed to address these issues, considering mass accuracy and alignment of retention times of peptides across various sets and peak abundance normalization, for example (Cox et al., 2014; Y. Zhang et al., 2013).

Label-free shotgun proteomics approaches have been popular due to their ease of application, even though quantitative methods involving, for example, isotope labeling or data-independent acquisition reduce missing values and improve reproducibility

(Aebersold & Mann, 2016). Missing values are a known problem of label-free shotgun proteomics and can be caused by biological variation or technical issues arising from sample storage, protein extraction, and mainly from stochastic sampling of peptide ions during MS acquisition (Christopher et al., 2021).

1.5.2. Spatial proteomics

1.5.2.1. Overview of the method

Spatial proteomics designates approaches for determining the localization and abundance of proteins in space (Lundberg & Borner, 2019). Here, we are using this term to refer to approaches that target protein localization in intricate subcellular structures, instead of whole-cell analysis in tissue-specific cell types.

In a typical spatial proteomics experiment, cells undergo biochemical fractionation for separation of organelles and proteins from each fraction are analyzed by LC-MS/MS. Subcellular fractionation is based on de Duve's principle, which states that proteins from same subcellular niche will share similar abundance profiles across a separation gradient (Christopher et al., 2021; de Duve, 1971). MS-based quantification of proteins provides systems-level information about subcellular localization and enables cellular model building (Christopher et al., 2021).

Various experimental designs involving MS-based proteomics and microscopy have been developed for investigation of organelle composition (Lundberg & Borner, 2019). Early MS-based studies have focused on the identification and quantification of proteins in single organelles by means of biochemical purification (Andersen et al., 2003). These approaches have established detailed inventories of organelles, shedding light on the composition of the nuclear membrane of mouse hepatocytes (Schirmer et al., 2003), mitochondria from different tissues (Pagliarini et al., 2008), peroxisomes (Islinger et al., 2007; Ray et al., 2020), autophagosomes (Goebel et al., 2020), lysosomes (Schmidtke et al., 2019), centrosomes (Andersen et al., 2003), lipid droplets (Krahmer et al., 2013), and vesicles (Borner et al., 2014). Organelle-purification based methods, however, suffer from two major drawbacks: i) targeted organelle constituents and contaminant co-purified proteins originated from non-targeted subcellular niches cannot be

distinguished, and ii) lack of a broader, more meaningful biological picture can lead to misleading associations (Gatto et al., 2014). To overcome the drawbacks of organelle-purification based approaches, other methods involving subcellular fractionation, such as protein correlation profiling, have focused on using more complex experimental designs to elucidate the broad subcellular diversity of the proteome of cells (Christopher et al., 2021).

In an experimental workflow of centrifugation-based methods for organelle fractionation, samples are usually kept on ice and the cellular membranes are lysed (Christopher et al., 2021). Disruption of organellar membranes should be avoided during this stage (Itzhak et al., 2016). This is usually achieved by performing hypotonic shock on cells and Dounce homogenization (Itzhak et al., 2016), ball bearing homogenization (Mulvey et al., 2017), or sonication in detergent-free lysis buffers, for example (Christopher et al., 2021; Shehadul Islam et al., 2017). After cell membrane lysis and removal of unlysed cells, intact organelles are usually separated by density or differential centrifugation into fractions (Geladaki et al., 2019) (**Fig. 9**). Density centrifugation involves the use of sucrose (Andersen et al., 2003; Krahmer et al., 2018), Nycodenz (Gronemeyer et al., 2013), iodixanol (Mulvey et al., 2017) or Percoll (Jethwaney et al., 2007) to produce discrete organellar fractions. Differential centrifugation, on the other hand, does not rely on the use of gradient-forming agents, but on performing sequential centrifugations of increasing centrifugal forces to partition the cell lysate into fractions (Itzhak et al., 2016). Both centrifugation-based methods have been successfully applied to generate detailed organellar maps of cells, with similar abilities to discriminate between multiple subcellular niches (Geladaki et al., 2019). Alternatively, detergent-based fractionation methods are also able to separate subcellular compartments based on their solubilization properties (Martinez-Val et al., 2021). This approach usually requires less starting material than centrifugation-based method and has also been successfully applied to generate organellar maps of cells (Christopher et al., 2021).
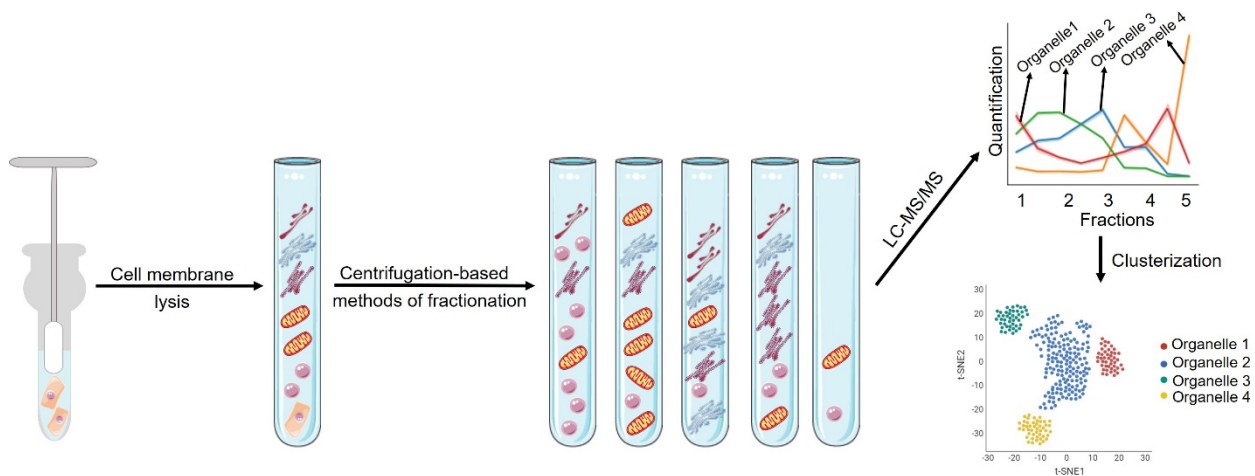
Fig. 9. Schematic representation of centrifugation-based methods of subcellular fractionation. (Image created with BioRender.com.)

The fractions obtained by centrifugation are enzymatically digested and injected into an LC-MS/MS system for protein identification and quantification. Protein quantification in spatial proteomics has been accomplished by using different methodologies, involving label-free quantification (Itzhak et al., 2017; Krahmer et al., 2018), tandem mass tags (Jean Beltran et al., 2016; Mulvey et al., 2017), and stable isotope labeling in cell culture (Itzhak et al., 2017), with the labeling methods yielding more accurate quantification data (Itzhak et al., 2017). Importantly, reduction of quantification noise leads to better resolution of subcellular niches (Gatto et al., 2014). Protein correlation profiling consists in obtaining multiple organelle profile plots, where the abundance of a protein is plotted across the biochemical fractionation gradient (Lundberg & Borner, 2019). Proteins with similar abundance profiles across fractions cluster together and can be assigned to their respective organelles, according to de Duve's principle (Christopher et al., 2021; de Duve, 1971).

As spatial proteomics datasets are complex and contain thousands of protein quantification data across different fractions, replicates and conditions, manual verification of individual profiling plots is not feasible. Thus, analysis of spatial proteomics datasets benefits from multivariate statistics, especially from dimensionality reduction (e.g., PCA and t-SNE) and clusterization methods (Hilario & Kalousis, 2008; Maaten & Hinton, 2008). These statistical and computational techniques enable visualization of the resolving power of the fractionation, quality control of the data and also extraction of biological information (Gatto et al., 2014) (**Fig. 10**).
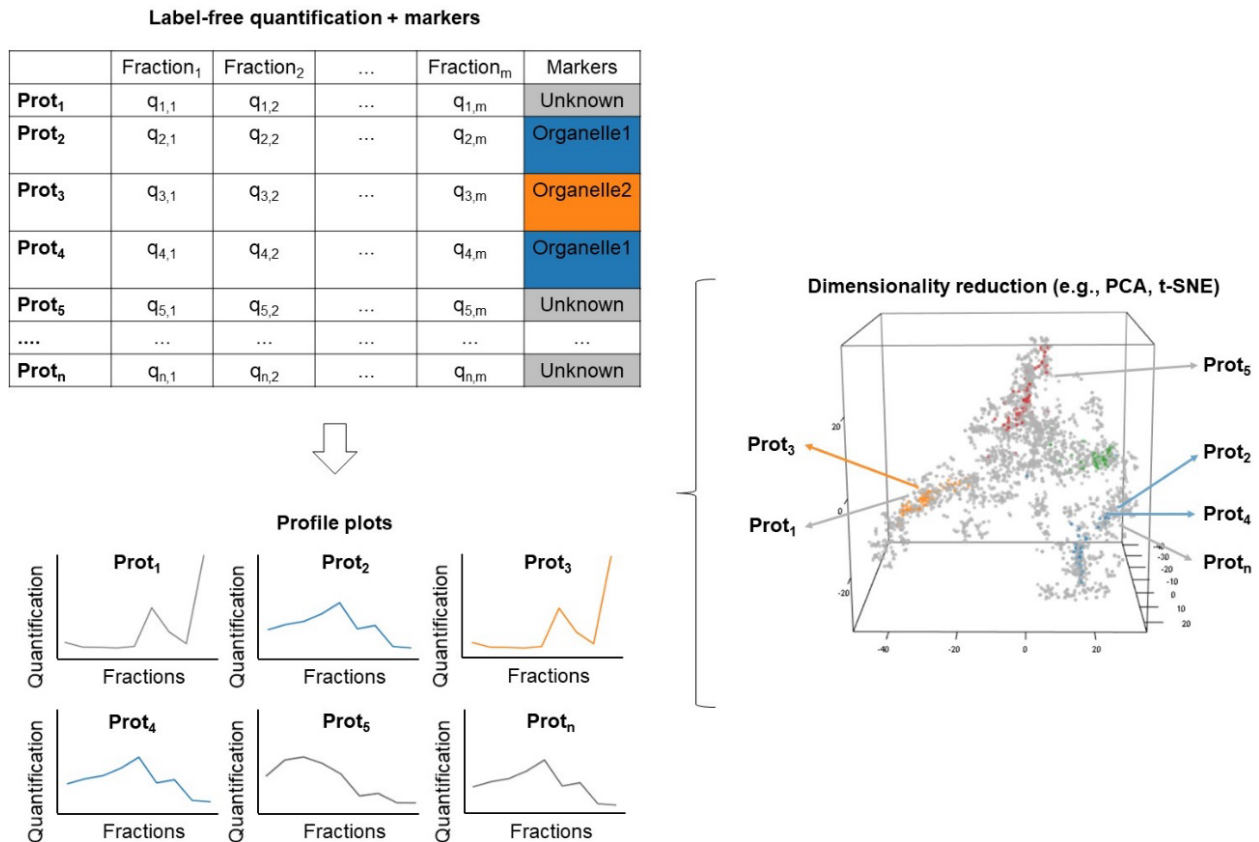
Fig. 10. Schematic representation of a spatial proteomics dataset containing quantitative data for n proteins along m fractions. Each protein is described by a fractionation profile, q is the quantification data in each fraction, n is the number of distinct proteins, while m stands for multiple fractions. Marker proteins are annotated with subcellular localization information from other sources (e.g., Uniprot, Gene Ontology and Cell Atlas). The data can be visualized in profile plots or via dimensionality reduction techniques. (Based on Gatto et al., 2014)

Since proteins from a given subcellular niche are expected to share similar profile plots, dimensionality reduction techniques allow inspection of the data and assessment of data structure (Mulvey et al., 2017). In a first instance, the data can be inspected in an unsupervised way, without overlaying of any additional information. This analysis provides a first quality assessment of the existence of clusters (Gatto et al., 2014). Ideally, there should be well-defined and structured clusters in the data, which will allow for reliable mapping of the points to subcellular niches (Gatto et al., 2014). A second assessment of the data involves overlaying data from other sources (e.g., Gene Ontology, Uniprot, Cell Atlas) on the PCA or t-SNE of observed points, for example. The

overlaying data should explain, at least to some extent, the underlying data structure and protein clusters (Breckels et al., 2018; Mulvey et al., 2017) (**Fig. 10**).

Spatial proteomics has benefitted from application of machine learning algorithms for subcellular localization and translocation prediction (Gatto et al., 2014; Kennedy et al., 2020). In spatial proteomics, the task of classification of subcellular localization and translocations falls under the area of supervised learning. As described in detail by Gatto et al., 2014, supervised learning aims to train a classifier into learning to map a set of observed points to a set of associated external attributes that are being predicted (class labels). Learning involves finding a mathematical function that approximates an underlying unknown target function, which describes how the observed points are related to their respective class labels (**Fig. 11A**). The set of points for which there are known class labels is called the training data. Each observation in the training data consists of a pair of inputs: a vector of numbers representing the observed data (for instance, the normalized ion intensities along a set of fractions for a given protein) and a class label, representing the membership of each protein to a given subcellular niche. As the classifier learns to discriminate the observed points of the training data into the correct class labels, the aim is to use the optimized mathematical function that separates the clusters to predict class labels on data with unknown attributes (**Fig. 11B**).

Almost all spatial proteomics methods to date have predicted protein localization and translocations using supervised learning algorithms (with the exception of the SubCellBarCode (Orre et al., 2019)). Furthermore, many machine learning algorithms have been extensively tested for spatial proteomics datasets, including support vector machines, neural networks, random forest models and naïve Bayes classifiers (Crook et al., 2018, 2020). These algorithms differ by the mathematical modeling underlying the classification of the predicted classes to the observed points and can have similar accuracies of classification on spatial proteomics datasets if the parameters of the model are properly optimized (Gatto et al., 2019; Jean Beltran et al., 2016).

A

Unknown target function
$$f: x \to y$$

Ideal function f that maps x (vector of ion intensities across fractions) to y (subcellular classifications)

Training set
$$(x_1, y_1), ..., (x_n, y_n)$$

Organellar markers of known-subcellular localizations

Error measure

Learning algorithm

$$g(x) \approx f(x)$$

Final hypothesis
$$g: x \to y$$

Final function g approximates the ideal function f

Hypothesis set

Set of candidate mathematical functions

B

Colored points represent organellar markers. Gray points represent proteins of unknown localization

Classification of subcellular localization for all non-marker proteins

Fig. 11. Machine learning algorithms applied to spatial proteomics.

(A) General scheme representing the training of a supervised machine learning algorithm (adapted from Abu-Mostafa et al., 2012). **(B)** Classification of proteins with unknown localization based on a mathematical function that separates the clusters.

The class label attribute of the training data in a spatial proteomics dataset is usually termed an organellar marker (Gatto et al., 2014). An organelle marker is a protein that resides in a known subcellular niche, considering the species and condition of interest. Organellar markers enable mapping of regions in the multidimensional space of the dataset to subcellular localizations. Organellar markers are commonly obtained from curation of proteins in the dataset according to subcellular information available in databases (Gatto et al., 2014). Gene Ontology (Ashburner et al., 2000), Uniprot (The UniProt Consortium, 2017) and the Cell Atlas (Rozenblatt-Rosen et al., 2017) classifications of subcellular localization are commonly used for curation of organellar markers (Itzhak et al., 2016; Mulvey et al., 2017). Curation of subcellular localization

according to multiple sources is necessary to counter unreliable annotation. It is not necessary to have organelle markers for every subcellular niche, especially given the complexity of subcellular organization. In general, reliable markers can be mapped to large and well-studied subcellular compartments for accurate classifications (Gatto et al., 2014).

Spatial proteomics experiments involving multiple biological conditions were frequently based on comparing the subcellular localization predictions across different conditions to detect translocations (Jean Beltran et al., 2016). Recently, a pipeline for direct modeling of translocation via machine learning was developed (TRANSPIRE for Translocation Analysis of Spatial pRotEomics (Kennedy et al., 2020)). This pipeline creates synthetic translocations profiles from experimental organellar markers of the dataset to train a classifier to identify true protein dynamic events.

1.5.2.2. Applications

Several approaches for protein correlation profiling have been implemented, differing in the methods used for subcellular fractionation, MS quantification and statistical/computational analysis. For comparative spatial proteomics experiments involving different biological conditions, three main approaches have been used in different biological contexts: protein correlation profiling (PCP), localization of organelle proteins by isotope tagging (LOPIT) and dynamic organellar maps (Lundberg & Borner, 2019).

PCP resolves organelles on a sucrose gradient (Foster et al., 2006; Krahmer et al., 2018). Subsequently, about 20 fractions are analyzed by label-free quantification. Comparative PCP has been used to detect subcellular reorganization in a hepatic steatosis model of mouse liver cells under a high-fat diet (Krahmer et al., 2018). Subcellular localization for over 4000 proteins were mapped and profound organellar rearrangements were detected. For example, translocation analysis revealed that the secretory capacity of steatotic cells was impaired because the Golgi apparatus was adsorbed into lipid droplets. Tracking of organellar contact-site proteins enabled the detection of enhanced interactions between mitochondria and lipid droplets. Additionally, this work achieved phosphopeptide profiling for over 150 phosphorylated proteins in an organellar-context.

LOPIT conventionally resolves different subcellular niches by density gradient centrifugation (Mulvey et al., 2017) (recently, this method was also adapted for differential centrifugation (Geladaki et al., 2019)). Protein quantification is performed on 10 fractions per sample via tandem mass tags. LOPIT has been initially used for static cell maps, providing detailed inventories of embryonic mouse stem cells (Christoforou et al., 2016) and U2OS (Thul et al., 2017), but recently this methodology has also been applied to dynamic organellar mapping. For example, the LOPIT methodology has been applied to investigate LPS-induced changes in subcellular organization in a human leukemia cell line (THP-1 cells) (Mulvey et al., 2021). Proteins not previously associated with LPS-induced responses were found to redistribute after treatment and the functional consequences of these redistributions remain to be explored. An approach similar to LOPIT has been used by another group to track subcellular rearrangements induced by cytomegalovirus infection in fibroblasts (Jean Beltran et al., 2016). A time-course experiment tracked localization for over 4000 host proteins and 100 viral proteins, implicating the host's unconventional myosin MYO18A in viral replication.

In dynamic organellar maps, organelles are separated into 8 fractions by differential centrifugation (Itzhak et al., 2016). Quantification is achieved by metabolic labeling of cells with SILAC. In parallel to fractionation, a total membrane fraction is prepared from labelled cells, and is added to all other fractions, providing an internal reference for MS quantification. This methodology was optimized for label-free quantification, stable isotope labeling in cell culture and tandem mass tags (Itzhak et al., 2017). Initially, dynamic organellar maps were applied to investigate EGFR signaling in HeLa cells by analyzing these cells before and after EGF-induced cellular perturbation (Itzhak et al., 2016). Later the same experiment was performed on primary neurons and revealed numerous known and novel translocations associated with EGFR signaling (Itzhak et al., 2017). Since then, the method has also been applied to compare the spatial organization of wild-type and AP-4 deficient cells (Davies et al., 2018). AP-4 is part of endosomal vesicles of unknown function. Congenital genetic defects in AP-4 are characterized by intellectual disability and paraplegia. By applying spatial proteomics to AP-4 deficient cells, AP-4 vesicles were shown to participate in the cellular redistribution of a protein required for autophagosome biogenesis and neuronal function (ATG9). The

same approach elucidated the role of the AP-5 adaptor protein in endosomal-to-Golgi trafficking (Hirst et al., 2018).

1.6. Overview of work described in this thesis

The interplay between UVA-induced damage and cell fate is mediated by the cell's proteome. In this sense, protein function is fine-tuned through mechanisms involving modulation in levels of specific proteins, chemical modifications, as well as spatial and temporal reorganization. A few proteomics studies have evaluated the oxidative effects of UVA radiation on the skin. These works demonstrate that acute doses of UVA radiation (>20 J/cm²) modulate the DNA damage response as well as antioxidant, inflammatory, and apoptotic mechanisms (Gęgotek et al., 2018, 2019; Narzt et al., 2019; Radrezza et al., 2021). However, systems-level information on how non-cytotoxic doses of UVA drive changes in protein expression, subcellular localization and cell fate are lacking.

In this context, we investigated the effects of 6 J/cm² of UVA radiation on the proteome of human keratinocytes. In preliminary experiments, we tested two different doses of UVA (12 and 6 J/cm²) and opted for the lowest, because our work is explicitly focused on evaluating the effects of a non-cytotoxic dose of UVA radiation in cells and 12 J/cm² of UVA generate considerable levels of metabolic stress (loss of reductive power) (as shown in the MTT assay of **Fig. 12**).
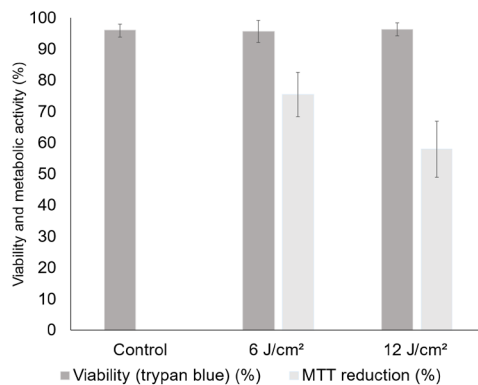
Fig. 12. Choice of UVA dose. MTT and trypan blue assays were used to evaluate the cellular viability of HaCaT cells under environmentally relevant UVA doses. Bars represent the mean, and error bars represent the standard deviation (n = 3). MTT reduction percentages were calculated relatively to controls (100%).

To investigate UVA's effects on human cells, we employed two *in vitro* models: primary normal human epidermal keratinocytes (NHEK), cultured as a monolayer and isolated from the skin of a healthy adult donor, and immortalized keratinocytes (HaCaT cells). HaCaT cells were used here as a pre-malignant model because they harbor UV-like mutations in p53, similar to the ones found in skin carcinomas and pre-malignant lesions (Ren et al., 2006). Importantly, a dose of 6 J/cm² of UVA radiation is relevant to routine exposure and equivalent to about 20 minutes of midday sun exposure (Halliday et al., 2011). By using a combination of mass spectrometry-based proteomics, bioinformatics, and conventional biochemical assays, we investigated:

1. The spatial subcellular remodeling of the proteome of human keratinocytes 30 minutes after UVA exposure.
2. Long-term changes in protein levels and secretion driven by UVA radiation in primary and pre-malignant human keratinocytes.

The following (second) chapter of this thesis was written in the form of a manuscript and addresses the spatial remodeling of keratinocytes under UVA exposure (first topic). In this work, we mapped the subcellular reorganization of the proteome of human keratinocytes in response to UVA radiation. Our workflow quantified and assigned subcellular localization for over 3000 proteins, of which about 600 were found to redistribute upon UVA exposure. Mitochondria were identified as the main target of UVA-induced stress. Further investigation demonstrated that mitochondrial fragmentation, up-regulation of redox-responsive proteins, and DNA damage drive protein redistribution. This manuscript was submitted to iScience.

The third chapter of this thesis was also written in the form of a manuscript and addresses long-term responses of keratinocytes to UVA-induced stress (second topic). Analysis of protein levels and secretion was conducted to derive the phenotypic signature induced by a low dose of the UVA component of the sunlight in primary human keratinocytes 24 h and 7 days after irradiation. Our results indicate that upon exposure to UVA-irradiation, keratinocytes enter senescence and elicit paracrine responses in neighboring pre-malignant cells via inflammatory mediators. We also investigated the differential sensitivity of NHEK and HaCaT cells to the radiation, demonstrating that HaCaT cells tend to be more resilient to UVA-induced stress, even though they are

susceptible to paracrine effects. This work has been published in Scientific Reports (doi.org/10.1038/s41598-021-02658-5).

CHAPTER 2 – Spatial proteomics reveals profound subcellular reorganization in human keratinocytes exposed to UVA radiation

2.1. Introduction

Ultraviolet-A (UVA) radiation (315–400 nm) constitutes about 95% of all ultraviolet radiation (UVR) that reaches the Earth (Schuch et al., 2017). The causal association between UVR exposure and skin cancer is well established, but epidemiology has little capacity to distinguish between the carcinogenic effects of UVA and UVB (El Ghissassi et al., 2009). At the molecular level, the effects of UVA and UVB in skin cells are of different natures, suggesting that each wavelength range defines a different path towards malignant transformation (Ridley et al., 2009).

For example, UVB is absorbed by pyrimidines, giving rise to cyclobutane pyrimidine dimers (CPD) and pyrimidine (6-4) pyrimidone photoproducts. Thus, UVB's carcinogenic action depends on the direct generation of mutagenic DNA lesions. On the other hand, UVA photons are poorly absorbed by the DNA, being more relevantly absorbed by other cellular chromophores (Ikehata, 2018). In this sense, UVA relies on the generation of photoexcited species, such as singlet oxygen, that may lead to oxidative damage (Wondrak et al., 2006).

Skin cells orchestrate complex responses to light stress, coordinating gene expression, metabolism and protein function (Chen et al., 2014). Protein function is fine-tuned in a sophisticated manner, involving modulations in abundance, chemical modifications, and spatial and temporal delimitations (Thul et al., 2017). Mutational dynamics is the primary driver of carcinogenesis. However, modulation of metabolism and protein function can contribute to this process by impacting signaling, organelle interactions and cell fate decisions towards apoptosis, senescence or malignant transformation (de Gruijl et al., 2001; El Ghissassi et al., 2009).

Even though the effects of UVR on DNA modification (Moreno et al., 2020), gene expression (He et al., 2004), protein expression (Edifizi et al., 2017) and post-

translational modifications (Elia et al., 2015; Zhou et al., 2016) have been investigated, information about how specific UVR components shape the subcellular organization of proteins in cells is still lacking. Advances in high-throughput mass spectrometry (Breker and Schuldiner, 2014; Larance and Lamond, 2015) and microscopy (Mattiazzi Usaj et al., 2016; Thul et al., 2017) and machine learning applications for these techniques (Gatto et al., 2014a; Lundberg and Borner, 2019) allow proteome-wide investigations into subcellular localization dynamics and organellar communication in cells under stress. Spatial or organellar proteomics workflows may combine cell fractionation with mass spectrometry to characterize changes in protein levels in multiple subcellular niches (Lundberg and Borner, 2019). Indeed, methods such as Protein Correlation Profiling (PCP) (Andersen et al., 2003; Foster et al., 2006) and Hyperplexed Localisation of Organelle Proteins by Isotope Tagging (LOPIT) (Geladaki et al., 2019; Mulvey et al., 2017) and other organellar mapping approaches (Itzhak et al., 2017; Jean Beltran et al., 2016) have been developed to monitor protein dynamics over space in an unbiased manner.

The principle behind these methodologies is to quantify the distribution of proteins across subcellular fractions under different biological conditions. The fractionation profiles of proteins reflect the complexity of subcellular localization better than the presence or absence in a single purified fraction. Thus, they are used as an input for learning algorithms, allowing the prediction and classification of subcellular localization. Recently, a machine learning pipeline predicted translocation events between subcellular niches by comparing fractionation profiles under different biological conditions (Kennedy et al., 2020).

In light of these advances, we used spatial proteomics coupled with machine learning techniques to systematically analyze the subcellular reorganization of the proteome of skin cells in response to UVA radiation. Our results show that a low UVA dose, equivalent to about 20 minutes of equatorial, midday sun exposure (Halliday and Rana, 2008), leads to a profound spatial remodeling of the skin cells' proteome. We found that the spatial stress response relies on changes in mitochondrial dynamics, nucleocytoplasmic translocations triggered by DNA damage, and protein degradation. Furthermore, our results provide a resource for further investigations of UVA-triggered protein dynamic events.

2.2. Results

2.2.1. Workflow used to investigate proteome remodeling in cells under UVA stress

An overview of the experimental protocol is shown in **Fig. 1A**. In the experimental pipeline, HaCaT skin cells were exposed to a non-cytotoxic low dose of UVA radiation (6 J/cm², using a simulator of the solar UVA spectrum) or kept in the dark under the same environmental conditions. Thirty minutes after exposure, mock-treated and UVA-exposed cells were collected, the plasma membranes were lysed in hypoosmotic solution, and the organelles were separated by differential centrifugation. We chose to evaluate keratinocyte's response 30 minutes after irradiation to account for possible early signaling events triggered by cellular stress. Fractions were collected after each centrifugation step, and proteins were quantified in each fraction by conventional label-free mass spectrometry. A total of 5351 protein groups were identified and quantified in 90 samples, comprising nine fractions for each of the five biological replicates of each condition. The dataset was filtered for proteins with label-free quantifications (LFQ) of greater than zero in at least one-third of all samples, yielding a matrix of 3287 protein groups. Then, the LFQ data of each proteins was scaled to a range between 0 and 1 for each subcellular map (the LFQ data is shown in **Spreadsheet S1** on **APPENDIX 1** and scaled LFQ data is shown in **Spreadsheet S2** on **APPENDIX 1**). This step was performed to exclude proteins that were very irregularly quantified across replicates and fractions. The missing values of the dataset were imputed as 0, but the use of more sophisticated methods of imputation or quantitative isobaric labeling of the samples for MS acquisition could decrease incorporation of errors into the analysis and lead to the curation of a more stringent list of possible translocation targets. Thus, this is a limitation of our work.

Next, to assess if the dataset's structure reflected subcellular localization, we used three complementary approaches to inspect data quality, predict subcellular localization and infer protein dynamic events. First, we used t-SNE as a dimensionality reduction method

overlaid with different databases (Uniprot, Gene Ontology and Cell Atlas) to inspect cluster formation. Second, we used a neural network algorithm to assess if subcellular localization could be predicted accurately by learning the fractionation patterns of organellar markers with well-established localization. Lastly, after validating the dataset's structure, we used the Translocation Analysis of Spatial Proteomics (TRANSPIRE) computational pipeline (Kennedy et al., 2020), which is based on a gaussian process classifier, to investigate changes in the subcellular landscape induced by UVA radiation in human keratinocytes. An overview of the computational workflow is presented in **Fig. 1B**. The results obtained by TRANSPIRE were further validated by conventional biochemical assays (**Fig. 1C**).
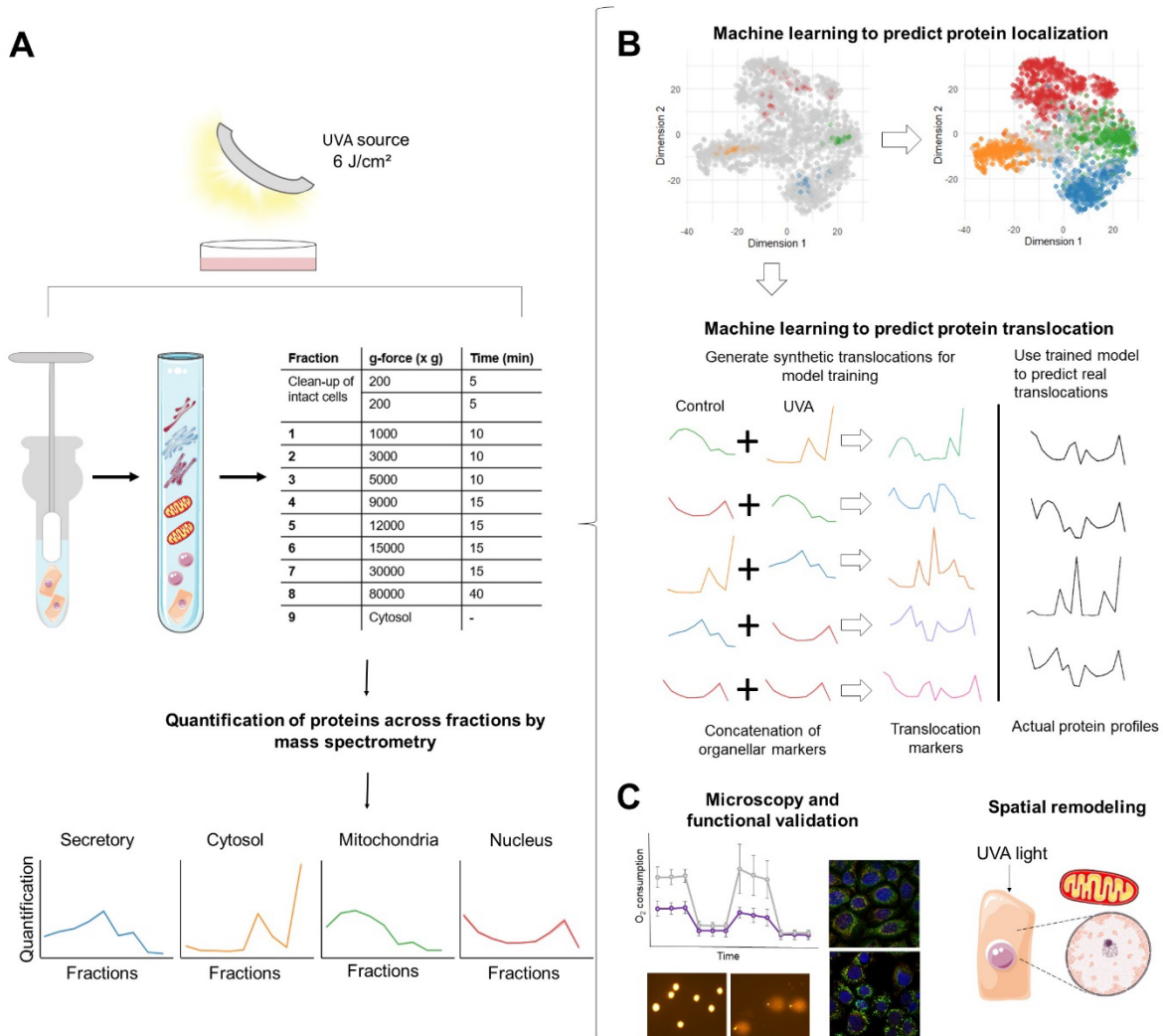
Fig. 1. Proteomic approach to define spatial changes in protein distribution upon stress. **(A)** Experimental protocol. **(B)** Computational pipelines used to define changes in subcellular

organization promoted by 6 J/cm² of UVA radiation 30 minutes after exposure in HaCaT cells. **(C)** Validation of results using traditional biochemical assays.

2.2.2. Validating the resolving power of the fractionation method

Following our workflow, we first inspected the t-SNE plot generated from the filtered dataset to reduce dimensionality and detect the presence of clusters. The plot revealed the presence of four main clusters in distinct regions (**Fig. S1A** on **APPENDIX 1**). When overlaid with the subcellular localization data from three different databases (Uniprot, Cell Atlas and Gene Ontology), we found that the four clusters represented four distinct subcellular environments: the nucleus, cytosol, mitochondria, and secretory organelles (**Fig. S1A** on **APPENDIX 1**). The database classifications were binned such that secretory organelles included proteins from the ER, peroxisome, Golgi, lysosome and plasma membrane. Additionally, hierarchical clustering was also performed on the data and revealed the presence of clusters enriched for different subcellular compartments (mainly nucleus, mitochondria, cytosol and membrane parts) (**Fig. S1B-C** on **APPENDIX 1**).

Since this analysis showed that the fractionation scheme provides the resolution necessary for differentiating these four main subcellular compartments, we curated organellar markers for each compartment to investigate if protein localization could be predicted based on the fractionation scheme. The Uniprot and Gene Ontology classifications of subcellular localization were used for curating the organellar markers. Thus, for a protein to be considered an organellar marker, it had to be classified in both databases as uniquely pertaining to one subcellular niche among the four compartments (i.e., cytosol, nucleus, mitochondria and secretory) established through dimensionality reduction. The fractionation profiles of uniquely localized proteins were then manually inspected to assure that the markers were reproducibly quantified. Proteins containing zeros were kept in as markers only if these values were reproducible across replicates in our experiment. We inspected the fractionation profiles manually to assure this conditions.

Based on these criteria, 247 organellar markers were curated into four subcellular niches: the cytosol (64), nucleus (75), mitochondria (60), and secretory organelles (48). The entire list of organellar markers used in this study is shown in **Spreadsheet S3** on **APPENDIX 1**. Fractionation profiles of markers from different compartments present characteristic shapes, demonstrating that proteins from the same subcellular niche tend to fractionate similarly (profile plots, **Fig. 2A**). The t-SNE supports the patterns observed in the profile plots, showing that organellar markers from different compartments cluster in separate plot regions, while markers of the same compartment cluster similarly (**Fig. 2B**).

Following this analysis, a neural networks algorithm implemented in pRoloc (Gatto et al., 2014b), utilizing references of each compartment the fractionation profiles of curated organellar markers, classified proteins into four discrete subcellular compartments. The results of this classification is shown in **Spreadsheet S4** on **APPENDIX 1.** To assess the reproducibility of prediction across replicates, we applied the algorithm to each of the five biological replicates of each condition separately. **Fig. 2C** contains the t-SNE plot representing the most frequent classification of each protein across the five replicates. All of the 3287 protein groups were classified into four subcellular niches: the cytosol (623 ± 47 proteins, considering the mean and standard deviation across replicates), nucleus (640 ± 144), mitochondria (1293 ± 179), and secretory organelles (707 ± 183), with slight differences for the total number of classifications between conditions (**Fig. 2D**). Classifications were highly reproducible, with 80 and 85% of all proteins in the treated and control samples, respectively, receiving the same classification in at least 3 out of 5 biological replicates (**Fig. 2E**). The cellular compartment classification obtained for each replicate was then compared to the GO classification. The results revealed that the neural networks algorithm achieved a mean prediction accuracy of 75% in control samples and 73% in treated samples (**Fig. 2F**). All classifications obtained from the machine learning algorithm are accompanied by classification probability scores that reflect the reliability of the assignment. In this context, low scores are often associated with profiles not directly modeled by the organellar markers used in the algorithm (e.g., multilocalized proteins) (Jean Beltran et al., 2016).
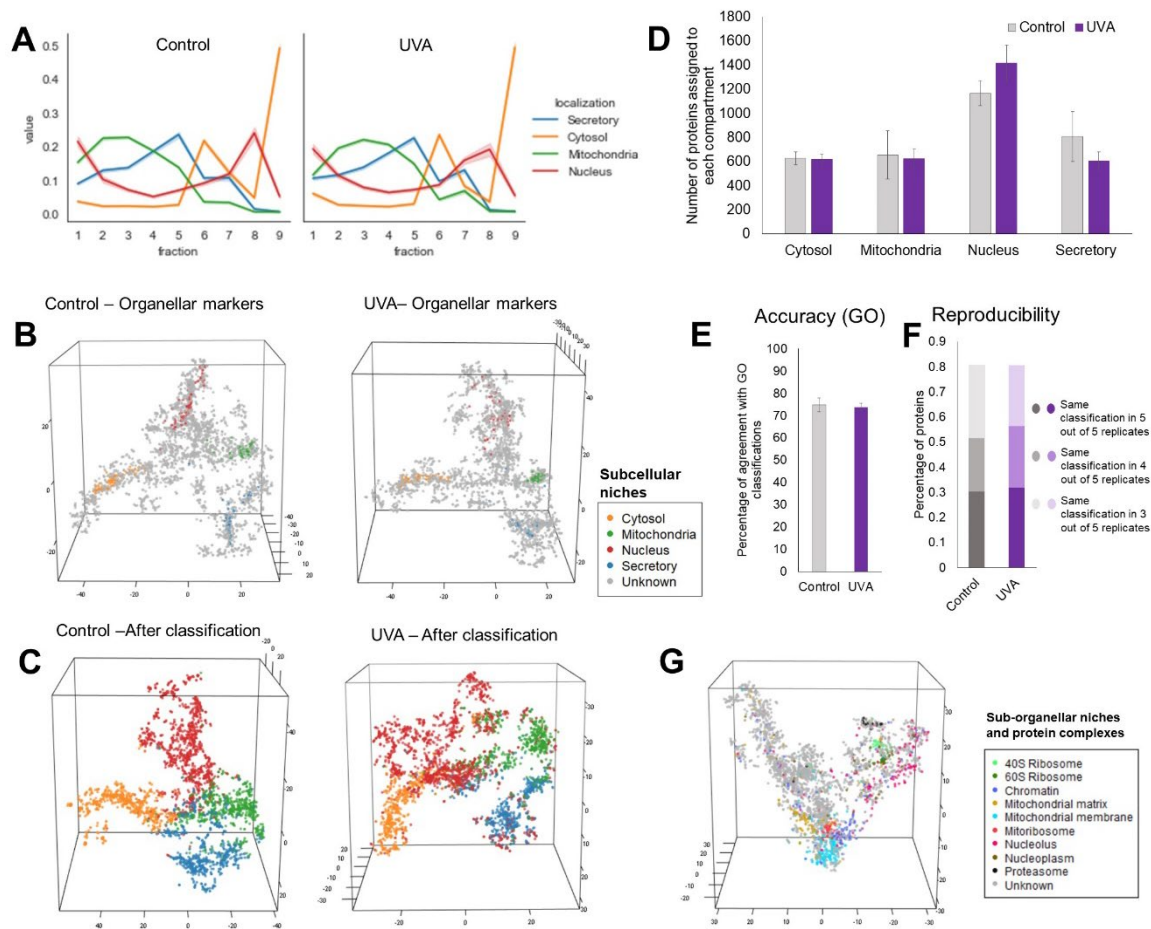
Fig. 2. Identification of subcellular patterns in HaCaT's spatial proteomics dataset. (A) Profile plots of organellar markers in the HaCaT dataset. Shadowed intervals represent standard errors, and values represent means. Five biological replicates per group were employed for the spatial proteomics experiment. **(B)** 3D representation of subcellular fractionation data using t-SNE. The maps were overlaid with organellar markers. **(C)** t-SNE plots of all control and irradiated samples overlaid with the most frequent classifications obtained for each protein across replicates using the neural network algorithm for predicting localization. **(D)** Numbers of proteins assigned to the cytosol, mitochondria nucleus and secretory organelles by condition. Bars represent the mean number of proteins assigned to each compartment, and error bars represent the standard deviation. **(E)** Reproducibility of classifications across replicates. Bars represent the percentage of proteins that received the same classification in 3, 4 or 5 biological replicates out of the total 5. **(F)** Accuracy of the neural network predictions obtained by comparing the predicted subcellular localizations with Gene Ontology information. Bars represent means per condition, and error bars represent standard deviations. **(G)** t-SNE plots overlaid with sub-organellar markers and colocalizing protein complexes.

In addition, we analyzed if the dataset could provide sub-organellar resolution by overlaying the t-SNE plot with markers of sub-organellar compartments (obtained from Uniprot, Cell Atlas and Gene Ontology). The results indicate a partial divide between the mitochondrial matrix, membrane and nuclear subniches, such as the nucleolus, nucleoplasm, and chromatin clusters (**Fig. 2G**). Moreover, the t-SNE plot also reveals that specific protein complexes colocalize *in vivo*. For example, our dataset's clustering of the heavy and light ribosome subunits and the proteasome supports the notion that the fractionation preserves the colocalization of interaction networks.

Altogether, these results indicate that the dataset is structured in a way that is dependent on subcellular localization, considering compartments delimited by membranes (i.e., organelles) and compartments delimited by protein complex formation (i.e., the nucleolus and the proteasome). This analysis provides a comprehensive investigation of HaCaT subcellular organization of the proteome, allowing for inferences about UVA-induced protein dynamic events.

2.2.3. UVA radiation elicits extensive changes in the subcellular distribution of proteins

Next, we used the recently developed TRANSPIRE pipeline (Kennedy et al., 2020) to predict UVA-triggered protein dynamic events in the spatial proteomics dataset. This pipeline creates synthetic translocation classes from organellar markers, trains a Gaussian process classifier based on the synthetic translocation classes and predicts translocations in the actual dataset. The basis of this approach relies on first concatenating the organellar markers between the different biological conditions to produce synthetic markers. Then the synthetic markers are further clustered to provide different translocation and non-translocation classes, allowing the algorithm to predict the directionality of protein trafficking across subcellular niches.

The algorithm performs all possible combinations of organellar markers between conditions to generate synthetic translocations of different classes. In this sense, "Nucleus to Cytosol" and "Mitochondria to Mitochondria" would represent two different classes. Thus, the algorithm's output consists of the translocation classes attributed to each protein and translocation scores, calculated as described by (Kennedy et al.,

2020). False-positive rates (FPR) were calculated based on the learning model, and a 0.5% FPR threshold was applied to define a true translocation event.

Importantly, changes in the fractionation profile may reflect diverse protein dynamic events, such as translocations (Itzhak et al., 2017), altered organellar dynamics (Jean Beltran et al., 2016), or possibly altered rates of synthesis and degradation of proteins within specific subcellular niches (Kennedy et al., 2020). Learning algorithms applied to spatial proteomics present limitations in differentiating among these events since they only classify proteins according to translocation classes (Jean Beltran et al., 2016; Lundberg and Borner, 2019). Here we used the TRANSPIRE algorithm to detect potential dynamic events triggered by UVA radiation in HaCaT cells. Subsequently, we validated a few of these targets using a microscopy-based approach, further characterizing the dynamic event.

As shown in **Fig. 3A**, training was achieved by maximizing the evidence lower bound (ELBO) using the Adam optimizer of the TRANSPIRE pipeline. As we can also see, the classifier achieved a high level of accuracy during training, reaching values above 90% (the metrics obtained for hyperparameter tuning are shown in **Fig S3A** of **APPENDIX 1,** the performance of the algorithm in the training set is shown in **Fig S3B** of **APPENDIX 1** and the performance of the algorithm in the test set is shown in **Fig S3C** of **APPENDIX 1**). The F1 metric used to evaluate the model performance ranges from 0 to 1 and our algorithm reaches values > 0.9.

Using this model, we identified 614 possible targets of dynamic events (FPR 0.5%) altogether. The entire TRANSPIRE analysis is shown in **Spreadsheet S5** on **APPENDIX 1.** We tested different FPR thresholds and observed that for an FPR lower than 0.5% the number of dynamic events remained relatively constant (**Fig. S1D** on **APPENDIX 1**) and **Fig. S3D** on **APPENDIX 1** shows false positive rates across the translocation scores. The number of proteins assigned to each translocation class is shown in **Fig 3B**. By aligning the translocation classes attributed by the algorithm in a circular plot (**Fig. 3C**), it is possible to see that they are not equally distributed across the four subcellular niches. Indeed the efflux is more intense for mitochondria and secretory organelles than for other compartments. This observation possibly reflects the crucial role secretory organelles play in protein trafficking between different subcellular niches.

Translocating proteins are significantly enriched for biological processes related to cellular localization ("cellular localization", "establishment of localization in cell', "cellular component organization") and mitochondrial translation ("mitochondrial translation elongation", "mitochondrial translation termination") (**Fig. 3D**). The GO terms for the cellular compartment indicate that translocating proteins are mainly cytosolic and mitochondrial, reinforcing the possible role of mitochondria in UVA-induced damage.

Further evaluation of the 12 highest scoring translocating proteins revealed that five (MAP2K3, PARP4, YTHDF2, OAS1 and RNF114) were reported to be multilocalized according to the GO and Uniprot classifications (**Fig. 3E**). Previously, MAP2K3, RPS6KA4 and CLDN7 were reported to be UV-responsive (Brzoska and Szumiel, 2008; Craxton et al., 2018; Hintsala et al., 2013; Remy et al., 2010). Notably, MAP2K3, a protein responsible for activating the p38-MAPK signaling and one of the most significant pathways involved in the response against UV-induced stress in human cells, had the highest score (Hildesheim et al., 2004).
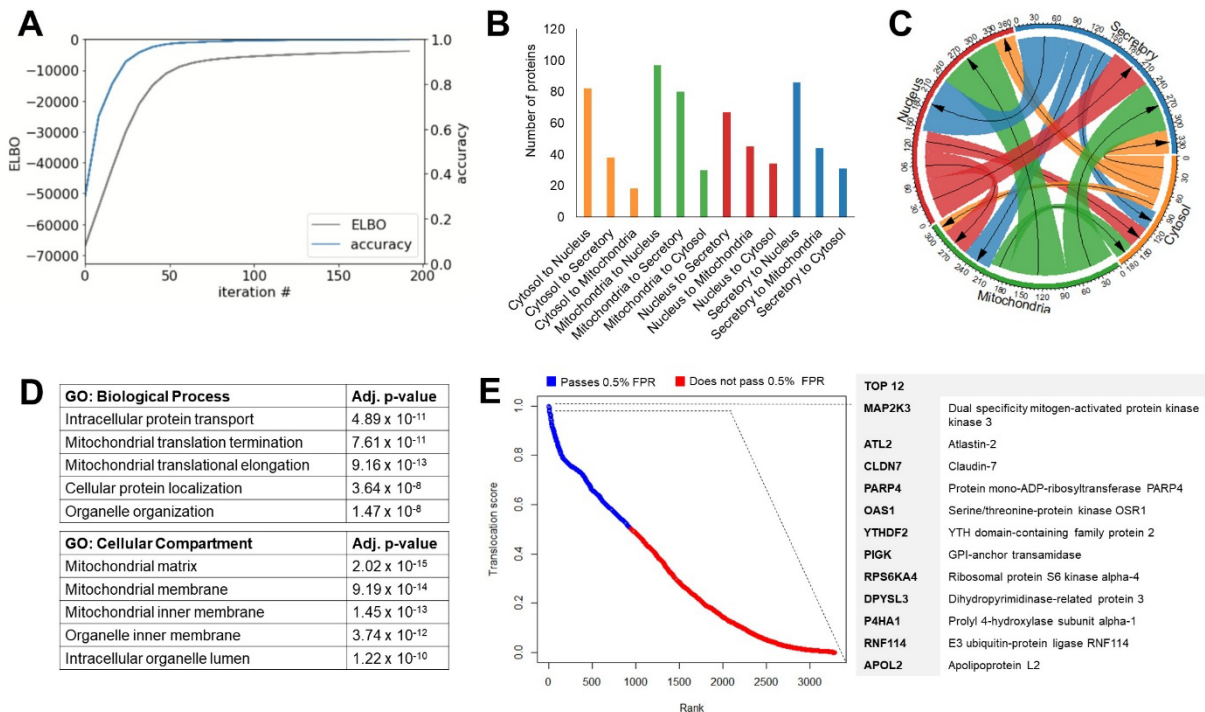
Fig. 3. Prediction of UVA-induced translocations in HaCaT cells (6 J/cm², 30 minutes after irradiation). (A) Accuracy and Evidence Lower Bounds (ELBO) obtained for the classifier during training. **(B)** Number of proteins of each translocation class assigned by the algorithm. **(C)** Circular plot representing UVA-induced translocations between subcellular niches as identified by the classifier. **(D)** Enrichment analysis of the translocation targets based on Gene Ontology

terms. **(E)** Rank order plot of the translocation scores obtained for each protein by the machine learning modeling. The top 12 highest scoring proteins are highlighted in a table to the right of the rank order plot.

Considering that nucleocytoplasmic and mitochondrial translocations were some of the most frequent types of events predicted by the algorithm and are unequivocally relevant to UVA's biological action, we explored these processes in more depth, validating some translocation targets involved in the response of keratinocytes to DNA damage and UVA-induced metabolic stress.

2.2.4. Spatial remodeling provides clues about UVA's oxidative action

We first focused on curating the translocation labels predicted by the algorithm using GO classifications and a review of the literature to validate specific UVA-triggered dynamic events between the cytoplasm and nucleus. The algorithm identified a total of 100 proteins that would possibly translocate between the cytosol and the nucleus, considering a 0.5% false-positive rate. The localization prediction of each protein in the control cells was compared to the respective GO classification to achieve a more stringent list of targets. We only kept proteins with concordant classifications for further analysis, which resulted in 67 out of the initial 100 proteins. Then, a literature review was performed to identify targets for which nucleocytoplasmic dynamic events had been previously identified, or at least for which dual nuclear-cytoplasmic localization and functions were previously reported. A total of 25 proteins fulfilled both conditions. These targets and their respective translocation scores are provided in **Table S1** on **APPENDIX 1**.

The 25 protein targets play diverse biological roles. While some are transcription factors, others participate in nuclear cytoskeleton remodeling, signaling pathways and RNA processing. Nucleocytoplasmic dynamic events induced by DNA damage have been previously reported for UBL4A (Krenciute et al., 2013), CETN2 (Nishi et al., 2005; Trojan et al., 2008, p. 2), FAF1 (Franz et al., 2016, p. 1), CTBP1 (Verger et al., 2006, p. 1), RELA (Wan and Lenardo, 2010), NFKB1 (Wan and Lenardo, 2010), CIAO2B (Ito et al., 2010) and CSNK2 (Filhol et al., 1992). Moreover, three proteins (CIAO2B (Ito et al., 2010), CETN2 (Nishi et al., 2005) and CSNK2 (Montenarh, 2016)) have been shown to interact with nucleotide-excision repair (NER) components, which are involved in

recognizing and repairing cyclobutane pyrimidine dimers (CPD) generated as a consequence of UVR exposure.

The β subunit of CSNK2 (CSNK2B), one of the possible translocation targets predicted by the TRANSPIRE algorithms, was first previously reported to be implicated in the DNA damage response through its interaction with the tumor suppressor p53 (Filhol et al., 1992). CSNK2 is also involved in the phosphorylation of two NER components (XPB, CETN2) (Coin et al., 2004; Grecu and Assairi, 2014). Additionally, it has been demonstrated that XPC- and XPD-deficient cells expressing higher levels of CSNK2B are more resistant to UV-induced death (Teitz et al., 1990), especially since increases in CSNK2B lead to dramatic increases in CSNK2 activity (Cochet and Chambaz, 1983). In our experiment, CSNK2B shifts from a central position in the cytosolic cluster in controls to the interface between the cytosolic and nuclear clusters in irradiated samples (**Fig. 4A**). This behavior is consistent with a significant difference between groups observed for this protein in the profile plot, especially in the last fraction that is enriched with cytosolic proteins (**Fig. 4B**). Redistribution of CSNK2B from the cytoplasm to the nucleus upon irradiation was corroborated by immunofluorescence, indicating that UVA exposure leads to the translocation of cytosolic CSNK2B to the nucleus (**Fig. 4C**).

To confirm that our irradiation conditions generated significant levels of DNA damage, we performed a modified version of the comet assay to detect different types of DNA lesions in cells following exposure to 6 J/cm² of UVA radiation (**Fig. 4D**). The comet assay was modified through the addition of formamidopyrimidine-DNA glycosylase (FPG), endonuclease V (endoV) and endonuclease III (endoIII) to detect oxidized pyrimidines, CPD and oxidized purines, respectively. The predominant types of lesions generated immediately after exposure to UVA are CPD and oxidized purines, in agreement with what has been previously described for this radiation dose (Delinasios et al., 2018). However, while oxidized purines seem to be efficiently removed from the DNA one hour after exposure to the radiation, CPD is more slowly repaired and persists in HaCaT cells for at least four hours after irradiation. The DNA lesion profile identified here and its repair kinetics are consistent with NER activation, and thus consistent with triggering of translocation events associated to this pathway. Even though UVA generates lower levels of CPD than UVB, CPD generation can still promote CSNK2B recruitment to the nucleus.
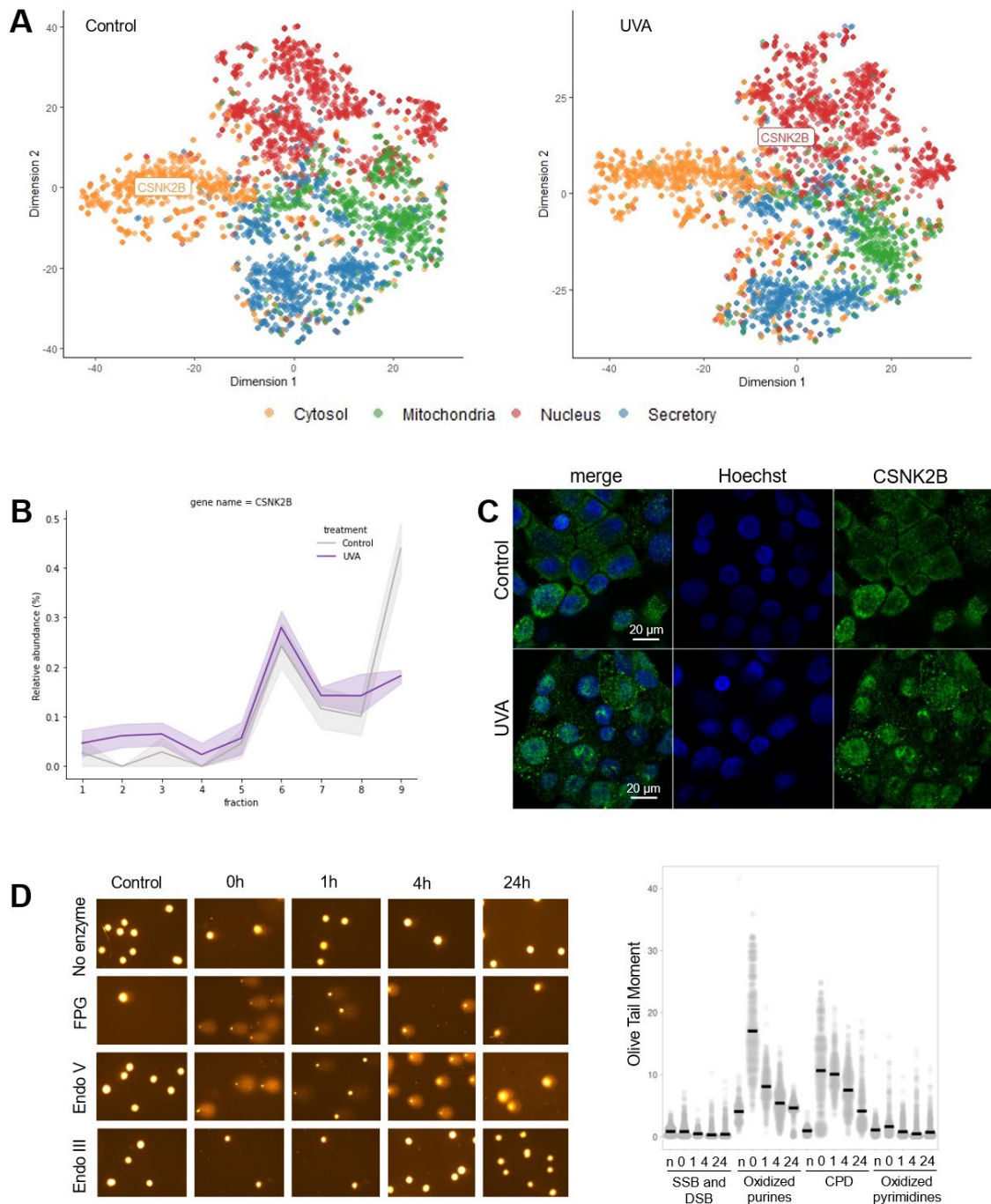
Fig. 4. CSNK2B translocates to the nucleus upon DNA damage induced 30 minutes after exposure to 6 J/cm² of UVA. (A) 2D t-SNE plots representing the migration of CSNK2B from the cytosolic cluster in control samples to the nuclear cluster in UVA-irradiated cells. Colors represent the translocations predicted by the classifier (organelle of origin in controls and destination in UVA plot). **(B)** Profile plot obtained for CSKN2B in controls and irradiated samples. Lines represent the means of relative abundance, and shadowed intervals represent the

standard errors. **(C)** Representative immunofluorescence images showing CSNK2B translocation from the cytosol to the nucleus after exposing HaCaT cells to UVA radiation. CSNK2B was immunostained (green), and the nucleus was stained with Hoechst (blue). Three independent replicates per group were analyzed. **(D)** Comet assay results for control and irradiated cells. Representative images of randomly scored comets in slides from all conditions are represented on the left. The graph shows the semi-quantification of each type of DNA damage over time. Points represent Olive Tail Moments scored for all measured cells, and black bars represent the medians of all points (n = 4 independent experiments).

The algorithm also predicted the movement of two NF-κB subunits (RELA and NFKB1). The RELA subunit contains the transactivation domain, responsible for the transcription factor function (Wan and Lenardo, 2010), and we chose this subunit for further validation by confocal microscopy (see below). In our spatial proteomics experiment, RELA of non-irradiated samples presents a typical cytosolic fractionation pattern, with peaks in the 6th and last fractions. However, upon irradiation, we observe a decrease in abundance in the 6th fraction and an increase in the 3rd fraction (**Fig. 5A**). Changes between conditions can also be observed in the t-SNE plots (**Fig. 5B**). Importantly, RELA is in the center of the cytoplasmic cluster in the control samples but shifts to the interface between the cytoplasmic and nuclear clusters following irradiation. To investigate NF-κB dynamics further, we immunolabeled the RELA subunit and performed immunofluorescence (IF) microscopy. Immunolabeling of the RELA subunit revealed a reduction in the overall levels of this transcription factor (**Fig. 5C**), which seems to be consistent with the attenuated abundance observed in the 6th fraction of irradiated cells. In control cells, RELA is present throughout the entire cytoplasm. However, in irradiated cells, RELA labeling weakens, assuming punctate structures and possibly reflecting the cellular compartmentalization of protein degradation. Previous studies addressing functional aspects of NF-κB in HaCaT cells exposed to UVA radiation revealed contradictory roles for this protein in this type of stress response (Djavaheri-Mergny et al., 1999; Saliou et al., 1999; Vile et al., 1995). It was reported that UVA doses lower than 1 J/cm² induce NF-κB activation, while higher doses lead to decreased NF-κB levels (Tebbe et al., 2001). Moreover, in agreement with our results, UVA radiation has been previously described to induce NF-κB degradation in human keratinocytes (Djavaheri-Mergny et al., 1999). In this context, deuterated water enhanced UVA-induced NF-κB degradation and low concentrations of sodium azide abolished this effect (Djavaheri-Mergny et al., 1999).

Importantly, since deuterated water prolongs the half-life of singlet oxygen and sodium azide is a singlet oxygen quencher, UVA-induced NF-κB degradation has been mainly attributed to singlet oxygen generation.
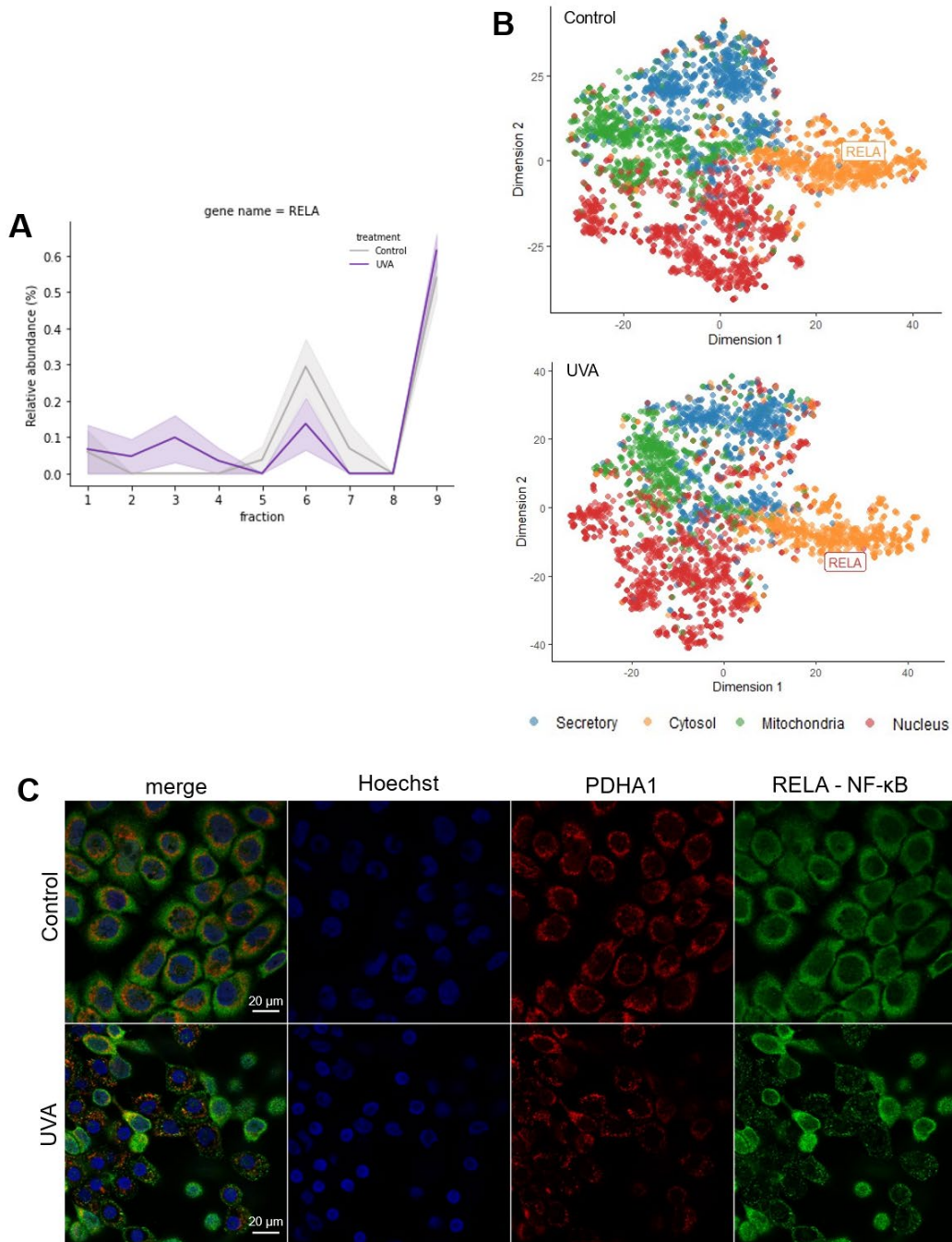
Fig. 5. UVA radiation induces NF-κB RELA subunit degradation (6 J/cm² of radiation, 30 minutes after exposure). (A) Profile plots obtained for RELA in controls and irradiated samples. Lines represent the means of relative abundance, and shadowed intervals represent the

standard errors. **(B)** 2D t-SNE plots representing the migration of RELA from the cytosolic cluster in control samples to the interface between the cytosolic and nuclear clusters in UVA-irradiated cells. Colors represent the translocations predicted by the classifier (organelle of origin in controls and destination in UVA plot). **(C)** Immunostaining of NF-κB RELA subunit (green) in control and UVA-irradiated samples. The nucleus was stained with Hoechst (blue). Mitochondria were stained by immunolabeling of pyruvate dehydrogenase (PDHA1, red). n = 3 independent biological replicates.

2.2.5. UVA radiation promotes metabolic stress through mitochondrial fragmentation

Since mitochondrial proteins have been detected as the significant pool of translocating targets, we investigated and validated the role of the spatial reorganization of mitochondrial components in the response against UVA-induced stress. Interestingly, most of the mitochondrial proteins classified as translocating are structural and uniquely localized to the mitochondria. These proteins are not usually involved in translocations across different subcellular niches. Examples include mitoribosomal subunits and electron transport chain components (**Fig. 6A**). We hypothesized that alterations in the fractionation profiling of these proteins between conditions might represent alterations in mitochondrial morphology and not necessarily translocations. Thus, we immunolabeled a respiratory chain component (COX4I1) and performed an IF experiment. As shown in **Fig. 6B**, in controls, COX4I1 displays the typical tubular appearance of the mitochondrial network and forms punctate structures in irradiated samples, a sign of UVA-induced mitochondrial fragmentation. Additionally, when we look at the fractionation profiles of structural mitochondrial proteins, including COX4I1, we observe a small shift between biological conditions (**Fig. 7C**). Even though the shift is subtle, it is consistent among many structural proteins, which suggests that mitochondrial fragmentation provokes a change in the fractionation profile of mitochondrial proteins.

Fig. 6. UVA radiation (6 J/cm²) induces changes in mitochondrial morphology in HaCaT cells 30 minutes after exposure and these changes are associated with altered fractionation profiles. (A) String network of proteins that the learning classifier identified as translocating from the mitochondria to other compartments in response to UVA. Nodes represent proteins, and the edges represent physical interactions between proteins. ETC = electron

transport chain **(B)** Immunostaining of COX4I1 (green). The nucleus was stained with Hoechst (blue). Two biologically independent experiments were performed, with similar results obtained.

Besides detecting changes in the fractionation profile of structural mitochondrial proteins, the TRANSPIRE algorithm also detected the movement of some proteins that have been previously described as migrating from the mitochondria to the nucleus. Thus, to determine if changes in the fractionation profiling of non-structural mitochondrial proteins predicted as translocations also reflect mitochondria fragmentation, we validated the spatial redistribution of fumarase (FH) and ornithine aminotransferase (OAT) in irradiated cells. Notably, both FH and OAT have been reported to translocate from the mitochondria to the nucleus (Wang et al., 2007; Yogev et al., 2010). We also monitored PDHA1 in the same experiment to check for colocalization of structural and non-structural mitochondrial proteins. The results showed that both FH and OAT display similar migration patterns in the t-SNE, shifting from the interface between the mitochondrial and nuclear clusters in control cells to the interface between the mitochondrial and cytosolic clusters in treated cells (**Fig. 7A**). Thus, both proteins display decreasing levels in the first fractions (1-3) of irradiated samples compared to control samples, accompanied by increased levels in the last fraction (**Fig. 7B**). Immunofluorescence images confirmed the same mitochondrial fragmentation phenomenon observed for labeling structural mitochondrial proteins (COX4I1 and PDHA1), reinforcing our previous results (**Fig. 7C-D**).
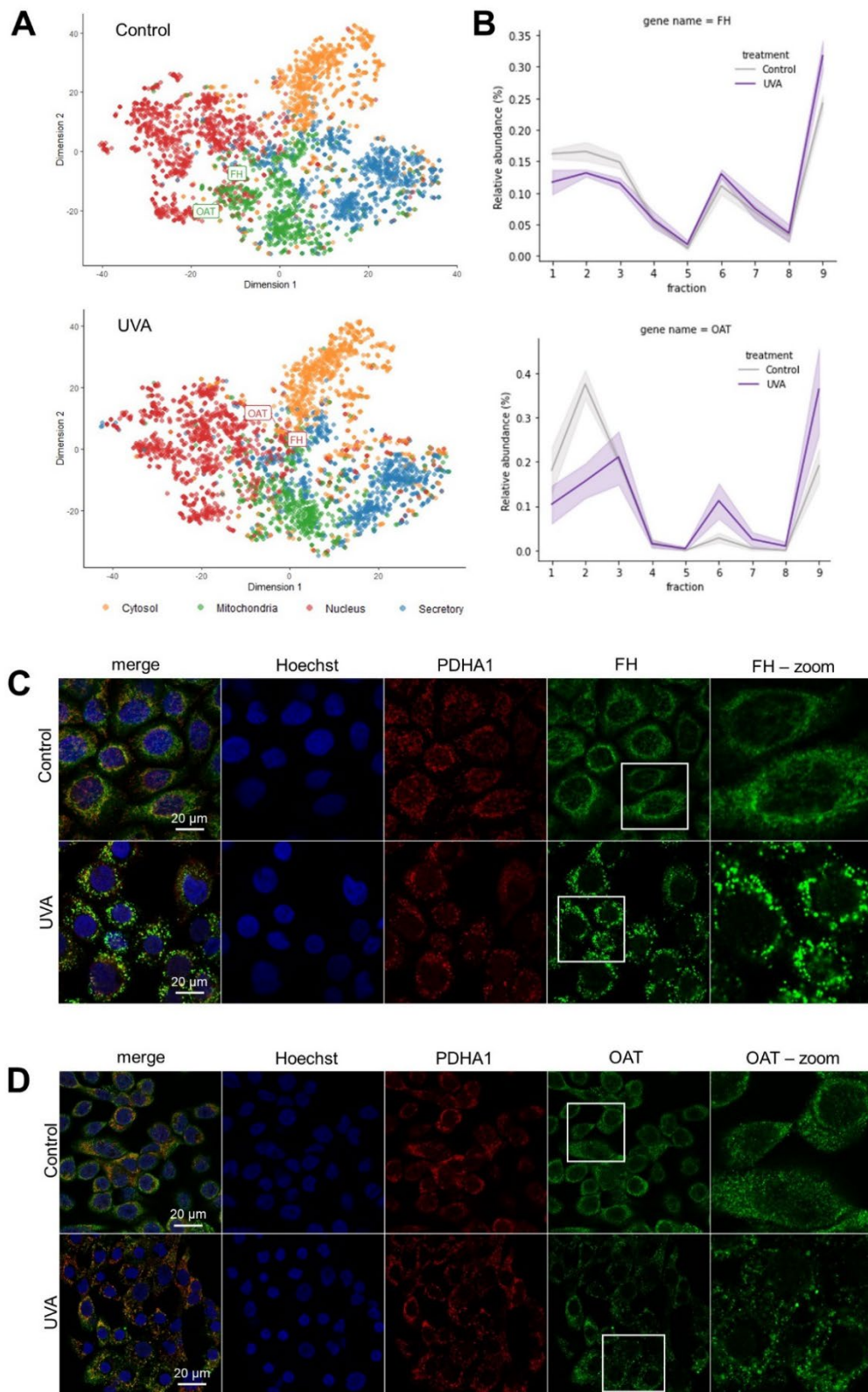
Fig. 7. Changes in the fractionation profiles of proteins from the mitochondrial matrix in UVA-exposed cells compared to controls reflect mitochondrial fragmentation (6 J/cm² of radiation, 30 minutes after exposure).

(A) t-SNE plots representing the migration of FH and OAT from the mitochondrial cluster in control samples to the nuclear cluster in UVA-irradiated cells. Colors represent the translocations predicted by the classifier (organelle of origin in controls and destination in UVA plot). **(B)** Profile plots obtained for FH and OAT in control and irradiated samples. Lines represent the means of relative abundance, and shadowed intervals represent standard errors. **(C)** Immunostaining of FH (green) in HaCaT cells exposed to UVA or mock-treated. PDHA1 (red) was immunolabeled as a structural mitochondrial marker. The nucleus was stained with Hoechst (blue). Three independent experiments were performed, and similar results were obtained. **(D)** Immunostaining of OAT (green) in HaCaT cells exposed to UVA or mock-treated. Similarly, PDHA1 (red) was used as a mitochondrial marker, and the nucleus was stained with Hoechst (blue). Three independent experiments were performed, and similar results were obtained.

Since cells displaying fragmented mitochondria usually have a reduced respiratory capacity (Sabouny and Shutt, 2020), we measured oxygen consumption rates in HaCaT cells exposed to UVA radiation using a Seahorse Analyzer XF24 to validate the functional impact of mitochondrial fragmentation. Accordingly, basal and maximal mitochondrial respiration are decreased in irradiated cells compared to control samples, supporting the notion of respiratory dysfunction (**Fig. 8A**). Changes in mitochondrial respiration were accompanied by a decrease in the cell's reductive power up to 24 hours after irradiation, without losses in viability, as inferred by the MTT results and the trypan blue exclusion assay (**Fig. S2B** on **APPENDIX 1**). The reduction in the cell's reductive power occurs in a radiation dose-dependent manner, as shown by the MTT assay (**Fig. S2B** on **APPENDIX 1**). Importantly, we did not observe leakage of cytochrome c from the mitochondria to the cytosol or BAX translocation, as would be expected of cells entering apoptosis, since these proteins are not present in the last, cytosolic-enriched fraction (**Fig. 2SC** on **APPENDIX 1**). We also searched for changes in the fractionation profiles of MFN1 and MFN2, two key regulators of mitochondrial dynamics, to further confirm mitochondrial fragmentation. Indeed, as shown in **Fig. 8B**, both proteins displayed differential fractionation profiles between biological conditions.

Since UVA radiation is known to cause oxidative and genotoxic stresses (Schuch et al., 2017) and help explain the changes in mitochondrial dynamics, we tested if 6 J/cm² of UVA could promote alterations in the levels of stress-responsive proteins one and a half hours after radiation exposure. After this period, 138 proteins were significantly

modulated between groups (**Fig. 8C**). Focusing on proteins responsive to DNA damage and oxidative stress (**Fig. 8C**), we observed the up-regulation of the DNA damage response components (RAD23B and XRCC6), a few DNA replication licensing factors, antioxidant enzymes (GSTP1 and PRDX1) and heat shock proteins. Additionally, a few subunits of the electron transport chain complexes and a few redox-responsive proteins (CAT and PRDX3) were diminished, possibly due to depletion.
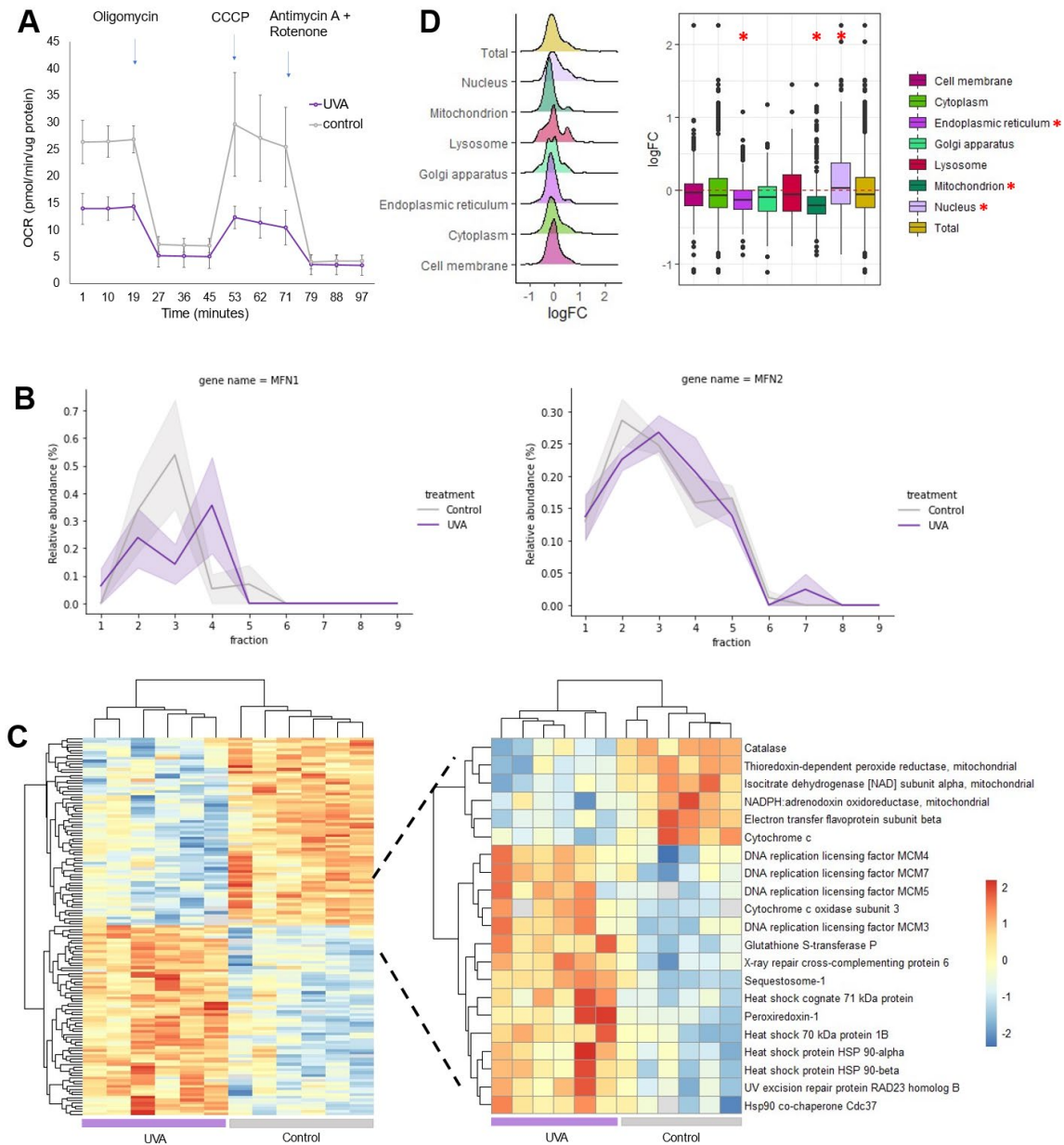
Fig. 8. UVA-induced changes in mitochondrial dynamics impact respiratory function (6 J/cm² of radiation, 30 minutes and 1h30 after exposure). (A) Oxygen consumption rates (OCR) were measured in irradiated and control cells before and after the addition of 1 μM

oligomycin, 1 μM CCCP and a solution containing 1 μM antimycin and 1 μM rotenone (n = 4). **(B)** Profile plots of MFN1 and MFN2. Lines represent the means of relative abundance, and shadowed intervals represent the standard errors. **(C)** Hierarchical clustering of differentially regulated proteins comparing HaCaT cells exposed to UVA versus controls (Student's T-test, 0.05 FDR correction). The color gradient represents z-scored LFQ intensities, and columns represent replicates (n = 6 per group). Proteins responsive to DNA damage and oxidative stress are highlighted. **(D)** Compartment-specific proteome changes in irradiated versus control HaCaT cells one and a half hours after UVA exposure (n = 6). Values are expressed in $\log_2$ (Fold Change UVA/control). The analysis of the $\log_2$(Fold Changes) of irradiated HaCaT cells in relation to controls was performed according to (Parca et al., 2018). Proteins were assigned to compartments according to GO-terms and each compartment was tested for difference against the whole proteome (Wilcoxon rank sum test with 0.5% FDR correction).

By analyzing the fold change of proteins between treatments in a compartment-specific fashion (**Fig. 8D**), we found that the fold change of mitochondrial proteins is significantly lower when compared to the whole proteome (p = 1.47×10^{-17}, Wilcox test, FDR correction), suggesting that decreasing levels of electron transport chain components recapitulate mitochondrial proteome changes as a whole. Importantly, mitochondrial fragmentation usually facilitates mitophagy of damaged mitochondria (Twig and Shirihai, 2011).

These results show that exposing skin cells to UVA radiation impacts mitochondrial dynamics, leading to fragmentation, respiratory dysfunction, and the upregulation of stress response proteins.

2.3. Discussion

The present study is the first to provide a map of subcellular protein reorganization induced by the UVA component of sunlight in a skin cell type. High sensitivity MS-based proteomics coupled to machine learning algorithms quantified and assigned subcellular localization and redistribution patterns for over 3000 proteins in human keratinocytes exposed to UVA radiation. Our unbiased approach revealed that a single low dose of UVA radiation could affect the proteomic architecture of skin cells, provoking the reorganization of subcellular structures due to genotoxic and metabolic stresses. Importantly, because we performed the spatial proteomics experiment 30 minutes after

exposure to UVA, our analysis provides a resource on early signaling events triggered by cellular stress.

In this work, about 20% of the identified and quantified proteins (over 600 proteins from a total of 3200) relocalized in response to UVA exposure. Our results showed that redistribution of proteins across subcellular niches encompass different phenomena, such as changes in organelle dynamics, translocation and targeting for degradation. After considering all redistribution events, important modulators of cellular metabolism, mitochondrial function, protein and vesicle trafficking, signaling pathways and DNA damage recognition and repair were identified.

Previously it was reported that DNA damage response rewires metabolic circuits, fine-tuning protein synthesis, trafficking and secretion (Chatzidoukaki et al., 2020). However, it is not clear how genotoxic components of the sunlight affect protein localization or organelle architecture and interactions. We showed that UVA exposure caused nucleocytoplasmic translocations induced by DNA damage. For instance, our algorithm detected the nucleocytoplasmic translocation of CSNK2B in UVA-irradiated cells, a finding further confirmed by confocal microscopy and coherent with previous literature information, even in the case of a non-cytotoxic dose of a low-energy UV radiation. CSNK2 has many biological targets, maintaining cellular viability and the DNA damage response (Gray et al., 2014; Montenarh, 2016; Yefi et al., 2011). Its role in the cellular response against UVR has been described in terms of its interaction with p53 and NER components (Montenarh, 2016). Indeed, using the Comet assay, we observed that UVA radiation leads to simultaneous CPD formation and CSNK2B translocation. We also monitored DNA damage over time and observed that CPDs are repaired over 24 hours, indicating NER activation. Collectively, these results demonstrate that UVA triggers a classical DNA damage signaling pathway, even though it generates lower levels of CPD than the more energetic UVB radiation.

Besides having oxidative effects on the DNA, we also provide evidence that UVA can target NF-κB's catalytic subunit for degradation, which likely occurs in a singlet oxygen-dependent manner, as previously proposed (Djavaheri-Mergny et al., 1999). Since NF-κB is ubiquitously distributed across the cytoplasm, the extensive degradation of this protein indicates that the oxidative potential of UVA may bear consequences for the

entire surface of cells. Importantly, this evidence also reinforces the differential immunomodulatory effects of UVA and UVB on the skin (Halliday and Rana, 2008) since UVB has been extensively reported to trigger NF-κB's nuclear translocation and subsequent activation of this transcription factor (Cooper and Bowden, 2007). In contrast, UVA seems to trigger the opposite effect.

The most notable result of our systematic proteomic profiling was identifying mitochondria as the main target of UVA-induced stress. Mitochondrial proteins are in a high proportion among the possible translocation targets predicted by TRANSPIRE. When we look at the fractionation profile of structural mitochondrial proteins, we observed a shift between biological conditions. Even though the shift is subtle, it is consistent among many structural proteins, suggesting that mitochondrial fragmentation provokes a change in the fractionation profile of mitochondrial proteins. To our knowledge, this has not been reported in the literature.

Further experiments demonstrated that UVA induces mitochondrial fragmentation, up-regulates redox-responsive proteins and reduces the respiratory rate, leading to changes in the cells' overall energetic status. These results expand on previous characterizations of mitochondrial dysfunction in response to UV radiation (Djavaheri-Mergny et al., 2001; Jugé et al., 2016) and show that alterations occur even with acute low-dose exposures to UVA, the least energetic component of the UV spectrum. It has been suggested that UVA-induced deletions in mtDNA underlie the long-term effects of UVA during photoaging (Berneburg et al., 2004). However, our results suggest that UVA also has short-term effects on the mitochondria, acting as a potent stressor immediately after exposure. Some endogenous metabolites have been proposed to play a role in UVA's photosensitization in skin cells, such as flavin-derivatives, NADH, NADPH, FADH, urocanic acid, porphyrins and some sterols (Wondrak et al., 2006). Mitochondria, in particular, contain high concentrations of putative UVA chromophores, such as flavin-derivatives, NADH, FADH and NADPH, which could mediate the damage to this organelle.

Several studies showed that high doses of UVB irradiation (e.g., > 100 mJ/cm²) trigger mitochondrial fragmentation in keratinocytes (Jugé et al., 2016; Wang et al., 2015, p. 1; Zhang et al., 2016, p. 1). On the other hand, UVC (60 mJ/cm²) leads to mitochondrial

hyperfusion instead of fragmentation in mouse fibroblasts, suggesting that UVR-induced modulations of mitochondrial dynamics are complex and context-dependent (Tondera et al., 2009). Our results show that even low doses of less energetic UVA radiation induce mitochondrial fragmentation.

UVB-induced mitochondrial fragmentation is dependent on DRP1 mitochondrial translocation, with partial roles for MFN1 and OPA1(Jugé et al., 2016), frequently followed by apoptosis (Wang et al., 2015; Zhang et al., 2016). In our experiments with UVA irradiation, we did not detect changes in molecular markers of apoptosis, such as cytochrome *c* leakage from mitochondria, BAX translocation, or attenuated cell viability. Moreover, we did not observe changes in the abundance or subcellular reorganization of DRP1 or OPA1. However, we did observe that MFN1 and MFN2 displayed a differential fractionation profile between conditions, suggesting that UVA may affect their function differently than other UV wavelength ranges. Importantly, MFN1 and MFN2 modulations have been reported to occur in response to oxidative stress (Willems et al., 2015). For example, fibroblasts exposed to exogenous H_2O_2 up-regulate the ubiquitination of MFN1 and MFN2, triggering mitochondrial fragmentation (Rakovic et al., 2011).

Our study has several strengths. First, machine learning predictions involving DNA damage response, inflammation and cellular metabolism were validated using confocal microscopy and functional assays. Second, our dataset opens up possibilities for further investigation of UVA-triggered dynamic events in less studied subcellular niches. Furthermore, ER and Golgi vesiculation occur in UV-exposed cells (Chatzidoukaki et al., 2020), and our data suggest that proteins from these compartments are redistributed upon stress.

Our work also has some limitations. The shotgun proteomics approach, due to semi-stochasticity of fragmentation, leads to high levels of missing values in the dataset. Here we simply imputed these values as 0, but the use of more sophisticated methods of imputation would improve the analysis and lead to prediction of a more stringent list of possible translocation targets, with a lower false-positive rate. Alternatively, isobaric labeling of the samples would also improve the analysis. Thus, this is a limitation of our work, which will be addressed in the future. Furthermore, machine learning algorithms applied to spatial proteomics are not developed to differentiate between protein

translocation events, altered organellar dynamics, or altered protein synthesis and degradation rates within specific subcellular niches. However, our biochemical validations unequivocally differentiated among these events. It is also worth mentioning that there are also few user-friendly algorithm options for modeling protein multilocalization, which is an important biological aspect to be taken into account. Future developments in the spatial proteomics field will likely address this limitation.

In summary, our dataset provides valuable information about UVA-triggered translocation events in subcellular niches. Our experimental strategy employing cellular fractionation, MS-based proteomics and machine learning algorithms revealed UVA redistributed approximately 20% of the skin cell proteome, highlighted by the up-regulation of redox-responsive proteins, DNA damage and mitochondrial fragmentation.

2.4. Materials and Methods

2.4.1. Experimental model

HaCaT cell line, a spontaneously immortalized human keratinocyte, was cultured in 5% CO_2 at 37°C and grown in Dulbecco's Modified Eagle's Medium (DMEM) supplemented with 10% fetal bovine serum, 100 U/mL penicillin and 100 ug/mL streptomycin. Professor Mauricio S. Baptista (Institute of Chemistry, University of São Paulo) provided the cell line, and it was tested for mycoplasma contamination. As subcellular fractionation requires high amounts of cells, we used an immortalized cell line, however HaCaT has a well-characterized genetic status. HaCaT cells do not harbor any viral sequences (Boukamp et al., 1997; Mueller et al., 2001) and were likely immortalized as a consequence of UV-like mutations in p53 (Lehman et al., 1993), similar to the ones found in skin carcinomas and pre-malignant lesions (Brash, 1997). Therefore, this lineage is commonly used as a model to study very early stages of skin tumorigenesis (Fusenig and Boukamp, 1998). HaCaT cells are also able to undergo tumorigenic conversion by overexpression of a single proto-oncogene (NF-κB) (Ren et al., 2006). Despite these alterations, HaCaT cells have a stable chromosome content and remain non-tumorigenic (Boukamp et al., 1997).

2.4.2. Irradiation conditions

An Oriel SOL-UV 2 solar simulator (Newport, USA) equipped with a Xenon arc lamp was used for cell irradiation. The simulator was equipped with an IR bandpass blocking filter plus a UVB-blocking filter (emission spectra of the simulator radiation with and without the UVB-blocking filter are displayed in **Fig. S2A** on **APPENDIX 1**). Before irradiation, the simulator's output was measured with a dosimeter from International Light Inc (Newburyport, MA, USA), model IL1700, with a SED033 detector. Using the IR and UVB blocking filters, the output measured in the area where the cell plates would be positioned, at a 10 cm distance from the radiation source, yielded a mean of 5.0 mW/cm², with a maximum variation of 10% between biological replicates. Each dish was irradiated for 26 minutes, corresponding to a total dose of 6 J/cm², which humans can be exposed to during routine daily living without affecting cellular viability (**Fig. S2B**). Cells were washed three times with phosphate-buffered saline (PBS) and kept in PBS during irradiation (26 minutes). Mock-treated controls were kept in PBS and maintained in the dark at room temperature for the same amount of time.

In preliminary experiments, we tested two different doses of UVA radiation (6 and 12 J/cm²). Upon irradiation with 6 J/cm², more than 90% of cells were viable (Supplemental information – Chapter 2). Thus, we chose this dose to evaluate non-citotoxic effects of UVA radiation on the proteome of skin cells.

2.4.3. Subcellular proteome sample preparation

For the spatial proteomics assay, two million cells were plated in 100 mm dishes 48 hours before the experiments (until cells reached 80-90% confluency). An entire dish containing around eight million cells yielded at least 10 µg of protein in the fraction with the lowest yield, which was enough for mass spectrometry analysis.

Cells were trypsinized and harvested by centrifugation 30 minutes after irradiation. The cell pellet was washed twice in PBS and incubated for 10 minutes in 1 mL of hypotonic lysis buffer (25 mM Tris-HCl, pH 7.5, 50 mM Sucrose, 0.5 mM $MgCl_2$, 0.2 mM EGTA) on ice. Cells were then transferred to a Potter-Elvehjem homogenizer and homogenized with 30 strokes on ice (until at least 70% of cells were stained with trypan blue). After homogenization, 110 µL of hypertonic sucrose buffer (2.5 M sucrose, 25 mM Tris pH 7.5, 0.5 mM $MgCl2$, 0.2 mM EGTA) was used to restore osmolarity. The cell lysate was

transferred to 2 mL tubes and centrifuged twice at 200 × *g* for 5 minutes to remove intact cells. The lysate was then subjected to a series of differential centrifugations: 1000 × *g* for 10 minutes, 3000 × *g* for 10 minutes, 5000 × *g* for 10 minutes, 9000 × *g* for 15 minutes, 12000 × *g* for 15 minutes, 15000 × *g* for 15 minutes, 30000 × *g* for 20 minutes and 80000 × *g* for 40 minutes. In total, each of the five biological replicates of each condition yielded nine fractions. The supernatant was collected because it contains the remaining cytosolic proteins. Afterward, fractions enriched with different organelles were lysed in 8 M urea containing 0.1% deoxycholate. The total protein concentrations were quantified using a BCA assay kit (Thermo Scientific), and 10 µg of protein per fraction were digested and analyzed by mass spectrometry.

2.4.4. Cell lysate sample preparation

For proteomics experiments, 400,000 cells were plated in 6-well plates 24 hours before the experiments. After irradiation, cells were washed five times with PBS, and scraped in 500 µL of a solution containing 100 mM ammonium bicarbonate, 8 M urea and protease inhibitors (cOmplete™ Protease Inhibitor Cocktail, Roche). Cell lysates were kept on ice for one hour and, after that, they were precipitated overnight with 3 volumes of cold (-20 °C) acetone. Precipitated proteins were collected by centrifugation. Pellets were air-dried for about 10 minutes and resuspended in 100 mM ammonium bicarbonate buffer containing 8 M urea. Protein concentration was measured using a Pierce™ BCA Protein Assay Kit (Thermo Fisher Scientific).

2.4.5. Protein digestion

Aliquots corresponding to 10 µg of protein per sample were reduced with 5 mM dithiothreitol for one hour and alkylated with 15 mM iodoacetamide for 30 minutes, at 30 °C with agitation (400 rpm). Then, the samples were diluted ten-fold with 100 mM ammonium bicarbonate, and digested by the addition of two aliquots of trypsin (in the proportions of 1:40 and 1:50 w/w, respectively, with an interval of four hours between the additions). The samples were digested overnight at 30°C with agitation (400 rpm). Digestion was stopped by adding 4% trifluoracetic acid (TFA), and then the samples were dried. Samples were desalted using the StageTip protocol (Rappsilber et al.,

2007). Peptides were washed ten times with 0.1% TFA in the StageTips and eluted with 50% acetonitrile and 0.1% TFA.

2.4.6. LC-MS/MS measurements

Each sample was injected in an Orbitrap Fusion Lumos mass spectrometer (Thermo Scientific, Bremen, Germany) coupled to a Nano EASY-nLC 1200 (Thermo Scientific, Bremen, Germany). Peptides were injected into a trap column (nanoViper C18, 3 μm, 75 μm × 2 cm, Thermo Scientific) with 12 μL of solvent A (0.1% formic acid) at 980 bar. After this period, the trapped peptides were eluted onto a C18 column (nanoViper C18, 2 μm, 75 μm × 15 cm, Thermo Scientific) at a flow rate of 300 nL/min and subsequently separated with a 5-28% acetonitrile gradient with 0.1% formic acid for 80 minutes, followed by a 28-40% acetonitrile gradient with 0.1% formic acid for 10 minutes.

The eluted peptides were detected in the data-dependent acquisition mode under positive electrospray ionization conditions. A full scan (*m/z* 400-1600) was acquired at a 60000 resolution, followed by HCD fragmentation of the most intense ions, considering an intensity threshold of 5×10^4. Ions were filtered for fragmentation by the quadrupole with a transmission window of 1.2 *m/z*. HCD fragmentation was performed with a normalized collision energy of 30, and the Orbitrap detector analyzed the fragments with a 30000 resolution. The number of MS2 events between full scans was determined by a cycle time of 3 seconds. A total of 5×10^5 and 5×10^4 ions were injected in the Orbitrap with accumulation times of 50 and 54 seconds for the full scan and MS2 acquisition, respectively. Monocharged ions or ions with undetermined charges were not selected for fragmentation.

2.4.7. Comet assay

A total of 500,000 cells were plated in 6-well plates 24 hours before the experiment (n = 3). After irradiation, cells were trypsinized and collected by centrifugation. The supernatant was discarded, and cell pellets were mixed with 100 μL of PBS. 10 μL of cell suspension was added to 90 μL of 0.5% low melting point agarose. Subsequently, 75 μL of this cell suspension was pipetted onto slides pre-coated with 1.5% normal melting point agarose. Slides were covered with coverslips and kept at 4°C for 30 minutes to allow the agarose to solidify. Next, the coverslips were removed, and the

slides were kept in a tank containing lysis buffer (2.5 M NaCl, 100 mM EDTA, 10 mM Tris, 1% Triton X-100, and 10% DMSO, pH 10) overnight at 4°C in the dark.

After lysis, slides were washed with cold PBS three times in the dark and immersed three times in cold reaction buffer (40 mM HEPES, 0.1 M KCl, 0.5 mM EDTA, 0.2 mg/mL BSA, pH 8) for 5 minutes each time. After that, the reaction buffer or reaction buffer containing T4 endonuclease V (0.1 U/mL), FPG (0.2 U/mL) or endonuclease III (10 U/mL) enzymes were pipetted onto each slide. Coverslips were placed over the slides, and they were incubated for 30 minutes at 37°C in the dark. The slides were then transferred to cold electrophoresis buffer (10 M NaOH, 200 mM EDTA, pH 13 in water) and incubated for 20 minutes. Then, the slides were submitted to electrophoresis for 20 minutes at 25 V, 300 mA. After electrophoresis, the slides were immersed in neutralizing solution (0.4 Tris, pH 7.5) three times for 5 minutes each time and fixed in methanol for 10 minutes. After washing, all the slides were air-dried at room temperature. The DNA was stained with 20 μL of a solution containing 2.5 ug/mL of propidium iodide for 10 minutes. Fifty randomly selected comets per sample were analyzed on a fluorescence microscope (Olympus BX51) using the Komet 6 software. Two technical and four biological replicates were analyzed per condition.

2.4.8. Immunofluorescence

Cells were seeded on 8-well Lab-Tek® II Chambered Coverglass plates (Thermo Scientific, # 155409) under standard cell culture conditions. Samples were fixed with ice-cold 4% paraformaldehyde in PBS without Ca^{2+} and Mg^{2+}. After removing the PFA, the cells were incubated for 20 minutes at room temperature with freshly prepared permeabilization buffer (0.1 % Triton X-100, PBS, pH 7.4). After that, cells were washed in PBS three times for 5 minutes each time.

For cell staining, samples were first rinsed for one hour with blocking buffer (3% fetal bovine serum, PBS, pH 7.4) at room temperature. Then, primary antibodies (OAT, Invitrogen #PA5-66715, 1:500; Fumarase, Invitrogen #PA5-82899, 1:500; Casein Kinase 2 beta, Abcam #ab151784, 1:500; PDHA1 [9H9AF5], Abcam #ab110330, 1:200, and COX4I1 Abcam #ab33985) were diluted (as indicated above) in blocking buffer and incubated overnight at 4°C. Next, the chambered coverglass plates were rinsed three

times with PBS and cells were labeled with fluorescently conjugated secondary antibody (anti-Rabbit Alexa Fluor 488, Invitrogen #A-11008, 1:500; anti-Mouse Alexa Fluor 647, Abcam # ab150119, 1:500) in blocking buffer for one hour at room temperature. Afterward, unbound secondary antibodies were removed by washing with PBS three times for 5 minutes each at room temperature. Finally, nuclei were labeled with 1 µg/mL Hoechst 33342 in PBS (Invitrogen #H1399). Imaging was performed in PBS. A Zeiss LSM 710 laser scanning confocal microscope was used, and cells were imaged using x63 oil immersion objective (Plan Apochromat NA 1.40).

2.4.9. Respirometry

One day before the experiment, on four different days, 60,000 cells were plated on XF24 cell plates (Agilent) to measure cell respiration. After irradiation, PBS was replaced by DMEM without sodium bicarbonate, and cells were incubated for 1 hour at 37°C and atmospheric pressure of CO_2. Oxygen consumption rate (OCR) was measured in a Seahorse XF24 Analyzer (Agilent), before and after subsequent additions of 1 µM oligomycin, 1 µM CCCP and a mix of 1 µM antimycin and 1 µM rotenone. Each compound was added after three cycles of measurements of 3 minutes each. The concentration of CCCP was determined through the previous titration. At the end of the experiments, each well was washed once with PBS and proteins were resuspended in 100 µM ammonium bicarbonate, containing 8 M urea and 1% sodium deoxycholate. After homogenization, protein concentration was determined by using a BCA assay kit. The OCR values were normalized by the amount of total protein in each well.

2.4.10. Descriptive data analysis

Raw files were processed using MaxQuant (Cox and Mann, 2008) (version 1.16.17.0). The Andromeda algorithm (Cox et al., 2011) was used for protein identification against the homo sapiens Uniprot database (downloaded August, 2019; 20416 entries). Error mass tolerance for precursors and fragments were set to 4.5 ppm and 20 ppm, respectively. Cysteine carbamidomethylation was selected as a fixed modification and methionine oxidation and *N*-terminal acetylation were selected as variable modification. Trypsin was set as digestion enzyme, with a maximum of 2 missed cleavages allowed. A maximum FDR of 1% was allowed both for peptides and proteins identification, and for

proteins it was calculated using a decoy database created from the reverse ordination of the protein sequences in the Uniprot database. Identification of at least two peptides (unique + razor) was set as a parameter for the identification of a protein. Protein abundances were quantified by the LFQ algorithm, based on the normalized chromatographic peak integrations generated by MaxQuant. Other parameters were kept as default.

Each fraction was considered a different sample in the experimental design annotation file required for the MaxQuant analysis. A matrix of relative quantification data (LFQ) (Cox et al., 2014) for proteins in each fraction was obtained and used for subsequent analysis. Missing values were kept as 0. Each protein was scaled by the total sum of the LFQs for a given replicate/cell map, yielding a value between 0 and 1. Proteins that were not quantified in at least 3 biological replicates of the 90 samples were filtered out to remove the most uninformative fractionation profiles with missing values generated by stochastic fragmentation in the shotgun proteomics approach.

Dimensionality reduction was achieved using the t-distributed stochastic neighbor embedding technique (t-SNE) (Maaten and Hinton, 2008). The fractionation data was plotted with different perplexity parameters (perplexity = 30 yielded the best cluster separation). The plots were overlaid with categorical subcellular classifications from the Cell Atlas initiative (Rozenblatt-Rosen et al., 2017), Uniprot (The UniProt Consortium, 2017) and Gene Ontology (Ashburner et al., 2000) databases, providing information on the clusterization of different subcellular compartments.

Organellar markers were curated based on classification from the Cell Atlas, Uniprot and Gene Ontology databases. Markers had to be reproducible across all replicates, and profile plots were manually curated to remove proteins with unreproducible missing values. Organellar markers from four different compartments (cytosol, mitochondria, nucleus, and secretory organelles) were assigned with different colors to visualize clusterization in the t-SNE plots. The secretory compartment comprises proteins initially assigned to peroxisomes, endoplasmic reticulum (ER), plasma membrane, Golgi apparatus and lysosomes. These organelles were grouped under the term "secretory" because they share similar fractionation profiles that were not well distinguished by the machine learning algorithms.

2.4.11. Localization prediction

As described previously (Breckels et al., 2018; Gatto et al., 2014b), a supervised machine learning approach was used for the subcellular localization prediction. We used a model of an averaged neural networks algorithm (Gatto et al., 2014b) to produce the paper's results, but a support vector machine was also tested and yielded similar results. The organellar markers were used to train the model for subcellular localization prediction. Organellar markers were divided into a training and validation set (80/20% proportion for each set) with a 5-fold cross-validation through 100 iterations of the algorithm. We used a grid search to achieve hyperparameter tuning. The accuracy of the classifier was estimated through the F1 score (Breckels et al., 2018), and the best hyperparameters were chosen according to the accuracy of the classifier. The best network size ranged from 4 to 6, and the best decay was 10^{-4}. These analysis were performed using the pRoloc (version 1.34.0) package on RStudio (version 2021.09.1+372).

2.4.12. Translocation prediction

The TRANSPIRE pipeline (version 0.1.1) was used for the translocation prediction, as developed and described by Kennedy et al. (2020). The analysis were performed using python (version 3.7.6). Curated organellar markers were utilized to generate synthetic translocations, which are then used to train the learning algorithm in distinguishing translocation classes and consequently translocating from non-translocating proteins. In brief, each organellar marker in the control samples is concatenated with every other organellar marker of the treated samples, producing synthetic translocations and non-translocations (when markers of the same compartment are concatenated). For example, a synthetic translocation that simulates the migration of a protein from the nucleus to the cytosol would have a fractionation profile that is characterized by the combination of a nuclear marker profile containing information for all control samples with the cytosolic marker profile containing information of all treated samples (yielding a total of 90 "fractions" per synthetic translocation).

Synthetic translocations were used to train a Stochastic Variational Gaussian Process Classifier (SVGPC) implemented in TRANSPIRE through the GPFlow package (built upon the TensorFlow platform in Python). This model is composed of a kernel function,

a likelihood function, n latent variables (which account for the number of translocation classes), a training set, and a subset of the training set used as inducing points (Kennedy et al., 2020). The model implemented in TRANSPIRE uses softmax as a likelihood function to improve score calibration.

Hyperparameter tuning involved choosing the kernel type (squared exponential, rational quadratic, exponential Matern32 and Matern52, as implemented by TRANSPIRE through GPFlow) and the number of inducing points (ranging from 1 to 500). The synthetic translocation data were divided into training, validation, and test sets in a 50/20/20% proportion, respectively, during training. The training data was further split into five balanced folds during hyperparameter tuning, allowing for a 5-fold cross-validation. A class imbalance was prevented by allowing the most frequent translocation classes to have, at most, three times more proteins than the least frequent. The best hyperparameters selected through the grid search were the squared exponential kernel and 30 inducing points (optimization plots are shown in the Supporting Information). The results were evaluated by maximizing the evidence lower bound (ELBO) using the Adam optimizer. Afterward, the resulting model was used to predict translocations in the actual dataset and performance was evaluated based on the held-out test partition of the synthetic translocation data.

The output of the TRANSPIRE pipeline entails the classification of a translocation class (e.g., "Nucleus to Cytosol") for each protein plus a classifier score. The classifier score ranges from 0 to 1 for each translocation class, and the sum of the scores for all classes for each protein should be equal to 1. Class prediction is based on the highest classifier score for a given translocation class. This score is referred to as "predicted scores" in the spreadsheets in the Supporting Information. Additionally, the TRANSPIRE pipeline provides a translocation score, defined as the sum of the predicted scores for all true translocation classes. This score accounts for situations in which high classifier scores are split among at least two translocation classes.

TRANSPIRE also allows for the computation of false-positive rates (FPR), based on the model's performance, setting thresholds for the translocation scores to minimize the likelihood of false positives. Herein, we adopted a 0.5% FPR to generate a more stringent list of translocation targets.

2.4.12. Data availability

The proteomic dataset generated during this study has been deposited to the ProteomeXchange Consortium (http://www.proteomexchange.org/) via the PRIDE repository (identifier: PXD027941). All processed data are available in the Supporting Information.

A

B

C

Cluster 1

Biological process	In cluster	Ben. Ho. FDR
membrane part	520	5.96E-96
endoplasmic reticulum part	207	2.11E-59
plasma membrane	304	2.69E-41
Golgi apparatus part	113	1.13E-16
cytoplasmic vesicle	113	4.91E-14
endosomal part	76	2.03E-12
vacuolar membrane	50	6.98E-08
lysosomal membrane	47	1.49E-07

Cluster 2

Biological process	In cluster	Ben. Ho. FDR
chromosomal part	67	1.45E-29
nuclear chromosome part	45	4.98E-24
chromatin	43	8.49E-24
mitochondrial matrix	49	8.19E-23
chromosome	33	1.84E-22
nuclear chromatin	33	6.12E-21
nuclear part	152	4.58E-17

Cluster 3

Biological process	In cluster	Ben. Ho. FDR
mitochondrial membrane	152	6.49E-61
mitochondrial membrane part	81	4.84E-54
mitochondrial part	172	1.40E-52
mitochondrial inner membrane	124	6.19E-50
organelle inner membrane	125	6.50E-48
mitochondrion	163	8.54E-33

Cluster 4

Biological process	In cluster	Ben. Ho. FDR
ribonucleoprotein complex	275	2.26E-98
nuclear part	478	5.06E-63
nucleolus	208	7.12E-53
spliceosomal complex	90	3.51E-40
non-membrane-bounded organelle	324	6.50E-32

Cluster 5

Biological process	In cluster	Ben. Ho. FDR
intrinsic to membrane	45	6.42E-18
integral to membrane	45	6.49E-18
membrane part	55	1.34E-16
Golgi apparatus part	26	5.88E-13
SNARE complex	11	4.40E-12
Golgi membrane	22	1.47E-11

Cluster 6

Biological process	In cluster	Ben. Ho. FDR
chromosomal part	56	1.40E-23
organelle inner membrane	63	2.76E-23
chromatin	38	3.55E-21
nuclear chromosome part	38	8.42E-20
nuclear chromatin	29	2.30E-18
mitochondrial inner membrane	55	2.60E-18

Cluster 7

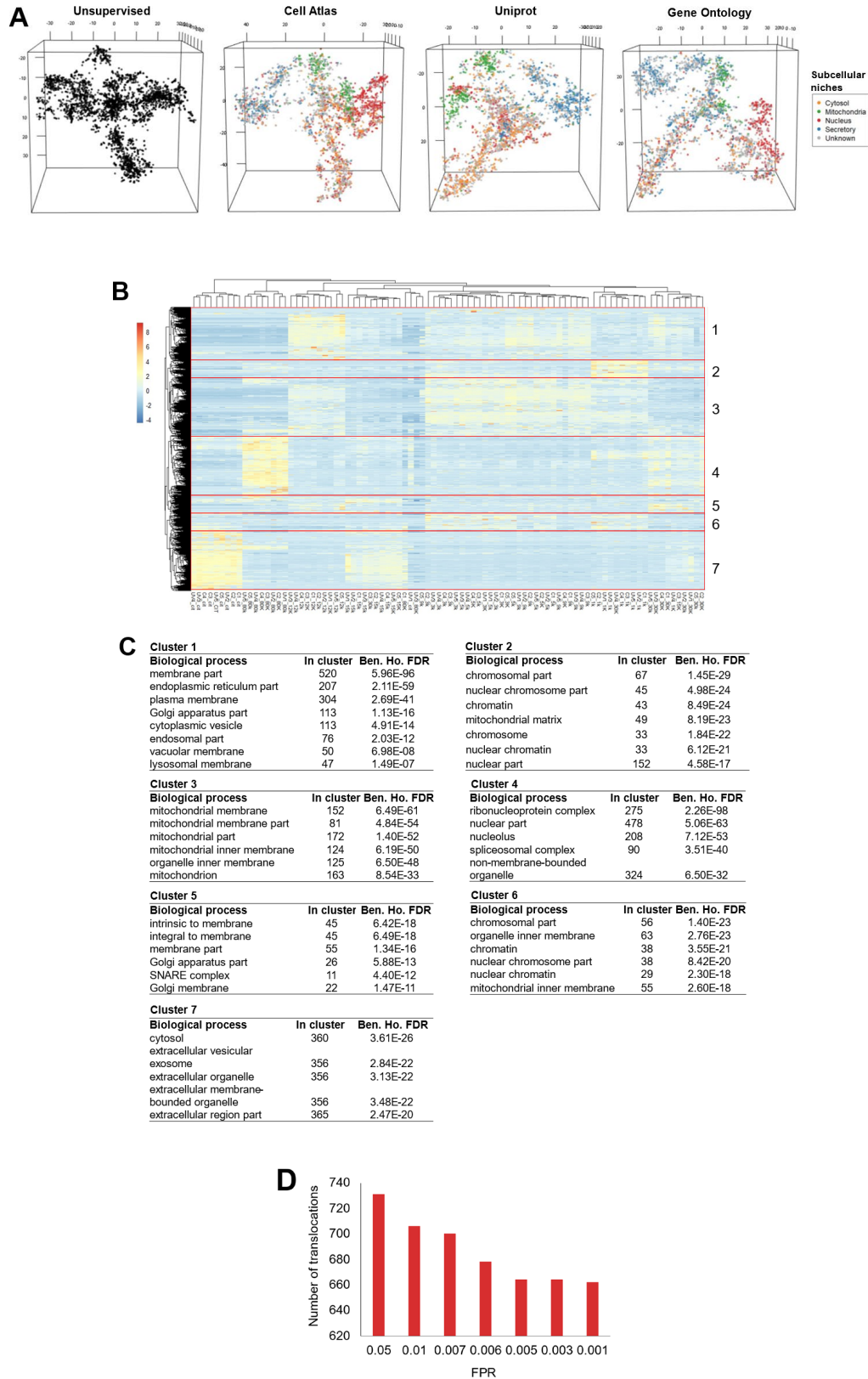| Biological process	In cluster	Ben. Ho. FDR
cytosol	360	3.61E-26
extracellular vesicular exosome	356	2.84E-22
extracellular organelle	356	3.13E-22
extracellular membrane-bounded organelle	356	3.48E-22
extracellular region part	365	2.47E-20

D

Fig. S1. Unsupervised and supervised clustering of the fractionation data.

(A) Unsupervised hierarchical clustering of the fractionation data based on Euclidian distances. The color gradient represents relative LFQ intensities, and columns represent samples. **(B)** Unsupervised and supervised t-SNE analysis of the fractionation dataset. For supervised analysis, proteins were overlaid with subcellular classifications from the Cell Atlas, Uniprot and Gene Ontology databases. All graphs were plotted with a perplexity parameter of 30. **(C)** Each heatmap cluster was enriched for GO terms. "In cluster" refers to the number of proteins associated with a given process, and "Ben. Ho. FDR" refers to Benjamin-Hochberg FDR corrected p-values. **(D)** Number of potential translocations as a function of the FPR threshold.
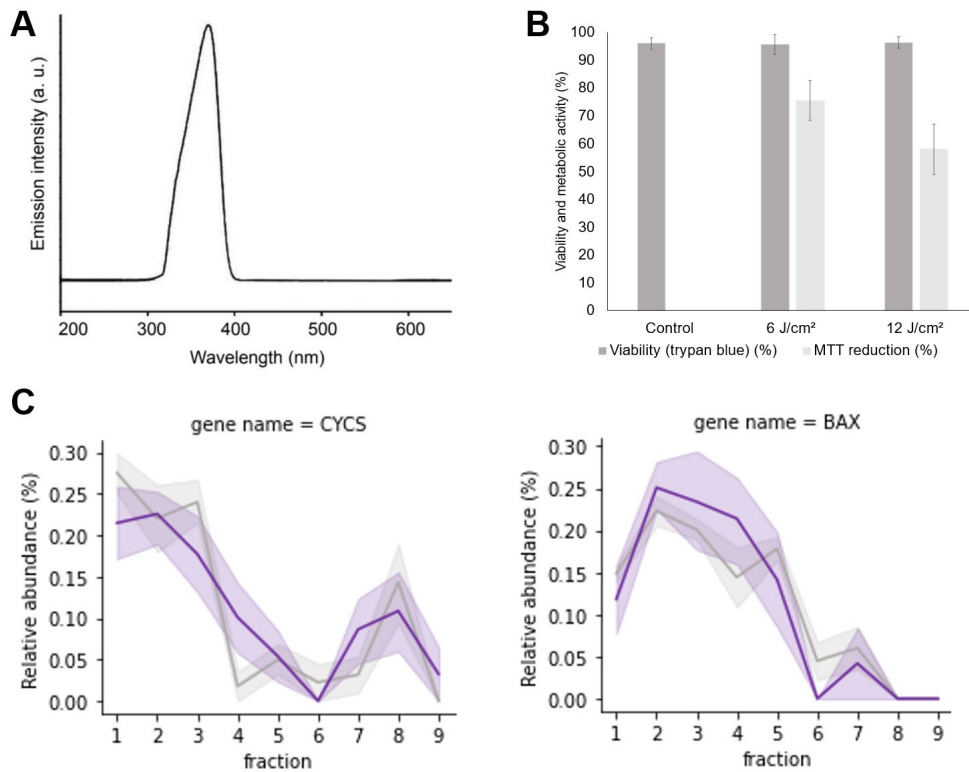
Fig. S2. Irradiation conditions and cellular viability.

(A) Emission spectrum of the SOL-UV solar simulator equipped with a Xenon arc lamp, IR bandpass blocking filter and UVB-blocking filter. **(B)** MTT and trypan blue assays were used to evaluate the cellular viability of HaCaT cells under environmentally relevant UVA doses. Bars represent the mean, and error bars represent the standard deviation (n = 3). **(C)** Profile plots of cytochrome *c* (CYCS) and apoptosis regulator BAX. Lines represent the means of relative abundance, and shadowed intervals represent the standard errors.
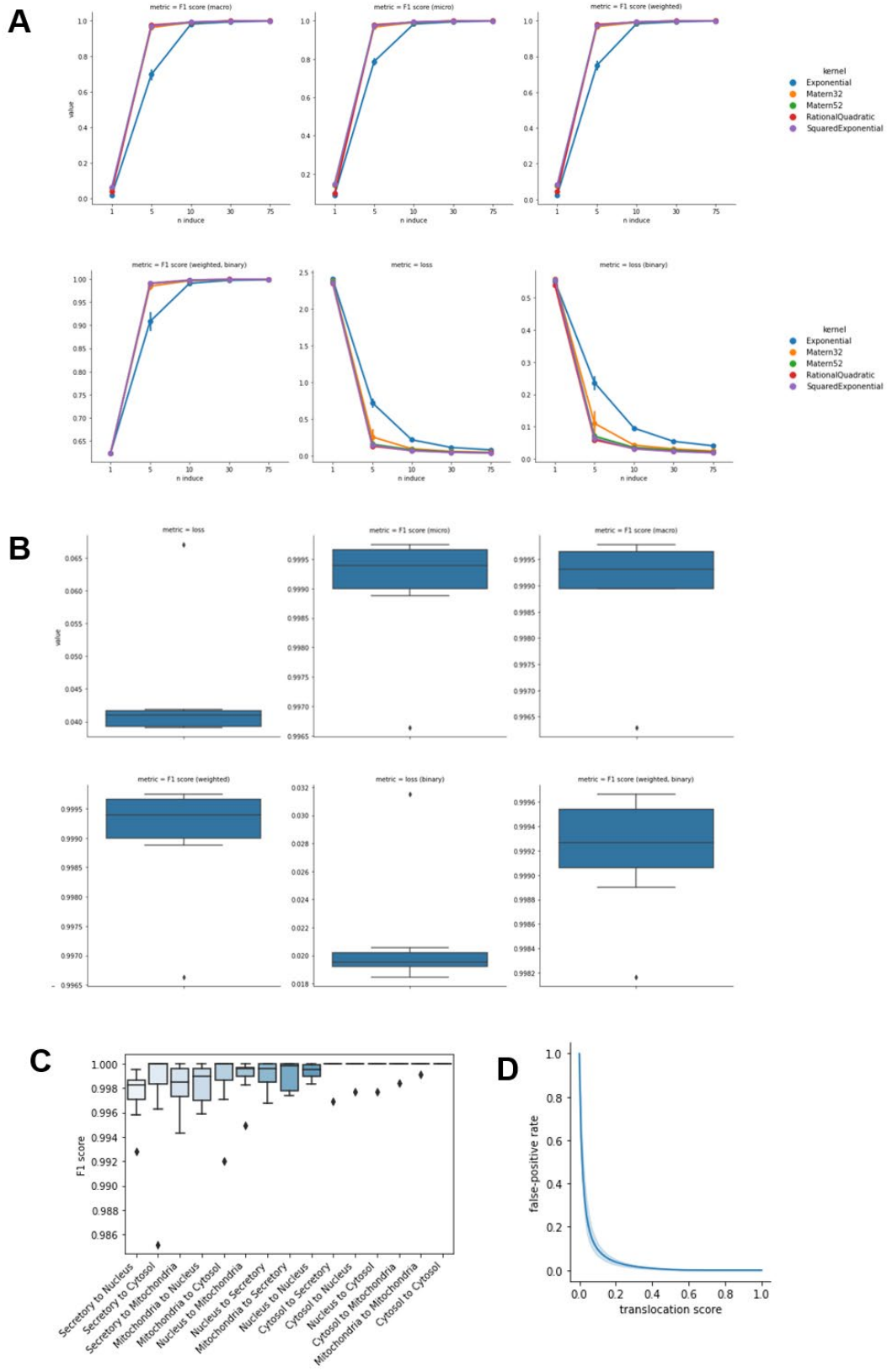
Fig. S3. Classifier performance and reliability.

(A) Optimization of the hyperparameters of the classifier (n induce and kernel type). The loss and F1 scores were used as metrics to define the optimal hyperparameters. **(B)** Performance of the classifier across five folds of the training data. **(C)** Boxplots of weighted F1 scores describing the classifier performance per class across eight folds of the test data. **(D)** False-positive rates for translocation prediction based on the classifier performance of the test data.

Table S1. Refined nucleocytoplasmic translocations predicted by TRANSPIRE according to a review of the literature

| Gene name | TRANSPIRE prediction | | Literature evidence of translocation or dual localization | |
	Predicted label	Translocation Score	Reference	Description
PFKFB2	Nucleus to Cytosol	0.51	(Ozcan et al., 2020)	Nucleocytoplasmic shuttling
URI1	Cytosol to Nucleus	0.80	(Tsuchiya et al., 2019; Tummala et al., 2014)	Dual localization
PARN	Nucleus to Cytosol	0.51	(Duan et al., 2019)	Nucleocytoplasmic shuttling
UBL4A	Cytosol to Nucleus	0.71	(Krenciute et al., 2013)	Translocates from the cytoplasm to the nucleus
CREB1	Nucleus to Cytosol	0.53	(Mroz et al., 2007)	Nucleocytoplasmic shuttling
CETN2	Cytosol to Nucleus	0.86	(Renaud et al., 2011)	Translocates from the cytoplasm to the nucleus
KPNA2	Cytosol to Nucleus	0.58	(Alshareeda et al., 2015)	Translocates from the cytoplasm to the nucleus
SMAD3	Nucleus to Cytosol	0.64	(Hill, 2009)	Nucleocytoplasmic shuttling
CENPE	Cytosol to Nucleus	0.65	(Barisic et al., 2015)	Dual localization
PRDX1	Cytosol to Nucleus	0.72	(Aeby et al., 2016; Ding et al., 2017)	Dual localization
TRAF2	Cytosol to Nucleus	0.54	(Min et al., 1998)	Dual localization
CTBP1	Nucleus to Cytosol	0.83	(Verger et al., 2006)	Nucleocytoplasmic shuttling
LASP1	Cytosol to Nucleus	0.65	(Frietsch et al., 2010)	Nucleocytoplasmic shuttling
RANBP10	Cytosol to Nucleus	0.71	(Yudin and Fainzilber, 2009)	Translocates from the cytoplasm to the nucleus
NELFCD	Nucleus to Cytosol	0.71	(Yung et al., 2009)	Nucleocytoplasmic shuttling
SPC24	Nucleus to Cytosol	0.84	(Ma et al., 2007)	Dual localization
SYMPK	Nucleus to Cytosol	0.53	(Tatomer et al., 2014; Zhang et al., 2017)	Dual localization
SMARCC1	Nucleus to Cytosol	0.55	(Scott et al., 2017)	Dual localization
LSM7	Cytosol to Nucleus	0.57	(Spiller et al., 2007)	Dual localization

FAF1	Cytosol to Nucleus	0.76	(Yu et al., 2016)	Translocates from the cytoplasm to the nucleus
CIAO2B	Cytosol to Nucleus	0.94	(Ben-Shimon et al., 2018)	Dual localization
ARFGEF1	Cytosol to Nucleus	0.74	(Padilla et al., 2004)	Translocates from the cytoplasm to the nucleus
CHCHD2	Nucleus to Cytosol	0.54	(Liu et al., 2015, p. 2; Wasilewski et al., 2017)	Dual localization
NFKB1	Cytosol to Nucleus	0.69	(Lessard et al., 2005)	Translocates from the cytoplasm to the nucleus
RELA	Cytosol to Nucleus	0.84	(King et al., 2011)	Translocates from the cytoplasm to the nucleus

Spreadsheet S1.

Label-free quantification of proteins across organelle fractions from the differential centrifugation

Spreadsheet S2.

Scaled protein abundance across organelle fractions

Spreadsheet S3.

List of refined organellar markers used to predict subcellular localization and translocations

Spreadsheet S4.

Neural network predictions of subcellular localization along with the respective prediction scores

Spreadsheet S5.

Translocation events predicted by the TRANSPIRE algorithm in HaCaT cells upon UVA exposure

The above spreadsheets can be found at:

https://www.biorxiv.org/content/10.1101/2021.09.01.458617v2.supplementary-material

CHAPTER 3 - A single dose of Ultraviolet-A induces proteome remodeling and senescence in primary human keratinocytes

3.1. Introduction

The solar ultraviolet radiation that reaches the Earth comprises about 5% of UVB (290-320 nm) and 95% of UVA radiation (320-400 nm), and both are strongly associated with skin photoaging and tumorigenesis (El Ghissassi et al., 2009). While the mechanisms underlying UVB carcinogenicity have been well-described for at least 60 years (Setlow and Setlow, 1962), involving direct generation of bipyrimidine photoproducts, UVA has only been classified as "probably carcinogenic to humans" by the Word Health Organization's International Agency for Research on Cancer in 2009 (El Ghissassi et al., 2009) and many of its cellular effects remain unknown. This is due to the fact that UVA is poorly absorbed by canonical nucleotides, causing much less direct DNA damage than UVB (Schuch et al., 2017). However, UVA can still be absorbed by other cellular chromophores, generating photoexcited species as singlet oxygen, as well as free radicals, and consequently causing oxidative damage in cells (Baier et al., 2006).

Ultraviolet radiation drives photoaging both at the level of the dermis and epidermis. UVA's effect on the dermis have been widely studied, likely because UVA is more efficient in reaching this skin layer than UVB (Battie et al., 2014). Dermal changes during aging reflect senescence as well as death of fibroblasts, which are constantly remodeling the connective tissue by secretion of soluble factors and extracellular matrix repertoire, both under homeostasis and cellular stress conditions (Wlaschek et al., 2021). In this sense, UVA have been shown to induce alterations in the gene expression signatures of fibroblasts, modulating their secretory capacity, and eventually leading to apoptosis and senescence (Battie et al., 2014; Cavinato and Jansen-Dürr, 2017). Similarly, aging also impacts ultrastructure and function of the epidermis, interfering with skin thickness, barrier capacity, prevention of water loss, hydration maintenance and reepithelization post wound healing (Gilhar et al., 2004). Epidermis balance is dependent on the proliferative and differentiation capacities of keratinocytes, which are the main cell type of this skin layer and are in constant renewal. While UVB's action on the epidermis is well-characterized (Fitsiou et al., 2020), UVA-induced cellular mechanisms underlying epidermal alterations during aging are not as well understood.

Lethal UVA doses have been shown to induce apoptosis in epidermal keratinocytes (Assefa et al., 2005) and melanocytes (Bivik et al., 2006), but to date the impact of low doses of UVA on epidermal photoaging has not been well characterized.

Here, proteomic analysis was conducted to derive the phenotypic signature induced by a low dose of the UVA component of the sunlight in primary human keratinocytes. Our results indicate that, upon exposure to UVA radiation, keratinocytes may enter senescence and elicit paracrine responses in neighboring pre-tumoral cells. We also investigated the effects of UVA on immortalized human keratinocytes that harbor potentially oncogenic mutations and dysfunctional components of the senescence machinery, providing a proteomic characterization of the differential sensitivity of the two cell types to the radiation.

3.2. Results

3.2.1. UVA radiation induces changes in protein levels in primary keratinocytes 24 hours after exposure

We first tested if exposure to an environmentally relevant and non-cytotoxic low dose of UVA radiation could promote changes in protein levels of normal human epidermal keratinocytes (NHEK cells). For that purpose, we irradiated NHEK cells with a dose of 6 J/cm² of UVA radiation using a solar UVA spectrum simulator, and monitored changes in protein levels by shotgun proteomics. Importantly, cell viability was above 90% with this UVA dose. Proteins were extracted from irradiated and mock-treated cells 24 hours after irradiation, digested into peptides and analyzed by mass spectrometry. Protein groups were considered differentially expressed if, after hypothesis testing (Student's T-test), the FDR-corrected p-values were lower than 0.05. Principal component analysis of the variables shows a radiation-dependent clusterization effect (**Fig. 1A**). Among the 2807 identified proteins, 253 were differentially regulated 24 hours after UVA irradiation, comprising a cluster of 205 up-regulated proteins and a cluster of 48 down-regulated proteins (**Fig. 1B**).

To evaluate systematically the biological meanings associated with these changes, significantly up and down-regulated proteins were used to generate an enrichment

network based on Gene Ontology's terms through ClueGO (Bindea et al., 2009) (**Fig. 1C**). Additionally, semantically related GO-terms were clustered and labeled with AutoAnnotate to facilitate visualization of the network. The ClueGO analysis revealed that the main biological processes associated with up-regulated proteins in NHEK cells are oxidative stress, immune response, nucleotide metabolism and mitochondrial metabolism, whereas down-regulated proteins are enriched for translation, cytoskeleton regulation, and cell adhesion (see **Fig. 1D** for a table containing key up-regulated proteins and significantly enriched biological processes).

Differential regulation of three markers of senescence (the tumor suppressor p16, histone H2A.J and caveolin-1) (Campisi, 2013; Contrepois et al., 2017; Hernandez-Segura et al., 2018) (**Fig. 1E**), together with exacerbated pro-inflammatory and antioxidant responses (**Fig. 1C**), led us to wonder if a single, low dose of UVA could impact cellular proliferation and induce cellular senescence. In addition, senescent cells usually display an increased number of mitochondria with decreased membrane potential (Passos et al., 2007) accompanied by a reduction in mitophagy (Korolchuk et al., 2017), leading to the release of mitochondrial proteins and intensified ROS production (Hernandez-Segura et al., 2018). Mitochondrial damage also plays an important role in UVA's biological action (Berneburg et al., 1999). The up-regulation of several structural mitochondrial proteins in irradiated NHEK cells, such as components of the respiratory chain, seems consistent with the increase in mitochondrial mass usually observed in senescent phenotypes (Korolchuk et al., 2017).

Furthermore, analysis of the differentially expressed proteins also shows that proteostasis is importantly affected by UVA radiation. It has been observed that accumulation of unfolded proteins during stress-induced senescence (Naidoo, 2009) may lead to the activation of the unfolded protein response in the endoplasmic reticulum, followed by a reduction in protein synthesis (Pluquet et al., 2014). However, protein synthesis is required for production of the senescence-associated secretory phenotype (SASP) and, as a consequence, senescent cells usually suffer from proteotoxic stress (Deschênes-Simard et al., 2014). Accordingly, we found down-regulation of ribosomal subunits and translation regulators, and up-regulation of several heat-shock proteins, transcription factors, translation regulators and proteasome

subunits in irradiated cells (**Supplementary Spreadsheet S1** on **APPENDIX 2** details all the differentially regulated proteins between groups in NHEK cells 24 hours after irradiation and **Supplementary Spreadsheet S2** shown in **APPENDIX 2** details the enrichment analysis).
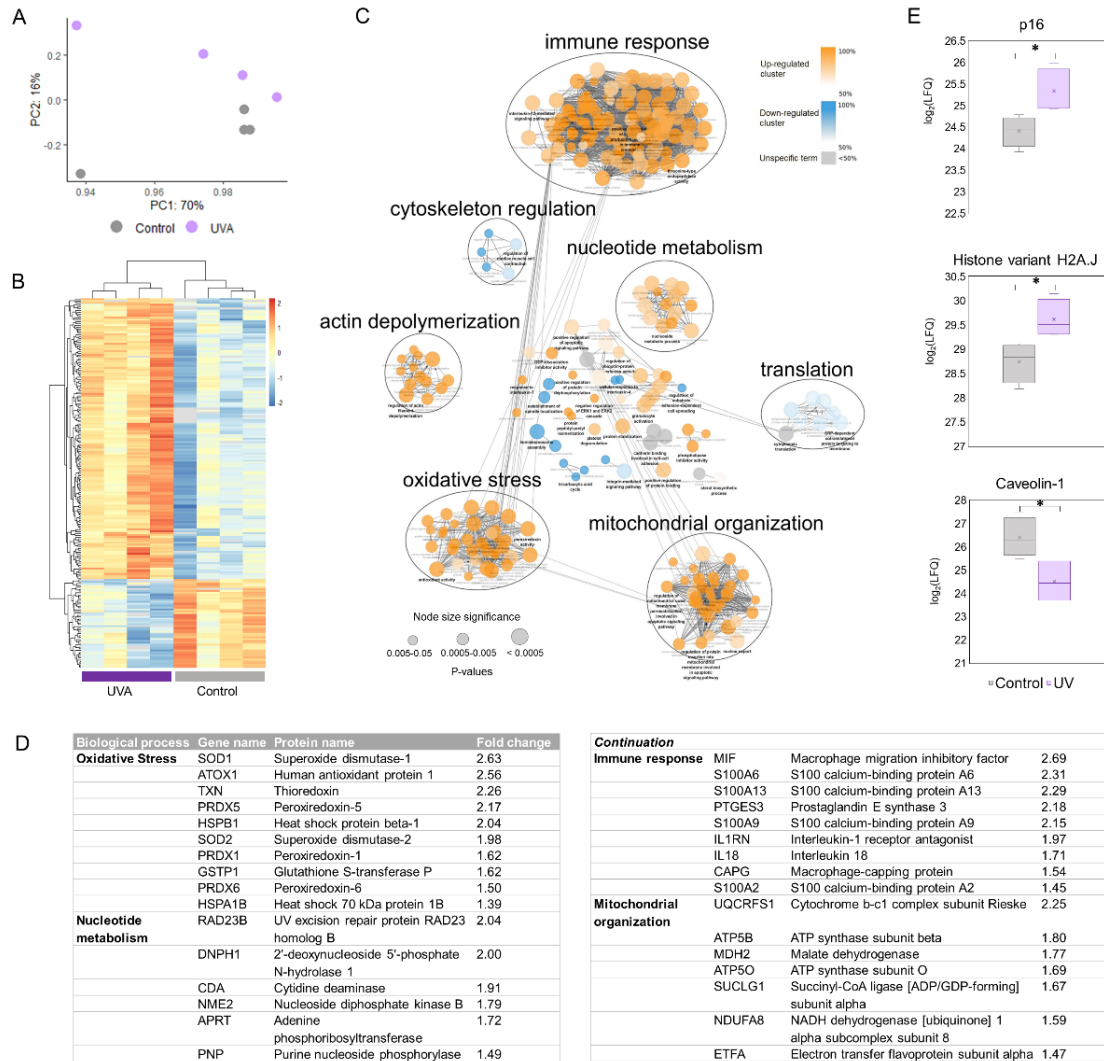
Fig. 1. Proteome remodeling induced by UVA radiation (6 J/cm²) in primary human keratinocytes 24 hours after exposure.

(A) Principal component analysis of UVA-irradiated and control samples obtained by analyzing NHEK cells proteome 24 hours after exposure to 6 J/cm² of radiation (n = 4 per group). **(B)** Hierarchical clustering of differentially regulated proteins (two-tailed Student's T-test, 0.05 FDR correction, with S_0 parameter value of 0.1) in NHEK cells 24 hours after exposure to UVA radiation. The color gradient represents z-scored Label Free Quantification (LFQ) intensities and columns represent replicates. **(C)** Enrichment network of the up and down-regulated clusters

identified in the heatmap. Enriched GO-terms for biological processes are shown as nodes, interconnected according to the number of genes shared between them. The size of the nodes reflects the significance of the terms (p-value < 0.05, right-sided hypergeometric test, Benjamin-Hochberg FDR correction). Semantically-related biological processes were clustered and labeled with AutoAnnotate. **(D)** Most significantly up-regulated proteins in NHEK cells 24 hours after exposure to UVA radiation. **(E)** Boxplots of the log_2 LFQ intensities of p16, caveolin-1 and histone H2A.J in irradiated and control NHEK cells 24 hours after treatment. Asterisks indicate significant differences (*corrected p-value < 0.05) determined by Student's t-test post FDR correction. The x inside the box represents the mean of all values.

3.2.2. UVA radiation induces a senescent phenotype in primary keratinocytes 7 days post irradiation

The up-regulation of immune and stress responses in UVA-exposed keratinocytes, together with differential organization of the mitochondrial proteome and altered proteostasis are coherent with some of the metabolic changes that have been previously described in senescence, such as increased mitochondrial mass and proteotoxic stress (Hernandez-Segura et al., 2018). To confirm that UVA was inducing a senescent phenotype in primary keratinocytes, we used two well-characterized senescence assays (**Fig. 2A**). First, we employed the crystal violet assay to assess cellular proliferation (Feoktistova et al., 2016). Cells were also counted by the trypan blue exclusion method to assure that crystal violet staining reflected growth rates and not viability loss. Our results showed that exposure to UVA radiation impacts cellular growth overtime until at least 7 days after exposure, without concomitant increases in membrane permeabilization to trypan blue (**Fig. 2B**). Second, cells were tested for one of the main hallmarks of senescence, the senescence-associated (SA) β-galactosidase (Dimri et al., 1995). Irradiated NHEK cells showed an increased accumulation of this protein in relation to controls 7 days after exposure to the radiation, besides also exhibiting morphological changes (a large and flat appearance, **Fig. 2C**).

The results obtained with the senescence assays lead us to explore the proteomic profiling of irradiated NHEK cells 7 days after exposure to UVA. Besides promoting a deep remodeling of the proteome after 24 hours of exposure, UVA radiation produced long-lasting effects on the proteome of primary keratinocytes, leading to clusterization of

the variables in a treatment-dependent fashion in the PCA (**Fig. 2D**). Importantly, our proteomic experiments showed an increase in β-galactosidase levels 7 days after UVA exposure in irradiated cells compared to controls (**Fig. 2E**), confirming the results obtained with the staining assay of SA β-galactosidase. By inspecting proteins with larger differences between UVA-treated and control cells (**Fig. 2F**), we found senescence-like changes in the proteome of UVA-exposed cells. Notably, irradiated cells have increased levels of laminin subunits (*LAMA3, LAMB3, LAMC*) and *SERPINE2*, proteins usually secreted in SASP (Coppé et al., 2010; Wiley et al., 2019) (**Fig. 2F-G**). Also, UVA-exposed cells have accumulation of core histone macro-H2A.1 (**Fig. 2H**), a key player in regulation of SASP gene expression (Chen et al., 2015), and a persistent, long-lasting up-regulation of redox-responsive proteins, such as catalase.
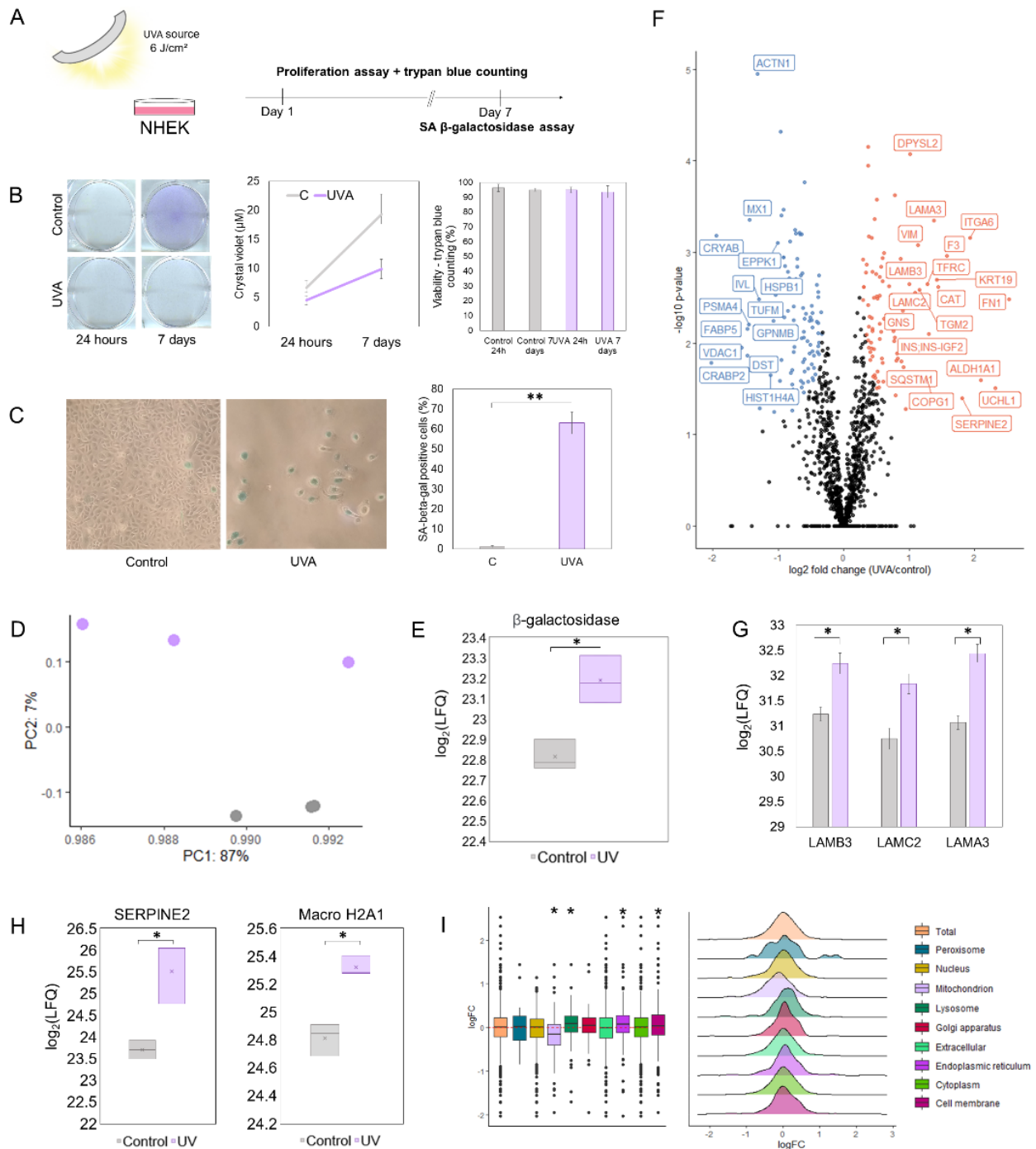
Fig. 2. Long-term implications of UVA-induced cellular senescence (6 J/cm² of radiation, 7 days post-exposure).

(A) Simplified workflow of the proliferation and β-galactosidase assays used to confirm senescence induction by UVA radiation in primary keratinocytes. **(B)** NHEK cells were exposed to UVA radiation or mock-treated and stained with crystal violet after 24 h and 7 days. Representative images of the stained plates are shown in the left and growth curves are shown

in the right, with points representing means, and error bars representing standard deviation values (n = 3). Trypan counting data is shown in the barplot, with bars representing means and error bars representing standard deviation (n = 3). **(C)** NHEK cells were stained for senescence-associated β-galactosidase 7 days after exposure. Representative images of control and UVA-irradiated cells are shown next to a barplot representing the means of the percentage of stained cells in each condition as well as standard deviations. Asterisks indicate significant differences (**p-value < 0. 0.001) determined by Student's t-test. **(D)** Principal component analysis of UVA-irradiated and control samples obtained by analyzing NHEK proteome 7 days after exposure to UVA radiation (n = 3 per group). **(E)** Boxplot of the $\log_2$ LFQ intensities of beta-galactosidase in irradiated and control NHEK cells 7 days after irradiation. The x represents the mean of all values. Asterisks indicate significant differences (*corrected p-value < 0.05) determined by Student's t-test post FDR correction. **(F)** Proteomics analysis of NHEK cells exposed or not to UVA radiation (cells were lysed 7 days post-treatment). Significantly up and down-regulated proteins are shown in the volcano plot, highlighted in orange and blue, respectively. Significance was defined in this plot by a 0.05 FDR and labels were shown for proteins with $\log_2$(Fold Change) > 0.5 or < 0.5 (n = 3). **(G)** Differential levels of laminin subunits (LAMB3, LAMC2, LAMA3) in irradiated and control samples 7 days post-exposure. Bars represent mean $\log_2$(LFQ) values as measured by mass spectrometry and error bars represent standard deviation. Asterisks indicate significant differences (*corrected p-value < 0.05) determined by Student's t-test post FDR correction. **(H)** Boxplot of the $\log_2$ LFQ intensities of SERPINE2 and core histone macro-H2A.1 in irradiated and control NHEK cells 7 days after irradiation. The x represents the mean of all values. Asterisks indicate significant differences (*corrected p-value < 0.05) determined by Student's t-test post FDR correction. **(I)** Compartment-specific proteomic analysis (Parca et al., 2018) of the $\log_2$ fold changes of irradiated NHEK cells in relation to controls. Proteins were assigned to compartments according to GO-terms and each compartment was tested for difference against the whole proteome (Wilcoxon rank sum test with 0.5% FDR correction).

Additionally, increased levels of sequestosome-1 (*SQSTM1*) were observed in irradiated cells (**Fig. 2H**), suggesting late activation of autophagic removal after light stress. In fact, by analyzing compartment-specific changes in the proteome according to the methodology developed by (Parca et al., 2018), we found a significant reduction in the fold changes of mitochondrial proteins in relation to the whole proteome in the long-term, as well as an increase in the fold changes of the lysosomal proteins (Wilcoxon test, 5% FDR correction) (**Fig. 2I**). In this regard, there are evidences that SASP production by

senescent cells elicit a proteotoxic response, affecting cellular metabolism and triggering autophagy as a mechanism for coping with protein unfolding (Dörr et al., 2013). UVA has also been described to impair autophagic flux, which could explain the late cellular repair response (Lamore and Wondrak, 2011).

3.2.3. UVA induces distinct phenotypic signatures in primary and pre-malignant human keratinocytes

We were also interested in how UVA radiation affects keratinocytes at very early stages of tumorigenesis. With that in mind, we used HaCaT cells as a model to understand the effects of UVA radiation in pre-malignant keratinocytes (**Fig. 3A**). HaCaT cells do not harbor any viral sequences (Boukamp et al., 1997; Mueller et al., 2001), and were likely immortalized as a consequence of UV-like mutations in p53 (Lehman et al., 1993), similar to the ones found in skin carcinomas and pre-malignant lesions (Brash, 1997). Therefore, this lineage is used as a model to study very early stages of skin tumorigenesis (Fusenig and Boukamp, 1998). Besides inactivation of the two alleles of p53, HaCaT presents other characteristics of a pre-tumoral, initiated cell line, such as increased telomerase activity, silencing of p16, and defective regulation of p21 expression and function (Ren et al., 2006), all key components of the senescence machinery. HaCaT cells are also able to undergo tumorigenic conversion by overexpression of a single proto-oncogene (NF-κB) (Ren et al., 2006). Despite these alterations, HaCaT cells have a stable chromosome content and remain non-tumorigenic (Boukamp et al., 1997).

HaCaT cells show a distinct pattern of proteome remodeling in response to UVA-induced stress when compared to NHEK cells. As expected, HaCaT cells do not show up-regulation of classical senescence markers, as p16, or of antioxidant and pro-inflammatory enzymes, and do not stain positive for the accumulation of SA β-galactosidase under exposure to UVA radiation in relation to controls (**Fig. 3B**). Moreover, while NHEK cells exhibit a pronounced difference in growth rates between groups, HaCaT cells present only a mild proliferation reduction when irradiated, recovering their proliferative capacity in the long-term (**Fig. 3C**). A proteomic screening of UVA-irradiated and control HaCaT cells in the short and long-terms (24 hours and 7

days after irradiation, respectively) reveals that in the short-term UVA impacts the proteome composition, but in the long-term the proteome returns to homeostasis (**Fig. 3D**). Therefore, under the analysed conditions, we do not have evidence that HaCaT enters senescence 24 hours after exposure to UVA radiation. However it is possible that this cell lineage may have a different senescent phenotype from NHEK cells or that it enters senescence under exposure to higher doses of radiation. For example, it has been shown that HaCaT and NHEK cells both down-regulate a protein involved in senescence, even though HaCaT cells do not stain positive for SA β-galactosidase (Liu et al., 2012).
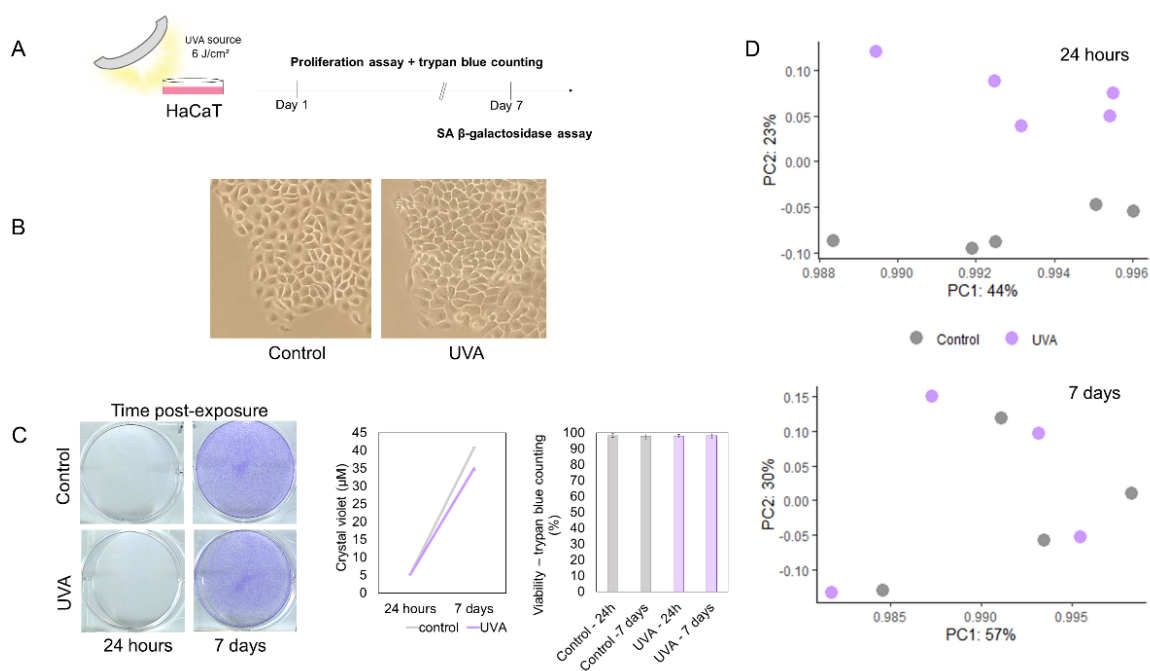
Fig. 3. Immortalized HaCaT cells are resilient to UVA radiation (6 J/cm².)
(A) Simplified workflow of the assays used to confirm senescence resistance in immortalized HaCaT cells exposed to UVA radiation. **(B)** Representative images of control and UVA-irradiated HaCaT cells after SA β-gal staining (n = 3 independent experiments). The assay was performed 7 days after irradiation and no staining was observed in any condition. **(C)** HaCaT cells were exposed to UVA radiation or mock-treated and stained with crystal violet after 24 hours and 7 days. Representative images of the stained plates are shown in the left, and growth curves are shown in the right, with points representing means and error bars representing standard deviation values (n = 3 independent experiments). Trypan counting data are shown in the bar plot, with bars representing means and error bars representing standard deviation (n = 3

independent experiments). **(D)** Principal component analysis of UVA-irradiated and control samples obtained by analyzing the proteome of HaCaT cells 24 hours after irradiation (n = 5 per group) as well as 7 days after exposure to the radiation (n = 4 per group).

A Student's T-test comparison, with 5% FDR correction, yielded 281 differentially abundant protein groups between control and irradiated HaCaT cells 24 hours after treatment. The heatmap of differentially abundant proteins shows separation into two clusters, an up-regulated one, consisting of 83 proteins, and a down-regulated cluster of 198 proteins (**Fig. 4A**). HaCaT cells mostly down-regulates protein levels in response to the radiation stress, in opposition to NHEK cells that show a majoritarian cluster of up-regulated proteins, mostly involved in a potent response against UVA-induced stress.

To compare the effects of UVA on HaCaT and NHEK cells in the short-term, we generated a joint enrichment network considering significantly up and down-regulated proteins of NHEK cells, together with up and down-regulated proteins in HaCaT cells in response to UVA (**Fig. 4B**). The enrichment network shows that UVA radiation leads to a general reduction in anabolic processes as well as a clear pattern of up-regulation in catabolic proteins in HaCaT cells. For example, translation and semantically related terms are the most significantly enriched GO biological terms among down-regulated proteins. Ribosomal subunits and translation initiation factors and activators comprise 22% of all significantly down-regulated proteins in this cell type 24 hours post-exposure to UVA. Epigenetic control of gene expression and RNA processing are also affected by radiation in immortalized cells (represented in the enrichment network by the term "chromatin silencing" (**Fig. 4B**)), with down-regulation of histone levels, i.e. subunits of histones H1, H2 and H3. Of note, core histone macro-H2A.1 is usually up-regulated in senescent cells, being required for SASP production (Contrepois et al., 2017), and has been detected as up-regulated in NHEK cells exposed to UVA, in opposition to the down-regulation observed in HaCaT cells.

Another important differential regulation between the two cell types encompasses the processes "oxidative stress", "chemotaxis", "immune response" and "outer mitochondrial membrane" (**Fig. 4B**). Proteins represented by the "oxidative stress" process are mainly up-regulated in NHEK, which is in line with the senescent phenotype, but are down-

regulated in HaCaT cells. Modulations in the levels of redox-responsive proteins by UVA in NHEK and HaCaT cells 24 hours after irradiation possibly reflects the ability of each of the cell types to deal with reactive oxygen species (ROS) generated by UVA. It has been demonstrated that HaCaT cells display a fast nuclear translocation of Nrf2, a key regulator in the transcription of genes encoding antioxidant enzymes, in response to UVA radiation. Importantly, the same study shows that NHEK and HaCaT cells display contrary responses in most of the Nrf2-controlled proteins, which suggests that these cell types have different antioxidant capacities (Ryšavá et al., 2020). Similarly, proteins involved in immune activation are only up-regulated in NHEK cells 24 hours after stress.

In opposition to the up-regulation of mitochondrial proteins observed in NHEK cells 24 hours after exposure to UVA, all differentially expressed mitochondrial proteins (27 in total) are down-regulated in HaCaT (**Fig. 4B**). Besides down-regulation of respiratory chain components in HaCaT, a few enzymes from the citric acid cycle are also down-regulated. Accordingly, by analyzing changes in the proteome in a compartment-specific fashion, after 24 hours we found a significant decrease in the fold changes of mitochondrial proteins of HaCaT cells in relation to the proteome (Wilcoxon test, 5% FDR correction) (**Fig. 4C**). These results are similar to those obtained with NHEK cells 7 days after irradiation, supporting the notion that HaCaT cells are more resilient to UVA-induced stress when compared to primary keratinocytes.
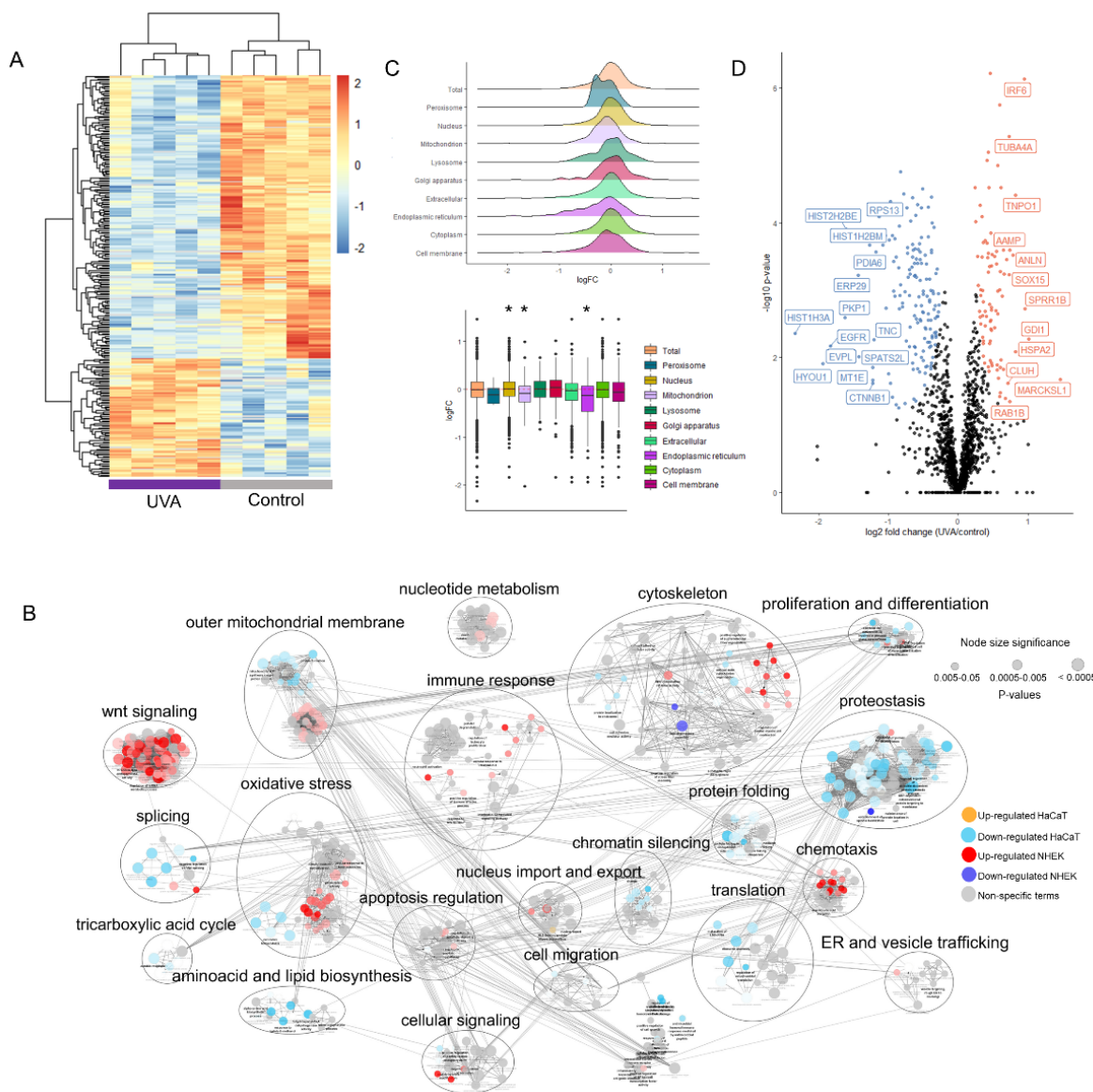
Fig. 4. Proteome remodeling of HaCaT cells in response to UVA radiation (6 J/cm²) 24 hours post-exposure.

(A) Hierarchical clustering of differentially regulated proteins (Student's T-test, 0.05 FDR correction) in HaCaT cells 24 hours after exposure to UVA radiation. The color gradient represents z-scored LFQ intensities and columns represent replicates (n = 5 per group). **(B)** Enrichment network of the up and down-regulated proteins of HaCaT and NHEK cells post-exposure to UVA. Enriched GO-terms for biological processes are shown as nodes, which are interconnected according to the number of genes shared between them. The size of the nodes reflects the significance of the terms (p-value < 0.05, right-sided hypergeometric test, Benjamin-Hochberg FDR correction). Semantically related biological processes were clustered and labeled with AutoAnnotate to facilitate visualization of the network. **(C)** Compartment-specific proteome

changes (Parca et al., 2018) in irradiated versus control HaCaT cells 24 hours after UVA exposure. Values represent $\log_2$(fold change UVA/control). **(D)** Volcano plot highlighting up and down-regulated proteins of irradiated HaCaT cells in relation to controls 24 hours after UVA exposure. Up-regulated proteins are highlighted in orange and down-regulated are highlighted in blue. Significance was defined in this plot by a 0.05 FDR and labels were shown if $\log_2$(Fold Change) > 0.5 or < 0.5.

Even though the majority of differentially regulated proteins are down-regulated in HaCaT 24 hours after irradiation, up-regulated proteins are specifically enriched for cytoskeleton reorganization (*MARCKSL1*, *SPRR1B*, *ANLN*, *TUBA4A*, *TUBA1C*, *MAPRE2*, *TUBB3*, *TTLL12*, *TUBA1B*, *EPPK1*). Cytoskeleton components and regulators of cytoskeleton organization are also among the proteins with the strongest statistical and practical significances between groups (e. g., *TUBA4A*, *ANLN*, *SPRR1B*, *MARCKSL1*) (**Fig. 4D**). *MARCKSL1*, the most up-regulated protein, is associated with increased migratory potential in cancer cells (Liang et al., 2020).

3.2.4. Senescent keratinocytes induce paracrine oxidative stress and immune system activation in pre-tumoral keratinocytes

The relationship between senescence and tumorigenesis has been described through the concept of antagonistic pleiotropy. Even though senescence is a mechanism of tumor suppression, senescent cells may secrete molecules that can stimulate tumorigenesis (Coppé et al., 2010). For example, senescent fibroblasts have been shown to stimulate proliferation of pre-malignant and malignant, but not normal, primary epithelial cells (Krtolica et al., 2001). On the other hand, primary human keratinocytes have been shown to be susceptible to paracrine senescence (Acosta et al., 2013; Nelson et al., 2012). Considering these evidences, we aimed at evaluating the paracrine effects of keratinocytes under UVA-induced senescence on the proteome of pre-tumoral, initiated HaCaT cells. HaCaT cells were used as a pre-tumoral model in this assay because they acquired p53 mutations during immortalization and have a defective senescence machinery. In this sense, HaCaT's genetic background predispose these cells to malignancy and prevent these cells from entering paracrine senescence. Even though there are limitations to using an immortalized cell line as a pre-tumoral model, HaCaT's acquired mutations in p53 can be useful in a pre-tumoral context because pre-

tumoral, p53-mutated cells are commonly found in the skin after exposure to UV (Murai et al., 2018).

For this assay, NHEK cells were irradiated with UVA radiation and maintained in culture for 7 days. On the first, third and fifth day after irradiation, conditioned medium containing NHEK-secreted molecules was centrifuged for removal of dead cells and transferred to HaCaT cells. In the seventh day, HaCaT cells were lysed and analyzed by mass spectrometry (a simplified scheme of the protocol is shown in **Fig. 5A**). In this experiment, control cells were treated with conditioned medium of non-irradiated primary cells.

Hierarchical clustering of 120 proteins with statistically different levels between HaCaT cells that received NHEK-irradiated secretome or the secretome of non-irradiated NHEK cells reveals the formation of up and down-regulated clusters, comprising 83 and 37 proteins, respectively (**Fig. 5B**). This result indicates the secretory phenotype of senescent keratinocytes is able to provoke changes in immortalized neighboring cells. The down-regulated cluster is mostly associated to translation, as has been previously observed to occur in UVA-exposed HaCaT cells (**Fig. 5C**). Interestingly, the up-regulated cluster is associated to immune system activation, detoxification of reactive species, and increased levels of structural mitochondrial proteins (**Fig. 5C**) (see Table 1 for specific proteins associated to these processes). These results suggest that exposure of immortalized HaCaT cells to senescent primary keratinocytes elicits a continuous anti-oxidant and pro-inflammatory response in these cells. Up-regulated proteins are also enriched for "keratinocyte proliferation", suggesting modulations in the differentiation and proliferation capabilities of these cells. Immortalized keratinocytes also mimic some the responses of senescent keratinocytes by up-regulating laminin subunits (LAMC2, LAMB3, LAMA3) and few members of the serpin family (SERPINB1 and SERPINB13), which are usually secreted in the SASP of senescent cells (Spreadsheet S1). A limitation of this experiment is that we transferred the medium of NHEK cells to HaCaT 7 days post-exposure, when cells display a difference in confluence between conditions. Therefore, the smaller amounts of senescent cells relatively to confluent controls may consume different nutrient amounts from the culture

medium and this may impact the mitochondrial metabolism of HaCaT cells exposed to it differently.
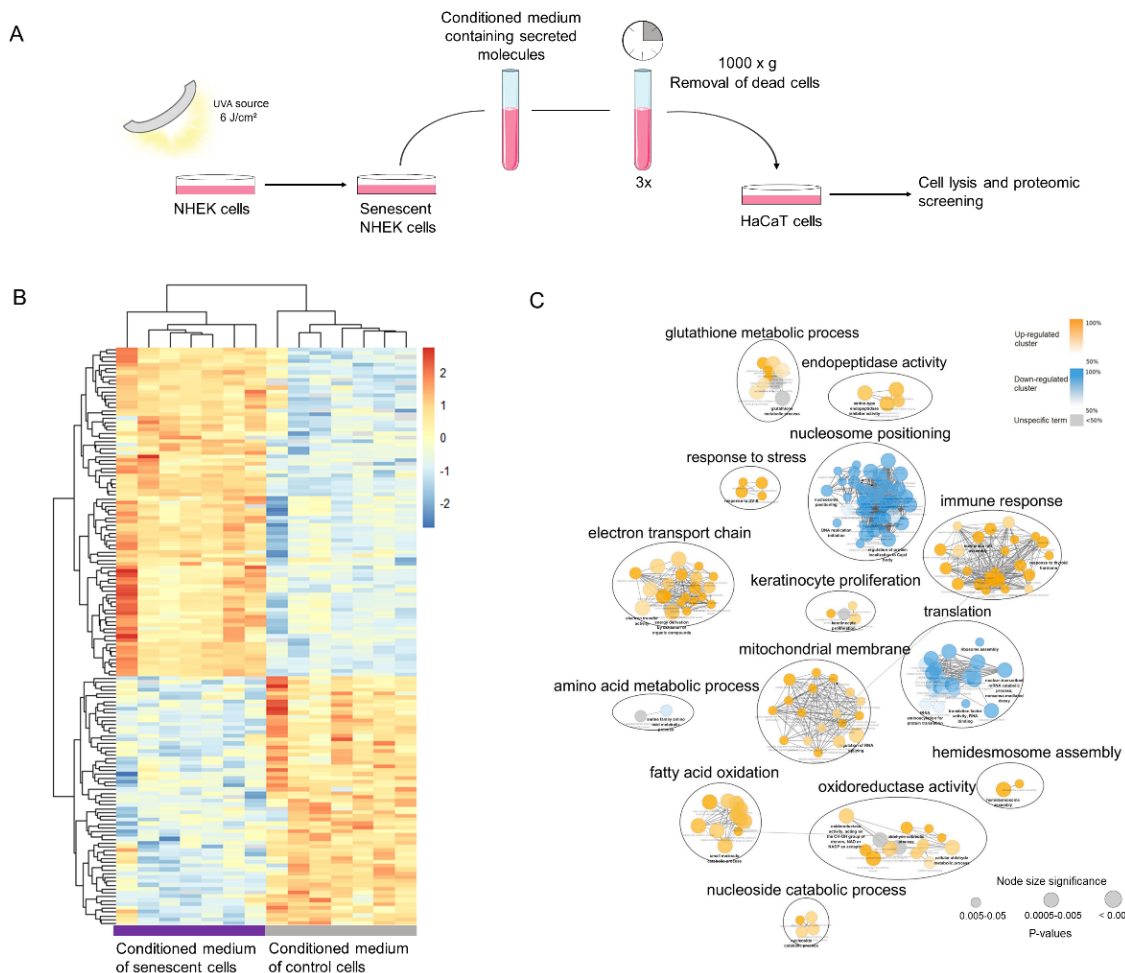
Fig. 5. Proteome response of HaCaT cells to conditioned medium of senescent primary keratinocytes.

(A) Scheme of the experimental approach performed to investigate bystander effects of senescent keratinocytes in immortalized cells. **(B)** Hierarchical clustering of differentially regulated proteins (Student's T-test, 0.05 FDR correction) comparing HaCaT cells that received NHEK-irradiated secretome with those receiving the secretome of non-irradiated NHEK cells. The color gradient represents z-scored LFQ intensities and columns represent replicates (n = 7 per group). **(C)** Enrichment network of the up and down-regulated clusters identified in the heatmap showed in b. Enriched GO-terms for biological processes are shown as nodes, which are interconnected according to the number of genes shared between them. The size of the nodes reflects the significance of the terms (p-value < 0.05, right-sided hypergeometric test,

Benjamin-Hochberg FDR correction). Related biological processes were clustered and labeled with AutoAnnotate.

Table 1. Differentially regulated proteins in HaCaT cells treated with conditioned medium from senescent keratinocytes (proteins are associated with major significantly enriched GO-terms).

Process	Gene name	Protein name	Fold Change
Immune system	LGALS7	Galectin-7	2.78
	S100A2	Protein S100-A2	2.78
	SERPINB1	Leukocyte elastase inhibitor	1.97
	SERPINB13	Serpin B13	1.87
	CAPG	Macrophage-capping protein	1.72
	LGALS3	Galectin-3	1.72
	SERPINB2	Plasminogen activator inhibitor 2	1.61
	CTSB	Cathepsin B	1.61
	SERPINB5	Serpin B5	1.58
	S100A14	Protein S100-A14	1.56
	S100A11	Protein S100-A11	1.52
	SERPINB8	Serpin B8	1.52
	S100A10	Protein S100-A10	1.39
	IRF6	Interferon regulatory factor 6	1.38
	S100A16	Protein S100-A16	1.32
Oxidative stress	PRDX5	Peroxiredoxin-5, mitochondrial	1.94
	GSTK1	Glutathione S-transferase kappa 1	1.51
	TXNDC17	Thioredoxin domain-containing protein 17	1.48
	AKR1A1	Alcohol dehydrogenase [NADP(+)]	1.43
	GSTP1	Glutathione S-transferase P	1.39
	GSR	Glutathione reductase, mitochondrial	0.75
Respiratory function	SQRDL	Sulfide:quinone oxidoreductase, mitochondrial	1.62
	COX6B1	Cytochrome c oxidase subunit 6B1	1.53
	SDHB	Succinate dehydrogenase [ubiquinone] iron-sulfur subunit	1.46
	NDUFA10	NADH dehydrogenase [ubiquinone] 1 alpha subcomplex subunit 10	1.39
Keratinocyte proliferation	IVL	Involucrin	4.19
	LAMA3	Laminin subunit alpha-3	2.37
	LAMC2	Laminin subunit gamma-2	2.37
	LAMB3	Laminin subunit beta-3	2.18
	CRABP2	Cellular retinoic acid-binding protein 2	2.00
	SERPINB13	Serpin B13	1.87
	PSAP	Prosaposin	1.86
	FERMT1	Fermitin family homolog 1	1.82
	ITG6A	Integrin alpha-6	1.60

|		
SRSF6	Serine/arginine-rich splicing factor 6	0.73
CD109	CD109 antigen	0.68
KRT18	Keratin, type I cytoskeletal 18	0.67

To investigate possible mediators of the paracrine responses in pre-tumoral HaCaT cells induced by keratinocytes under UVA-induced senescence, we analyzed the secretome of NHEK cells 24 hours after exposure to 6 J/cm² of UVA. A total of 254 proteins were quantified in all samples. Additionally, a total of 5 and 297 proteins were exclusively quantified in controls and UVA-irradiated samples, respectively (**Fig. 6A**). For a protein group to be considered present only in one condition, it had to be consistently quantified in all 3 biological replicates of this condition and completely absent in the other.

Consistently with our previous results, the levels of proteins involved in inflammatory processes were increased in the secretome of irradiated cells (**Fig. 6B**). Notably, p16 levels were also increased in irradiated cells compared to controls, consistently with the up-regulation we observed in cell lysates. The most enriched terms for up-regulated proteins in the secretome of irradiated cells are "neutrophil degranulation", "neutrophil activation in immune response" and "neutrophil mediated immunity", reinforcing the role of pro-inflammatory proteins in the paracrine effects triggered by cells under UVA-induced senescence in pre-tumoral keratinocytes.

For instance, we detected up-regulation in the secretion of a few members of the SERPIN and S100 family (*S100A8, S100A13, S100A16, S100A2, SERPINB6, SERPINB8, SERPINB5, SERPINB1*), similarly to the trend we observed in lysates of cells exposed to UVA and conditioned medium (**Fig. 6C-D**). Cells under UVA-induced stress also differentially secrete *IL1RN*, *TOLLIP*, *MIF*, in agreement with the up-regulation observed for these proteins in lysates of NHEK cells 24 hours after exposure to UVA. Furthermore, the levels of other relevant mediators of inflammation were altered in the secretome of irradiated cells, such as *IRF6, MX1, ILF3*. In this sense, *IRF6* and *MX1*, are involved in interferon signaling and are differentially regulated across most of the datasets we analyzed in this study. *MX1* is particularly up-regulated in NHEK cells 7 days post-exposure to UVA. *IRF6* is increased in HaCaT cells exposed to UVA and to the conditioned medium of senescent keratinocytes. *STAT1*, a transcription factor

responsible for mediating type I interferon responses, is up-regulated in NHEK cells 24 hours and 7 days post-exposure to UVA.

Additionally, the levels of redox-responsive enzymes were also increased in the secretome of irradiated cells compared to controls (*CAT*, TXN isoforms, PRDX isoforms, PDI isoforms, as well as a few HSP). It is possible that some of these proteins are secreted by cells under oxidative stress. It has been shown that cells under starvation, for example, increase ROS production and secrete antioxidant enzymes to prevent ROS-mediated damage in the extracellular space (Cruz-Garcia et al., 2020). A complete list of up and down-regulated proteins in NHEK secretome is available in **Supplementary Spreadsheet S3** on **APPENDIX 2**.
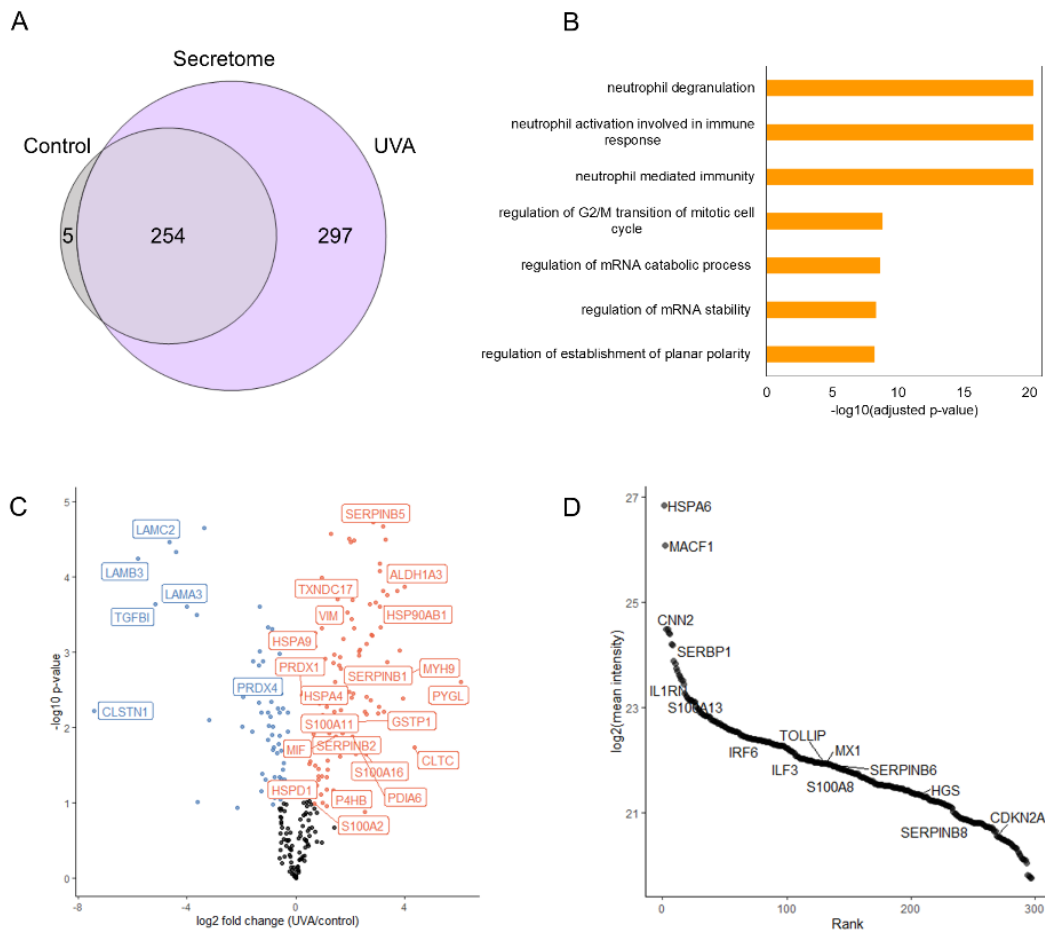
Fig. 6. Secretome of NHEK cells irradiated with UVA radiation (6 J/cm², 24 hours post-exposure).

(A) Venn diagram representing the secretome of control and irradiated cells (n = 3 per group). **(B)** Enrichment analysis of up-regulated proteins in the secretome of irradiated NHEK cells. **(C)** Volcano plot representing up and down-regulated proteins in the secretome of irradiated NHEK cells in comparison to controls 24 hours after UVA exposure. Up-regulated proteins are highlighted in orange and down-regulated -proteins are highlighted in blue. Significance was defined in this plot by a 0.05 FDR and labels were shown if $\log_2$(Fold Change) > 0.5 or < 0.5. **(D)** Intensity-based ranking of proteins identified exclusively in the secretome of irradiated NHEK cells.

3.3. Discussion

Skin aging is thought to be driven by intrinsic and extrinsic damage to biomolecules (Hernandez-Segura et al., 2018). Cells burdened with accumulated damage may die and not be replaced, contributing to the functional decline of tissues (Battie et al., 2014). On the other hand, cells may undergo phenotypic reprogramming and lose their proliferative capacity, a process that has been termed senescence (Campisi, 1998). In this context, UVA has been described to induce apoptosis in dermal fibroblasts, leading to dermal alterations usually observed during aging (Battie et al., 2014; Bernerd and Asselineau, 1998). UVA has also been reported to induce senescence in skin fibroblasts, up-regulating p16, p21, p53, SA β-galactosidase, and *MMP1* (Fagot et al., 2004; Fitsiou et al., 2020), thus playing a key role in dermal photoaging. Much less is known about the impact of UVA on the decline in epidermal function, even though epidermal aging is a risk factor for skin cancer and other skin diseases.

While UVB-induced senescence has been well-characterized (Debacq-Chainiaux et al., 2005), the only evidence to date suggesting senescence induction by UVA on keratinocytes relies on the fact that UVA modulates the levels of p63, ki67, and activated caspase-3 in the germinative layer of the epidermis (Casale et al., 2018). Importantly, senescence is a dynamic cellular reprogramming that may assume different phenotypes depending on the inducer and cell type (Lee and Schmitt, 2019). For example, there are differences in the secretory profile of senescent epithelial cells and fibroblasts (Basisty et al., 2020). Here, we characterized for the first time UVA-induced senescence in primary keratinocytes as dependent on anti-oxidant and pro-inflammatory responses, agreeing with UVA's acknowledged oxidative action (Schuch et al., 2017). Senescence

induction was confirmed by well-recognized senescence hallmarks (e.g., p16, SA β-galactosidase staining and impaired proliferation). In the short-term, up-regulation of structural mitochondrial proteins and alterations in translation components and regulators could reflect increases in mitochondrial mass and proteotoxic stress generally observed in stress-induced senescent phenotypes (Deschênes-Simard et al., 2014; Korolchuk et al., 2017). In the long-term, UVA-exposed cells still bear senescence markers, while exhibiting increased levels of lysosomal proteins and up-regulation of sequestosome-1, that could indicate the development of a late cellular repair response to cope with radiation stress. Senescent phenotypes have been shown to lead to ER stress, unfolded protein response and consequently autophagy as a mechanism for coping with proteotoxic stress (Dörr et al., 2013). UVA has also been reported to induce autophagic-lysosomal alterations that could result in impaired or late autophagic response (Lamore and Wondrak, 2011). On the other hand, HaCaT keratinocytes were not observed to be as susceptible to the effects of direct UVA exposure as primary cells under our experimental conditions, recovering completely from UVA-stress in less than 7 days, probably due to adaptations developed by these cells during immortalization. As mentioned previously, it is possible that this cell lineage may have a different senescent phenotype from NHEK cells (Liu et al., 2012). It is also possible that these cells may enter senescence under exposure to higher doses of radiation or at longer periods after exposure.

A few proteomics studies have evaluated the effects of UVA radiation on skin cells. In rats, chronic exposure to UVA modulates anti-oxidant proteins, inflammatory mechanisms and apoptosis in the skin (Atalay et al., 2021). In hairless mice, an acute dose of 20 J/cm² of UVA radiation on the dermis affected mitochondrial function, calcium metabolism and cytoskeleton signaling. These effects were prevented by carnosine, a free radicals scavenger (Radrezza et al., 2021). Exposure of hairless mice to 15 J/cm² of UVA radiation lead to fibroblast senescent patterns characterized by accumulation of 4-hydroxynonenal (HNE) adducts, DNA damage and ubiquitinated proteins. Topical application of carnosine, prevented adducts formation, DNA damage and senescence induction (Swiader et al., 2021). In cultured fibroblasts, exposure to 20 J/cm² of UVA radiation lead to changes in the levels of proteins associated with inflammation, anti-oxidant response and apoptosis. This study also revealed that rutin, an antioxidant with

polyphenolic structure, protected fibroblasts from UVA-induced effects more efficiently than from UVB damage (Gęgotek et al., 2018). Moreover, Gęgotek and collaborators (Gęgotek et al., 2019) found that 20 J/cm² of UVA up-regulates components of the DNA damage response, antioxidant proteins (peroxiredoxin-1, superoxide dismutase, glutathione reductase and glutathione S-transferase), as well as pro-apoptotic and inflammatory mechanisms in 3D cultured keratinocytes. Finally, another study (Narzt et al., 2019) based on a multi-omics approach revealed that 40 J/cm² of UVA lead to the generation of phospholipid hydroperoxides, with consequent up-regulation of antioxidant enzymes (peroxiredoxin 6 and glutathione peroxidase) in primary keratinocytes. Importantly, both UVA exposure and administration of *in-vitro* UVA-oxidized phospholipids to keratinocytes lead to modulations in lipid metabolism and antioxidant mechanisms. Our work is in agreement with previous findings, reinforcing the role of oxidant and inflammatory mechanisms in the stress response of keratinocytes to UVA. In addition, our results show that stress response may accompany the development of a senescent phenotype in keratinocytes, and is relevant in an environmental context of exposure to a considerably low UVA dose of 6 J/cm².

The control of the proliferative potential of keratinocytes in response to sun damage is at the heart of skin tumorigenesis, since all forms of skin cancer develop from epidermal cells and mainly from keratinocytes (Leiter et al., 2014). While senescent fibroblasts have been shown to stimulate the proliferation and malignancy of epithelial pre-tumoral cells, information about the paracrine effects of senescent cells on the proteome of pre-tumoral keratinocytes remains elusive. With that in mind, we characterized the response of pre-malignant HaCaT cells to neighboring senescent primary keratinocytes. HaCaT cells exposed to conditioned medium of senescent keratinocytes mimic the antioxidant and inflammatory responses developed during senescence, even though they do not suffer from permanent cell cycle arrest, as would be expected of primary cells susceptible to paracrine senescence (Acosta et al., 2013; Nelson et al., 2012). Triggering of antioxidant response in HaCaT cells exposed to conditioned medium could reflect paracrine damage induction in HaCaT cells by senescent keratinocytes, as has been previously reported to occur in senescence phenotypes (Nelson et al., 2012; Victorelli et al., 2019). Secretome analysis revealed pro-inflammatory mediators are the main drivers of intercellular communication between primary and pre-tumoral cells.

99

Importantly, phenotypic changes in both normal and pre-tumoral cells, accumulating oxidative damage and mutational load in combination with altered inflammation over time are factors contributing to how aging favors skin cancer (Persa et al., 2021) (a simplified scheme of our proposed model is shown in **Fig. 7**).
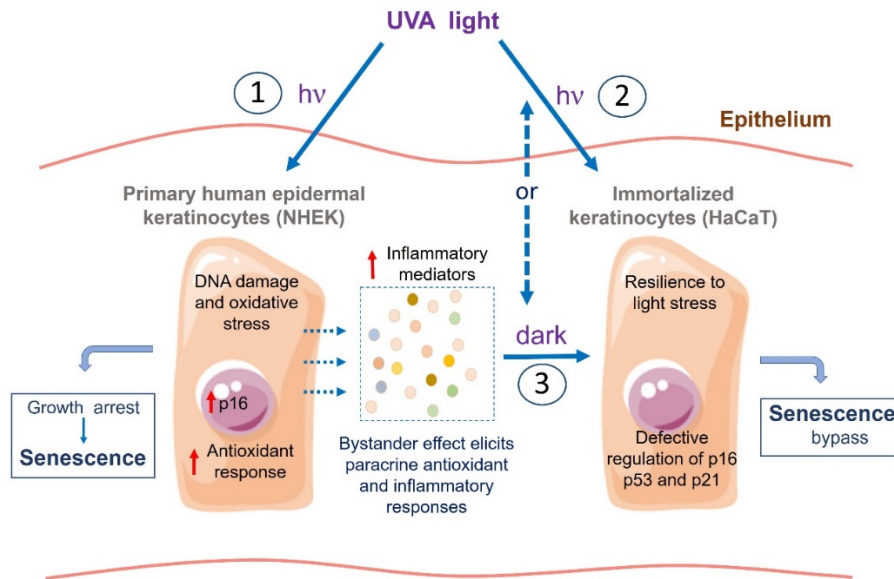
Figure 7: Proposed model of UVA-induced senescence in the epidermis.
Genotoxic and oxidative stresses are biological effects of UVA light leading to the accumulation of senescent cells over time in the skin. Using cell-culture models, we show that UVA induces senescence in primary keratinocytes **(1)**. Pre-malignant HaCaT cells are not as susceptible to the effects of direct UVA exposure as primary cells, probably due to adaptations developed by these cells during immortalization **(2)**. However, HaCaT cells are susceptible to the effects of inflammatory mediators secreted by senescent keratinocytes **(3)**.

3.4. Materials and methods

3.4.1. Experimental model

HaCaT cells were kindly provided by Professor Mauricio S. Baptista (Institute of Chemistry, University of São Paulo) and were grown in DMEM basal medium supplemented with 10% fetal bovine serum, 100 U/mL penicillin and 100 ug/mL streptomycin. Normal human epidermal keratinocytes (NHEK) were obtained from Lonza and were cultured in Keratinocyte SFM basal medium supplemented with human

recombinant epidermal growth factor and bovine pituitary extract (Thermo Scientific). Cells were tested for mycoplasma contamination.

3.4.2. Irradiation conditions

An Oriel SOL-UV 2 solar simulator (Newport) equipped with a Xenon arc lamp was used for cellular irradiation. The simulator was equipped with an infrared bandpass and a UVB blocking filter (emission spectra of the radiation emitted by the simulator is provided in **Figure S1** on **APPENDIX 2**). Before irradiation, the output of the simulator was measured with a dosimeter from International Light Inc (Newburyport), model IL1700, with a SED033 detector. The output of the simulator was measured at a 10 cm distance from the radiation source, where the plates were positioned, yielding a mean of 4.2 mW/cm² with maximum variation of 10% between biological replicates. Each cell plate was irradiated for 26 minutes to deliver a total dose of 6 J/cm². In preliminary experiments, we tested two different doses of UVA radiation (6 and 12 J/cm²). Upon irradiation with 6 J/cm², more than 90% of cells were viable (as shown in more detail in the previous chapter). Thus, we chose this dose to evaluate non-citotoxic effects of UVA radiation on the proteome of skin cells.

After irradiation, cells were washed three times with Phosphate Buffer Saline (PBS), and kept in PBS during the irradiation. Control cells were kept in PBS and in the dark at room temperature during the whole irradiation period.

3.4.3. Senescence associated β-galactosidase assay

Cells were irradiated and processed for the senescence-associated (SA) β-galactosidase assay (Dimri et al., 1995) seven days after treatment. Cells were washed two times with PBS, fixed for 4 minutes with 3% formaldehyde at room temperature, washed four times with PBS, and incubated at 37º C (in the absence of CO_2) with the staining solution (1 mg/mL x-gal, 40 mM citric acid/Na phosphate buffer, 5 mM potassium ferrocyanide, 5 mM potassium ferricyanide, 150 mM sodium chloride, 2 mM

magnesium chloride in water at pH 6), according to (Dimri et al., 1995). For each experiment and condition, 100 cells were counted.

3.4.4. Proliferation assay

Cells were irradiated with UVA and processed 24 hours and 7 days after exposure. For the proliferation assay (Feoktistova et al., 2016), cells were washed two times with PBS and incubated for 20 minutes at room temperature under agitation with 0.5% crystal violet. Cells were washed again 5 times with PBS, plates were scanned, crystals were resuspended in methanol (2 mL for each well of a 6-well plate) and the absorbance of each sample was measured. Measurements are accompanied by the trypan counting (Strober, 1997) to assure that the assay assessed proliferation and not cell death.

3.4.5. Secretome transfer

NHEK cells were irradiated with UVA and maintained in culture for 7 days in order to develop a senescent phenotype. On the first, third and fifth day after irradiation, the conditioned medium containing secreted molecules was centrifuged three times for 15 minutes at 1000 x g for removal of dead cells and transferred to HaCaT cells. On the seventh day, HaCaT cells were washed 5 times with PBS, lysed and proteins were analyzed by mass spectrometry. Control cells were treated with the conditioned medium of non-irradiated primary cells. Since NHEK and HaCaT cells were cultured in different mediums, NHEK's conditioned medium was added to HaCaT in a 1:1 (v/v) proportion in relation to DMEM. Controls were exposed to the same medium mixture.

3.4.6. Secretome sample preparation

NHEK cells were irradiated in PBS and kept overnight in DMEM basal medium, supplemented with KGM™ Gold Keratinocyte Growth Medium SingleQuots™ Supplements and Growth Factors (Lonza), without fetal bovine serum and phenol red. The supernatants were collected and centrifuged 3 times for 15 minutes at 3000 x g. Afterwards, the samples were concentrated in 3kDa Amicon® Ultra cut-off filters (Millipore). Final protein concentration was measured using a Pierce™ BCA Protein Assay Kit (Thermo Scientific), according to the manufacturer's instructions.

3.4.7. Cell lysate sample preparation

For proteomics experiments, 400,000 cells were plated in 6-well plates 24 hours before the experiments. After irradiation, cells were washed five times with PBS, and scraped in 500 µL of a solution containing 100 mM ammonium bicarbonate, 8 M urea and protease inhibitors (cOmplete™ Protease Inhibitor Cocktail, Roche). Cell lysates were kept on ice for one hour and, after that, they were precipitated overnight with 3 volumes of cold (-20 °C) acetone. Precipitated proteins were collected by centrifugation. Pellets were air-dried for about 10 minutes and resuspended in 100 mM ammonium bicarbonate buffer containing 8 M urea. Protein concentration was measured using a Pierce™ BCA Protein Assay Kit (Thermo Scientific).

3.4.8. Protein digestion

Aliquots corresponding to 10 µg of protein per sample were reduced with 5 mM dithiothreitol for one hour and alkylated with 15 mM iodoacetamide for 30 minutes, at 30 °C with agitation (400 rpm). Then, the samples were diluted ten-fold with 100 mM ammonium bicarbonate, and digested by the addition of two aliquots of trypsin (in the proportions of 1:40 and 1:50 w/w, respectively, with an interval of four hours between the additions). The samples were digested overnight at 30°C with agitation (400 rpm). Digestion was stopped by adding 4% trifluoracetic acid (TFA), and then the samples were dried. Samples were desalted using the StageTip protocol (Rappsilber et al., 2007). Peptides were washed ten times with 0.1% TFA in the StageTips and eluted with 50% acetonitrile and 0.1% TFA.

3.4.9. LC-MS/MS measurements

Each sample was analyzed in an Orbitrap Fusion Lumos mass spectrometer coupled to a Nano EASY-nLC 1200 (Thermo Scientific, Bremen, Germany). Peptides were injected into a trap column (nanoViper C18, 3 µm, 75 µm × 2 cm, Thermo Scientific) with 12 µL of solvent A (0.1% formic acid) at 980 bar. After this period, the trapped peptides were eluted onto a C18 column (nanoViper C18, 2 µm, 75 µm × 15 cm, Thermo Scientific) at a flow rate of 300 nL/min and separated with a gradient of 5-28% acetonitrile with 0.1% formic acid for 80 minutes, followed by 28-40% acetonitrile with formic acid for 10

minutes. The eluting peptides were detected in data-dependent acquisition mode using positive electrospray ionization. A full scan (m/z 400-1600) was acquired at a 60000 resolution, followed by HCD fragmentation of the most intense ions, considering an intensity threshold of 5×10^4. Ions were filtered for fragmentation by a quadrupole with a transmission window of 1.2 *m/z*. HCD fragmentation was performed with a normalized collision energy of 30 and the fragments were analyzed by the Orbitrap at resolution of 30000. The number of MS2 events between full scans were determined by a cycle time of 3 seconds. A total of 5×10^5 and 5×10^4 ions were injected in the Orbitrap with an accumulation time of 50 and 54 seconds for the full scan and MS2 acquisition, respectively. Monocharged ions or ions with undetermined charge were not selected for fragmentation.

3.4.10. Proteomics data analysis

Raw files were processed using MaxQuant version 1.6.17.0 (Cox and Mann, 2008). The Andromeda algorithm (Cox et al., 2011) was used for protein identification against the homo sapiens Uniprot database (downloaded August, 2019; 20416 entries). Error mass tolerance for precursors and fragments were set to 4.5 ppm and 20 ppm, respectively. Cysteine carbamidomethylation was selected as a fixed modification and methionine oxidation and *N*-terminal acetylation were selected as variable modification. Trypsin was set as digestion enzyme, with a maximum of 2 missed cleavages allowed. A maximum FDR of 1% was allowed both for peptides and proteins identification, and for proteins it was calculated using a decoy database created from the reverse ordination of the protein sequences in the Uniprot database. Identification of at least two peptides (unique + razor) was set as a parameter for the identification of a protein. Protein abundances were quantified by the LFQ algorithm, based on the normalized chromatographic peak integrations generated by MaxQuant. Other parameters were kept as default.

Before statistical analysis, the data were log-transformed, and matches to the contaminants and reverse database, as well as proteins identified only by modified sites, and missing values (< 30% in all samples) were filtered out. Statistical significance was assessed using a two-tailed Student's T-test in Perseus version 1.5.5.3 (Tyanova et al., 2016) with a permutation-based false discovery rate (FDR) of 5% and a S_0 parameter of 0.1. The plots were displayed in the R statistical computing environment (RStudio

version 2021.09.1+372), using libraries, ggplot2 (version 3.3.5) and pheatmap (version 1.0.12). The number of independent replicates for each experiment is specified in the legends of their respective figures.

3.4.11. Network Analysis

For functional network analysis, we used the ClueGO (version 2.5.4) (Bindea et al., 2009) and AutoAnnotate (version 1.3) (Kucera et al., 2016) apps in Cytoscape (version 3.7.1) (Shannon et al., 2003). ClueGO presents enrichment analysis as a network of interconnected nodes representing gene ontology (GO) biological processes, with edges representing kappa scores (a statistic based on the number of genes shared between different biological processes) (Bindea et al., 2009). Benjamin-Hochberg correction for multiple hypotheses was applied to the results of a hypergeometric test based on the enrichment analysis and all networks represent processes that have a corrected p-value lower than 0.05. Clusterization of semantically-related terms was performed with AutoAnnotate to facilitate visualization of the network.

3.4.12. Data availability

The proteomic datasets generated during this study have been deposited to the ProteomeXchange Consortium (http://www.proteomexchange.org/) via the PRIDE repository (identifier: PXD025191).

APPENDIX 2: SUPPLEMENTAL INFORMATION – CHAPTER 2
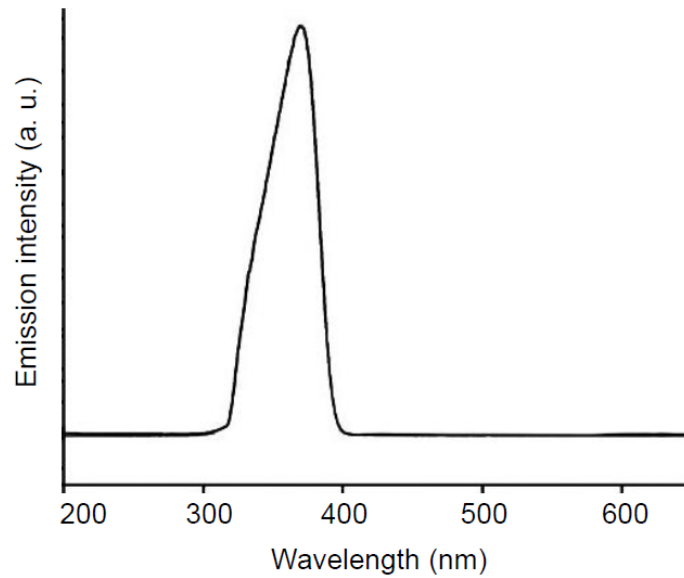
Figure 1S: Emission spectrum of the UVA radiation emitted by the Oriel SOL-UV 2 solar simulator.

Spreadsheets

Spreadsheet S1.

Perseus data table output for the datasets involving changes in protein levels

Spreadsheet S2.

ClueGO enrichment data output

Spreadsheet S3.

Protein-level Perseus data table output for the secretome dataset

The datasets generated during this study are available at doi.org/10.1038/s41598-021-02658-5 .

4. CONCLUSION AND PERSPECTIVES

In this work, we were able to provide a detailed inventory about the effects of a low, non-cytotoxic dose of UVA radiation on the proteome of human keratinocytes.

First, we mapped changes in protein subcellular localization triggered by UVA immediately after irradiation. Our experimental strategy employing subcellular fractionation, MS-based proteomics and machine learning algorithms revealed that UVA redistributed approximately 20% of the proteome of human keratinocytes. Validated protein redistributions were driven mainly by mitochondrial fragmentation, DNA damage and redox modulations, consistently with UVA's known biological action. Mitochondria were particularly affected by UVA radiation, displaying decreased respiratory rates upon fragmentation. In this sense, our study opens up possibilities for further investigations of endogenous UVA chromophores involved in mitochondrial damage. Our dataset also opens up possibilities for further investigation of UVA-triggered translocation events in less studied subcellular niches. It has been shown that ER and Golgi vesiculation occur in UV-exposed cells and our approach detected redistributions of proteins from these compartments upon stress. Importantly, because we performed the spatial proteomics experiment 30 minutes after exposure to UVA, our analysis provides information on early signaling events triggered by cellular stress.

In the long-term, UVA radiation affects the cell fate of primary keratinocytes by leading to a senescent phenotype and impairing cellular proliferation. Changes in protein levels revealed that UVA-induced senescence is accompanied by antioxidant and pro-inflammatory responses, as expected from UVA's biological action. We also demonstrated that primary cells and the pre-malignant HaCaT lineage are differentially affected by UVA radiation, with HaCaT cells being more resilient to light stress. However, HaCaT cells are susceptible to the paracrine effects of primary keratinocytes under UVA-induced senescence. Using a secretomics assay, we demonstrate that UVA-

107

induced paracrine effects in pre-malignant cells are elicited by release of inflammatory mediators from senescent keratinocytes. Altogether, these results provide a more detailed view of UVA's immunomodulatory effects, particularly upon exposure to a low radiation dose.

Finally, we hope that this thesis can contribute to further investigations of skin photobiology. For example, examination of the less well-known effects of other radiations (infrared or visible light, e.g.) on the proteome of skin cells is very scarce. Alternatively, investigation of the response of different cell types to these radiations also remains to be further explored.

5. REFERENCES

Abu-Mostafa, Y. S., Magdon-Ismail, M., & Lin, H. (2012). Learning from data : a short course. [United States]: AMLBook.com.

Acosta, J. C., Banito, A., Wuestefeld, T., Georgilis, A., Janich, P., Morton, J. P., Athineos, D., Kang, T.-W., Lasitschka, F., Andrulis, M., Pascual, G., Morris, K. J., Khan, S., Jin, H., Dharmalingam, G., Snijders, A. P., Carroll, T., Capper, D., Pritchard, C., … Gil, J. (2013). A complex secretory program orchestrated by the inflammasome controls paracrine senescence. Nature Cell Biology, 15(8), 978–990. https://doi.org/10.1038/ncb2784

Aebersold, R., Agar, J. N., Amster, I. J., Baker, M. S., Bertozzi, C. R., Boja, E. S., Costello, C. E., Cravatt, B. F., Fenselau, C., Garcia, B. A., Ge, Y., Gunawardena, J., Hendrickson, R. C., Hergenrother, P. J., Huber, C. G., Ivanov, A. R., Jensen, O. N., Jewett, M. C., Kelleher, N. L., … Zhang, B. (2018). How many human proteoforms are there? Nature Chemical Biology, 14(3), 206–214. https://doi.org/10.1038/nchembio.2576

Aebersold, R., & Mann, M. (2016). Mass-spectrometric exploration of proteome structure and function. Nature, 537(7620), 347–355. https://doi.org/10.1038/nature19949

Agar, N. S., Halliday, G. M., Barnetson, R. S., Ananthaswamy, H. N., Wheeler, M., & Jones, A. M. (2004). The basal layer in human squamous tumors harbors more UVA than UVB fingerprint mutations: A role for UVA in human skin carcinogenesis. Proceedings of the National Academy of Sciences, 101(14), 4954–4959. https://doi.org/10.1073/pnas.0401141101

Aird, K. M., Worth, A. J., Snyder, N. W., Lee, J. V., Sivanand, S., Liu, Q., Blair, I. A., Wellen, K. E., & Zhang, R. (2015). ATM Couples Replication Stress and Metabolic

Reprogramming during Cellular Senescence. *Cell Reports*, *11*(6), 893–901. https://doi.org/10.1016/j.celrep.2015.04.014

An, M., Colarelli, S. M., O'Brien, K., & Boyajian, M. E. (2016). Why We Need More Nature at Work: Effects of Natural Elements and Sunlight on Employee Mental Health and Work Attitudes. PLOS ONE, 11(5), e0155614. https://doi.org/10.1371/journal.pone.0155614

Andersen, J. S., Wilkinson, C. J., Mayor, T., Mortensen, P., Nigg, E. A., & Mann, M. (2003). Proteomic characterization of the human centrosome by protein correlation profiling. Nature, 426(6966), 570–574. https://doi.org/10.1038/nature02166

Archier, E., Devaux, S., Castela, E., Gallini, A., Aubin, F., Le Maître, M., Aractingi, S., Bachelez, H., Cribier, B., Joly, P., Jullien, D., Misery, L., Paul, C., Ortonne, J.-P., & Richard, M.-A. (2012). Carcinogenic risks of psoralen UV-A therapy and narrowband UV-B therapy in chronic plaque psoriasis: A systematic literature review. Journal of the European Academy of Dermatology and Venereology: JEADV, 26 Suppl 3, 22–31. https://doi.org/10.1111/j.1468-3083.2012.04520.x

Asgatay, S., Martinez, A., Coantic-Castex, S., Harakat, D., Philippe, C., Douki, T., & Clivio, P. (2010). UV-Induced TA Photoproducts: Formation and Hydrolysis in Double-Stranded DNA. Journal of the American Chemical Society, 132(30), 10260–10261. https://doi.org/10.1021/ja1023173

Ashburner, M., Ball, C. A., Blake, J. A., Botstein, D., Butler, H., Cherry, J. M., Davis, A. P., Dolinski, K., Dwight, S. S., Eppig, J. T., Harris, M. A., Hill, D. P., Issel-Tarver, L., Kasarskis, A., Lewis, S., Matese, J. C., Richardson, J. E., Ringwald, M., Rubin, G. M., & Sherlock, G. (2000). Gene Ontology: Tool for the unification of biology. Nature Genetics, 25(1), 25–29. https://doi.org/10.1038/75556

Assefa, Z., Van Laethem, A., Garmyn, M., & Agostinis, P. (2005). Ultraviolet radiation-induced apoptosis in keratinocytes: On the role of cytosolic factors. Biochimica et Biophysica Acta (BBA) - Reviews on Cancer, 1755(2), 90–106. https://doi.org/10.1016/j.bbcan.2005.04.001

Atalay, S., Gęgotek, A., Wroński, A., Domigues, P., & Skrzydlewska, E. (2021). Therapeutic application of cannabidiol on UVA and UVB irradiated rat skin. A proteomic study. Journal of Pharmaceutical and Biomedical Analysis, 192, 113656. https://doi.org/10.1016/j.jpba.2020.113656

Bachelor, M. A., & Bowden, G. T. (2004). UVA-mediated activation of signaling pathways involved in skin tumor promotion and progression. Seminars in Cancer Biology, 14(2), 131–138. https://doi.org/10.1016/j.semcancer.2003.09.017

Bahar, R., Hartmann, C. H., Rodriguez, K. A., Denny, A. D., Busuttil, R. A., Dollé, M. E. T., Calder, R. B., Chisholm, G. B., Pollock, B. H., Klein, C. A., & Vijg, J. (2006). Increased cell-to-cell variation in gene expression in ageing mouse heart. *Nature*, *441*(7096), 1011–1014. https://doi.org/10.1038/nature04844

Bai, G.-L., Wang, P., Huang, X., Wang, Z.-Y., Cao, D., Liu, C., Liu, Y.-Y., Li, R.-L., & Chen, A.-J. (2021). Rapamycin Protects Skin Fibroblasts From UVA-Induced Photoaging by Inhibition of p53 and Phosphorylated HSP27. Frontiers in Cell and Developmental Biology, 9, 134. https://doi.org/10.3389/fcell.2021.633331

Baier, J., Maisch, T., Maier, M., Landthaler, M., & Bäumler, W. (2007). Direct Detection of Singlet Oxygen Generated by UVA Irradiation in Human Cells and Skin. Journal of Investigative Dermatology, 127(6), 1498–1506. https://doi.org/10.1038/sj.jid.5700741

Baier, J., Maisch, T., Maier, M., Engel, E., Landthaler, M., & Bäumler, W. (2006). Singlet Oxygen Generation by UVA Light Exposure of Endogenous Photosensitizers. Biophysical Journal, 91(4), 1452–1459. https://doi.org/10.1529/biophysj.106.082388

Baker, D. J., Childs, B. G., Durik, M., Wijers, M. E., Sieben, C. J., Zhong, J., A. Saltness, R., Jeganathan, K. B., Verzosa, G. C., Pezeshki, A., Khazaie, K., Miller, J. D., & van Deursen, J. M. (2016). Naturally occurring p16Ink4a-positive cells shorten healthy lifespan. *Nature*, *530*(7589), 184–189. https://doi.org/10.1038/nature16932

Baker, D. J., Wijshake, T., Tchkonia, T., LeBrasseur, N. K., Childs, B. G., van de Sluis, B., Kirkland, J. L., & van Deursen, J. M. (2011). Clearance of p16Ink4a-positive senescent cells delays ageing-associated disorders. *Nature*, *479*(7372), 232–236. https://doi.org/10.1038/nature10600

Banyasz, A., Martinez-Fernandez, L., Ketola, T.-M., Muñoz-Losa, A., Esposito, L., Markovitsi, D., & Improta, R. (2016). Excited State Pathways Leading to Formation of Adenine Dimers. The Journal of Physical Chemistry Letters, 7(11), 2020–2023. https://doi.org/10.1021/acs.jpclett.6b00660

Baptista, M. S., Cadet, J., Greer, A., & Thomas, A. H. (2021). Photosensitization Reactions of Biomolecules: Definition, Targets and Mechanisms. Photochemistry and Photobiology, 97(6), 1456-1483. https://doi.org/10.1111/php.13470

Basisty, N., Kale, A., Jeon, O. H., Kuehnemann, C., Payne, T., Rao, C., Holtz, A., Shah, S., Sharma, V., Ferrucci, L., Campisi, J., & Schilling, B. (2020). A proteomic atlas of senescence-associated secretomes for aging biomarker development. *PLOS Biology*, *18*(1), e3000599. https://doi.org/10.1371/journal.pbio.3000599

Basu-Modak, S., Ali, D., Gordon, M., Polte, T., Yiakouvaki, A., Pourzand, C., Rice-Evans, C., & Tyrrell, R. M. (2006). Suppression of UVA-mediated release of labile iron by epicatechin—A link to lysosomal protection. Free Radical Biology and Medicine, 41(8), 1197–1204. https://doi.org/10.1016/j.freeradbiomed.2006.06.008

Basu-Modak, S., Lüscher, P., & Tyrrell, R. M. (1996). Lipid metabolite involvement in the activation of the human heme oxygenase-1 gene. Free Radical Biology and Medicine, 20(7), 887–897. https://doi.org/10.1016/0891-5849(95)02182-5

Batista, L. F. Z., Kaina, B., Meneghini, R., & Menck, C. F. M. (2009). How DNA lesions are turned into powerful killing structures: Insights from UV-induced apoptosis. Mutation Research/Reviews in Mutation Research, 681(2), 197–208. https://doi.org/10.1016/j.mrrev.2008.09.001

Battie, C., Jitsukawa, S., Bernerd, F., Bino, S. D., Marionnet, C., & Verschoore, M. (2014). New insights in photoaging, UVA induced damage and skin types. Experimental Dermatology, 23(s1), 7–12. https://doi.org/10.1111/exd.12388

Beauséjour, C. M., Krtolica, A., Galimi, F., Narita, M., Lowe, S. W., Yaswen, P., & Campisi, J. (2003). Reversal of human cellular senescence: Roles of the p53 and p16 pathways. *The EMBO Journal*, *22*(16), 4212–4222. https://doi.org/10.1093/emboj/cdg417

Ben-Porath, I., & Weinberg, R. A. (2005). The signals and pathways activating cellular senescence. *The International Journal of Biochemistry & Cell Biology*, *37*(5), 961–976. https://doi.org/10.1016/j.biocel.2004.10.013

Berent-Maoz, B., Montecino-Rodriguez, E., Signer, R. A. J., & Dorshkind, K. (2012). Fibroblast growth factor-7 partially reverses murine thymocyte progenitor aging by repression of Ink4a. *Blood*, *119*(24), 5715–5721. https://doi.org/10.1182/blood-2011-12-400002

Berneburg, M., Grether-Beck, S., Kürten, V., Ruzicka, T., Briviba, K., Sies, H., & Krutmann, J. (1999). Singlet oxygen mediates the UVA-induced generation of the photoaging-associated mitochondrial common deletion. The Journal of Biological Chemistry, 274(22), 15345–15349. https://doi.org/10.1074/jbc.274.22.15345

Berneburg, M., Plettenberg, H., Medve-König, K., Pfahlberg, A., Gers-Barlag, H., Gefeller, O., Krutmann, J. (2004). Induction of the Photoaging-Associated Mitochondrial Common Deletion In Vivo in Normal Human Skin. Journal of Investigative Dermatology 122, 1277–1283. https://doi.org/10.1111/j.0022-202X.2004.22502.x

Bernerd, F., & Asselineau, D. (1998). UVA exposure of human skin reconstructed in vitro induces apoptosis of dermal fibroblasts: Subsequent connective tissue repair and implications in photoaging. Cell Death & Differentiation, 5(9), 792–802. https://doi.org/10.1038/sj.cdd.4400413

Besaratinia, A., Synold, T. W., Chen, H.-H., Chang, C., Xi, B., Riggs, A. D., & Pfeifer, G. P. (2005). DNA lesions induced by UV A1 and B radiation in human cells: Comparative analyses in the overall genome and in the p53 tumor suppressor gene. Proceedings of the National Academy of Sciences, 102(29), 10058–10063. https://doi.org/10.1073/pnas.0502311102

Besaratinia, A., Synold, T. W., Xi, B., & Pfeifer, G. P. (2004). G-to-T Transversions and Small Tandem Base Deletions Are the Hallmark of Mutations Induced by Ultraviolet A Radiation in Mammalian Cells. Biochemistry, 43(25), 8169–8177. https://doi.org/10.1021/bi049761v

Bikle, D. D., Xie, Z., & Tu, C.-L. (2012). Calcium regulation of keratinocyte differentiation. Expert Review of Endocrinology & Metabolism, 7(4), 461–472. https://doi.org/10.1586/eem.12.34

Bivik, C. A., Larsson, P. K., Kågedal, K. M., Rosdahl, I. K., & Öllinger, K. M. (2006). UVA/B-Induced Apoptosis in Human Melanocytes Involves Translocation of Cathepsins and Bcl-2 Family Members. Journal of Investigative Dermatology, 126(5), 1119–1127. https://doi.org/10.1038/sj.jid.5700124

Bindea, G., Mlecnik, B., Hackl, H., Charoentong, P., Tosolini, M., Kirilovsky, A., Fridman, W.-H., Pagès, F., Trajanoski, Z., & Galon, J. (2009). ClueGO: A Cytoscape plug-in to

decipher functionally grouped gene ontology and pathway annotation networks. Bioinformatics, 25(8), 1091–1093. https://doi.org/10.1093/bioinformatics/btp101

Blander, G., Oliveira, R. M. de, Conboy, C. M., Haigis, M., & Guarente, L. (2003). Superoxide Dismutase 1 Knock-down Induces Senescence in Human Fibroblasts *. *Journal of Biological Chemistry*, *278*(40), 38966–38969. https://doi.org/10.1074/jbc.M307146200

Blanpain, C., & Fuchs, E. (2006). Epidermal Stem Cells of the Skin. Annual review of cell and developmental biology, 22, 339–373. https://doi.org/10.1146/annurev.cellbio.22.010305.104357

Bond, J. A., Wyllie, F. S., & Wynford-Thomas, D. (1994). Escape from senescence in human diploid fibroblasts induced directly by mutant p53. *Oncogene*, *9*(7), 1885–1889.

Boquoi, A., Arora, S., Chen, T., Litwin, S., Koh, J., & Enders, G. H. (2015). Reversible cell cycle inhibition and premature aging features imposed by conditional expression of p16Ink4a. *Aging Cell*, *14*(1), 139–147. https://doi.org/10.1111/acel.12279

Borner, G. H. H., Hein, M. Y., Hirst, J., Edgar, J. R., Mann, M., & Robinson, M. S. (2014). Fractionation profiling: A fast and versatile approach for mapping vesicle proteomes and protein–protein interactions. Molecular Biology of the Cell, 25(20), 3178–3194. https://doi.org/10.1091/mbc.e14-07-1198

Boukamp, P., Bleuel, K., Popp, S., Vormwald-Dogan, V., & Fusenig, N. E. (1997). Functional evidence for tumor-suppressor activity on chromosome 15 in human skin carcinoma cells and thrombospondin-1 as the potential suppressor. Journal of Cellular Physiology, 173(2), 256–260. https://doi.org/10.1002/(SICI)1097-4652(199711)173:2<256::AID-JCP31>3.0.CO;2-B

Brash, D. E. (1997). Sunlight and the onset of skin cancer. Trends in Genetics, 13(10), 410–414. https://doi.org/10.1016/S0168-9525(97)01246-8

Brash, D. E., Goncalves, L. C. P., Bechara, E. J. H., & Excited-State Medicine Working Group. (2018). Chemiexcitation and Its Implications for Disease. Trends in Molecular Medicine, 24(6), 527–541. https://doi.org/10.1016/j.molmed.2018.04.004

Brash, D. E., Rudolph, J. A., Simon, J. A., Lin, A., McKenna, G. J., Baden, H. P., Halperin, A. J., & Pontén, J. (1991). A role for sunlight in skin cancer: UV-induced p53 mutations in squamous cell carcinoma. Proceedings of the National Academy of Sciences, 88(22), 10124–10128. https://doi.org/10.1073/pnas.88.22.10124

Breckels, L. M., Mulvey, C. M., Lilley, K. S., & Gatto, L. (2018). A Bioconductor workflow for processing and analysing spatial proteomics data. F1000Research, 5, 2926. https://doi.org/10.12688/f1000research.10411.2

Breker, M., Schuldiner, M. (2014). The emergence of proteome-wide technologies: systematic analysis of proteins comes of age. Nature Reviews Molecular Cell Biology 15, 453–464. https://doi.org/10.1038/nrm3821

Brown, J. P., Wei, W., & Sedivy, J. M. (1997). Bypass of Senescence After Disruption of p21CIP1/WAF1 Gene in Normal Diploid Human Fibroblasts. *Science*. https://doi.org/10.1126/science.277.5327.831

Brzoska, K., Szumiel, I. (2008). Signalling loops and linear pathways: NF- B activation in response to genotoxic stress. Mutagenesis 24, 1–8. https://doi.org/10.1093/mutage/gen056

Buckel, T. B. H., Goldstein, A. M., Fraser, M. C., Rogers, B., & Tucker, M. A. (2006). Recent Tanning Bed Use: A Risk Factor for Melanoma. Archives of Dermatology, 142(4), 485–488. https://doi.org/10.1001/archderm.142.4.485

Cadet, J., & Douki, T. (2018). Formation of UV-induced DNA damage contributing to skin cancer development. Photochemical & Photobiological Sciences, 17(12), 1816–1841. https://doi.org/10.1039/C7PP00395A

Cadet, J., Douki, T., & Ravanat, J.-L. (2008). Oxidatively Generated Damage to the Guanine Moiety of DNA: Mechanistic Aspects and Formation in Cells. Accounts of Chemical Research, 41(8), 1075–1083. https://doi.org/10.1021/ar700245e

Cadet, J., Douki, T., & Ravanat, J.-L. (2015). Oxidatively Generated Damage to Cellular DNA by UVB and UVA Radiation,. Photochemistry and Photobiology, 91(1), 140–155. https://doi.org/10.1111/php.12368

Cadet, J., Douki, T., Ravanat, J.-L., & Mascio, P. D. (2009). Sensitized formation of oxidatively generated damage to cellular DNA by UVA radiation. Photochemical & Photobiological Sciences, 8(7), 903–911. https://doi.org/10.1039/B905343N

Cadet, J., Mouret, S., Ravanat, J.-L., & Douki, T. (2012). Photoinduced Damage to Cellular DNA: Direct and Photosensitized Reactions†. Photochemistry and Photobiology, 88(5), 1048–1065. https://doi.org/10.1111/j.1751-1097.2012.01200.x

Campisi, J. (1998). The Role of Cellular Senescence in Skin Aging. Journal of Investigative Dermatology Symposium Proceedings, 3(1), 1–5. https://doi.org/10.1038/jidsymp.1998.2

Campisi, J. (2013). Aging, Cellular Senescence, and Cancer. Annual Review of Physiology, 75(1), 685–705. https://doi.org/10.1146/annurev-physiol-030212-183653

Casale, C., Imparato, G., Urciuolo, F., Rescigno, F., Scamardella, S., Escolino, M., & Netti, P. A. (2018). Engineering a human skin equivalent to study dermis remodelling and epidermis senescence in vitro after UVA exposure. Journal of Tissue Engineering and Regenerative Medicine, 12(7), 1658–1669. https://doi.org/10.1002/term.2693

Cavinato, M., & Jansen-Dürr, P. (2017). Molecular mechanisms of UVB-induced senescence of dermal fibroblasts and its relevance for photoaging of the human skin. Experimental Gerontology, 94, 78–82. https://doi.org/10.1016/j.exger.2017.01.009

Chatzidoukaki, O., Goulielmaki, E., Schumacher, B., Garinis, G.A. (2020). DNA Damage Response and Metabolic Reprogramming in Health and Disease. Trends in Genetics 36, 777–791. https://doi.org/10.1016/j.tig.2020.06.018

Chen, H., Weng, Q.Y., Fisher, D.E. (2014). UV Signaling Pathways within the Skin. J Invest Dermatol 134, 2080–2085. https://doi.org/10.1038/jid.2014.161

Chen, H., Ruiz, P. D., McKimpson, W. M., Novikov, L., Kitsis, R. N., & Gamble, M. J. (2015). MacroH2A1 and ATM Play Opposing Roles in Paracrine Senescence and the Senescence-Associated Secretory Phenotype. Molecular Cell, 59(5), 719–731. https://doi.org/10.1016/j.molcel.2015.07.011

Choi, M., Chang, C.-Y., Clough, T., Broudy, D., Killeen, T., MacLean, B., & Vitek, O. (2014). MSstats: An R package for statistical analysis of quantitative mass spectrometry-based proteomic experiments. Bioinformatics, 30(17), 2524–2526. https://doi.org/10.1093/bioinformatics/btu305

Christoforou, A., Mulvey, C. M., Breckels, L. M., Geladaki, A., Hurrell, T., Hayward, P. C., Naake, T., Gatto, L., Viner, R., Arias, A. M., & Lilley, K. S. (2016). A draft map of the mouse pluripotent stem cell spatial proteome. Nature Communications, 7(1), 9992. https://doi.org/10.1038/ncomms9992

Christopher, J. A., Stadler, C., Martin, C. E., Morgenstern, M., Pan, Y., Betsinger, C. N., Rattray, D. G., Mahdessian, D., Gingras, A.-C., Warscheid, B., Lehtiö, J., Cristea, I. M., Foster, L. J., Emili, A., & Lilley, K. S. (2021). Subcellular proteomics. Nature Reviews Methods Primers, 1(1), 1–24. https://doi.org/10.1038/s43586-021-00029-y

Chung, J. H., & Eun, H. C. (2007). Angiogenesis in skin aging and photoaging. The Journal of Dermatology, 34(9), 593–600. https://doi.org/10.1111/j.1346-8138.2007.00341.x

Courdavault, S., Baudouin, C., Charveron, M., Canguilhem, B., Favier, A., Cadet, J., & Douki, T. (2005). Repair of the three main types of bipyrimidine DNA photoproducts in

human keratinocytes exposed to UVB and UVA radiations. DNA Repair, 4(7), 836–844. https://doi.org/10.1016/j.dnarep.2005.05.001

Cochet, C., Chambaz, E.M. (1983). Oligomeric structure and catalytic activity of G type casein kinase. Isolation of the two subunits and renaturation experiments. J Biol Chem 258, 1403–1406.

Coin, F., Auriol, J., Tapias, A., Clivio, P., Vermeulen, W., Egly, J.-M. (2004). Phosphorylation of XPB helicase regulates TFIIH nucleotide excision repair activity. The EMBO Journal 23, 4835–4846. https://doi.org/10.1038/sj.emboj.7600480

Contrepois, K., Coudereau, C., Benayoun, B. A., Schuler, N., Roux, P.-F., Bischof, O., Courbeyrette, R., Carvalho, C., Thuret, J.-Y., Ma, Z., Derbois, C., Nevers, M.-C., Volland, H., Redon, C. E., Bonner, W. M., Deleuze, J.-F., Wiel, C., Bernard, D., Snyder, M. P., … Mann, C. (2017). Histone variant H2A.J accumulates in senescent cells and promotes inflammatory gene expression. Nature Communications, 8(1), 1–18. https://doi.org/10.1038/ncomms14995

Cooper, S.J., Bowden, G.T. (2007). Ultraviolet B Regulation of Transcription Factor Families. Curr Cancer Drug Targets 7, 325–334.

Coppé, J.-P., Desprez, P.-Y., Krtolica, A., & Campisi, J. (2010). The Senescence-Associated Secretory Phenotype: The Dark Side of Tumor Suppression. Annual review of pathology, 5, 99–118. https://doi.org/10.1146/annurev-pathol-121808-102144

Coppé, J.-P., Patil, C. K., Rodier, F., Sun, Y., Muñoz, D. P., Goldstein, J., Nelson, P. S., Desprez, P.-Y., & Campisi, J. (2008). Senescence-Associated Secretory Phenotypes Reveal Cell-Nonautonomous Functions of Oncogenic RAS and the p53 Tumor Suppressor. PLOS Biology, 6(12), e301. https://doi.org/10.1371/journal.pbio.0060301

Cosgrove, B. D., Gilbert, P. M., Porpiglia, E., Mourkioti, F., Lee, S. P., Corbel, S. Y., Llewellyn, M. E., Delp, S. L., & Blau, H. M. (2014). Rejuvenation of the muscle stem cell population restores strength to injured aged muscles. Nature Medicine, 20(3), 255–264. https://doi.org/10.1038/nm.3464

Courdavault, S., Baudouin, C., Charveron, M., Favier, A., Cadet, J., & Douki, T. (2004). Larger yield of cyclobutane dimers than 8-oxo-7,8-dihydroguanine in the DNA of UVA-irradiated human skin cells. Mutation Research/Fundamental and Molecular Mechanisms of Mutagenesis, 556(1), 135–142. https://doi.org/10.1016/j.mrfmmm.2004.07.011

Courtois-Cox, S., Jones, S. L., & Cichowski, K. (2008). Many roads lead to oncogene-induced senescence. *Oncogene*, *27*(20), 2801–2809. https://doi.org/10.1038/sj.onc.1210950

Cox, J., Hein, M. Y., Luber, C. A., Paron, I., Nagaraj, N., & Mann, M. (2014). Accurate Proteome-wide Label-free Quantification by Delayed Normalization and Maximal Peptide Ratio Extraction, Termed MaxLFQ *. Molecular & Cellular Proteomics, 13(9), 2513–2526. https://doi.org/10.1074/mcp.M113.031591

Cox, J., & Mann, M. (2008). MaxQuant enables high peptide identification rates, individualized p.p.b.-range mass accuracies and proteome-wide protein quantification. Nature Biotechnology, 26(12), 1367–1372. https://doi.org/10.1038/nbt.1511

Cox, J., Neuhauser, N., Michalski, A., Scheltema, R. A., Olsen, J. V., & Mann, M. (2011). Andromeda: A Peptide Search Engine Integrated into the MaxQuant Environment. Journal of Proteome Research, 10(4), 1794–1805. https://doi.org/10.1021/pr101065j

Craxton, A., Munnur, D., Jukes-Jones, R., Skalka, G., Langlais, C., Cain, K., Malewicz, M. (2018). PAXX and its paralogs synergistically direct DNA polymerase λ activity in DNA repair. Nature Communications 9, 3877. https://doi.org/10.1038/s41467-018-06127-y

Crook, O. M., Mulvey, C. M., Kirk, P. D. W., Lilley, K. S., & Gatto, L. (2018). A Bayesian mixture modelling approach for spatial proteomics. PLOS Computational Biology, 14(11), e1006516. https://doi.org/10.1371/journal.pcbi.1006516

Crook, O. M., Smith, T., Elzek, M., & Lilley, K. S. (2020). Moving Profiling Spatial Proteomics Beyond Discrete Classification. PROTEOMICS, 20(23), 1900392. https://doi.org/10.1002/pmic.201900392

Cruz-Garcia, D., Brouwers, N., Malhotra, V., & Curwin, A. J. (2020). Reactive oxygen species triggers unconventional secretion of antioxidants and Acb1. Journal of Cell Biology, 219(4). https://doi.org/10.1083/jcb.201905028

Cursons, J., Gao, J., Hurley, D. G., Print, C. G., Dunbar, P. R., Jacobs, M. D., & Crampin, E. J. (2015). Regulation of ERK-MAPK signaling in human epidermis. BMC Systems Biology, 9(1), 41. https://doi.org/10.1186/s12918-015-0187-6

d'Adda di Fagagna, F. (2008). Living on a break: Cellular senescence as a DNA-damage response. *Nature Reviews. Cancer*, *8*(7), 512–522. https://doi.org/10.1038/nrc2440

Damiani, E., Rosati, L., Castagna, R., Carloni, P., & Greci, L. (2006). Changes in ultraviolet absorbance and hence in protective efficacy against lipid peroxidation of organic sunscreens after UVA irradiation. Journal of Photochemistry and Photobiology B: Biology, 82(3), 204–213. https://doi.org/10.1016/j.jphotobiol.2005.03.011

Dau, T., Bartolomucci, G., & Rappsilber, J. (2020). Proteomics Using Protease Alternatives to Trypsin Benefits from Sequential Digestion with Trypsin. Analytical Chemistry, 92(14), 9523–9527. https://doi.org/10.1021/acs.analchem.0c00478

Davies, A. K., Itzhak, D. N., Edgar, J. R., Archuleta, T. L., Hirst, J., Jackson, L. P., Robinson, M. S., & Borner, G. H. H. (2018). AP-4 vesicles contribute to spatial control of autophagy via RUSC-dependent peripheral delivery of ATG9A. Nature Communications, 9(1), 3958. https://doi.org/10.1038/s41467-018-06172-7

de Duve, C. (1971). Tissue Fraction-Past and Present. The Journal of Cell Biology, 50(1), 20.

de Gruijl, F.R., van Kranen, H.J., Mullenders, L.H.F. (2001). UV-induced DNA damage, repair, mutations and oncogenic pathways in skin cancer. Journal of Photochemistry and Photobiology B: Biology, Consequences of exposure to sunlight: elements to assess protection 63, 19–27. https://doi.org/10.1016/S1011-1344(01)00199-3

de Laat, A., van der Leun, J. C., & de Gruijl, F. R. (1997). Carcinogenesis induced by UVA (365-nm) radiation: The dose-time dependence of tumor formation in hairless mice. Carcinogenesis, 18(5), 1013–1020. https://doi.org/10.1093/carcin/18.5.1013

de Mol, N. J., Beijersbergen van Henegouwen, G. M. J., Mohn, G. R., Glickman, B. W., & van Kleef, P. M. (1981). On the involvement of singlet oxygen in mutation induction by 8-methoxypsoralen and UVA irradiation in Escherichia coli K-12. Mutation Research/Fundamental and Molecular Mechanisms of Mutagenesis, 82(1), 23–30. https://doi.org/10.1016/0027-5107(81)90134-2

Debacq-Chainiaux, F., Borlon, C., Pascal, T., Royer, V., Eliaers, F., Ninane, N., Carrard, G., Friguet, B., de Longueville, F., Boffe, S., Remacle, J., & Toussaint, O. (2005). Repeated exposure of human skin fibroblasts to UVB at subcytotoxic level triggers premature senescence through the TGF-β1 signaling pathway. Journal of Cell Science, 118(4), 743–758. https://doi.org/10.1242/jcs.01651

Delinasios, G. J., Karbaschi, M., Cooke, M. S., & Young, A. R. (2018). Vitamin E inhibits the UVAI induction of "light" and "dark" cyclobutane pyrimidine dimers, and oxidatively generated DNA damage, in keratinocytes. Scientific Reports, 8(1), 1–12. https://doi.org/10.1038/s41598-017-18924-4

Deng, C., Zhang, P., Wade Harper, J., Elledge, S. J., & Leder, P. (1995). Mice Lacking p21CIP1/WAF1 undergo normal development, but are defective in G1 checkpoint control. Cell, 82(4), 675–684. https://doi.org/10.1016/0092-8674(95)90039-X

Deschênes-Simard, X., Lessard, F., Gaumont-Leclerc, M.-F., Bardeesy, N., & Ferbeyre, G. (2014). Cellular senescence and protein degradation. Cell Cycle, 13(12), 1840–1858. https://doi.org/10.4161/cc.29335

Di Mascio, P., Martinez, G. R., Miyamoto, S., Ronsein, G. E., Medeiros, M. H. G., & Cadet, J. (2019). Singlet Molecular Oxygen Reactions with Nucleic Acids, Lipids, and Proteins. Chemical Reviews, 119(3), 2043–2086. https://doi.org/10.1021/acs.chemrev.8b00554

Di Mascio, P., Wefers, H., Do-Thi, H.-P., Lafleur, M. V. M., & Sies, H. (1989). Singlet molecular oxygen causes loss of biological activity in plasmid and bacteriophage DNA and induces single-strand breaks. Biochimica et Biophysica Acta (BBA) - Gene Structure and Expression, 1007(2), 151–157. https://doi.org/10.1016/0167-4781(89)90033-X

Diedrich, J. K., Pinto, A. F. M., & Yates, J. R. (2013). Energy dependence of HCD on peptide fragmentation: Stepped collisional energy finds the sweet spot. Journal of the American Society for Mass Spectrometry, 24(11), 10.1007/s13361-013-0709–7. https://doi.org/10.1007/s13361-013-0709-7

Dimri, G. P., Lee, X., Basile, G., Acosta, M., Scott, G., Roskelley, C., Medrano, E. E., Linskens, M., Rubelj, I., & Pereira-Smith, O. (1995). A biomarker that identifies senescent human cells in culture and in aging skin in vivo. Proceedings of the National Academy of Sciences of the United States of America, 92(20), 9363–9367.

Djavaheri-Mergny, M., Gras, M.-P., Mergny, J.-L., Dubertret, L. (1999). UV-A-induced decrease in nuclear factor-κB activity in human keratinocytes. Biochemical Journal 338, 607–613. https://doi.org/10.1042/bj3380607

Djavaheri-Mergny, M., Marsac, C., Mazière, C., Santus, R., Michel, L., Dubertret, L., Mazière, J.C. (2001). UV-A irradiation induces a decrease in the mitochondrial respiratory activity of human NCTC 2544 keratinocytes. Free Radical Research 34, 583–594. https://doi.org/10.1080/10715760100300481

Dörr, J. R., Yu, Y., Milanovic, M., Beuster, G., Zasada, C., Däbritz, J. H. M., Lisec, J., Lenze, D., Gerhardt, A., Schleicher, K., Kratzat, S., Purfürst, B., Walenta, S., Mueller-Klieser, W., Gräler, M., Hummel, M., Keller, U., Buck, A. K., Dörken, B., … Schmitt, C. A.

(2013). Synthetic lethal metabolic targeting of cellular senescence in cancer therapy. Nature, 501(7467), 421–425. https://doi.org/10.1038/nature12437

Douki, T. (2013). The variety of UV-induced pyrimidine dimeric photoproducts in DNA as shown by chromatographic quantification methods. Photochemical & Photobiological Sciences, 12(8), 1286–1302. https://doi.org/10.1039/C3PP25451H

Douki, T. (2016). Relative Contributions of UVB and UVA to the Photoconversion of (6-4) Photoproducts into their Dewar Valence Isomers. Photochemistry and Photobiology, 92(4), 587–594. https://doi.org/10.1111/php.12605

Douki, T., & Cadet, J. (2001). Individual Determination of the Yield of the Main UV-Induced Dimeric Pyrimidine Photoproducts in DNA Suggests a High Mutagenicity of CC Photolesions. Biochemistry, 40(8), 2495–2501. https://doi.org/10.1021/bi0022543

Douki, T., Perdiz, D., Grof, P., Kuluncsics, Z., Moustacchi, E., Cadet, J., & Sage, E. (1999). Oxidation of Guanine in Cellular DNA by Solar UV Radiation: Biological Role†. Photochemistry and Photobiology, 70(2), 184–190. https://doi.org/10.1111/j.1751-1097.1999.tb07988.x

Douki, T., Reynaud-Angelin, A., Cadet, J., & Sage, E. (2003). Bipyrimidine Photoproducts Rather than Oxidative Lesions Are the Main Type of DNA Damage Involved in the Genotoxic Effect of Solar UVA Radiation. Biochemistry, 42(30), 9221–9226. https://doi.org/10.1021/bi034593c

Du, L., Chen, E., Wu, T., Ruan, Y., & Wu, S. (2019). Resveratrol attenuates hydrogen peroxide-induced aging through upregulation of autophagy in human umbilical vein endothelial cells. *Drug Design, Development and Therapy*, *13*, 747–755. https://doi.org/10.2147/DDDT.S179894

Dumont, E., Grüber, R., Bignon, E., Morell, C., Moreau, Y., Monari, A., & Ravanat, J.-L. (2016). Probing the reactivity of singlet oxygen with purines. Nucleic Acids Research, 44(1), 56–62. https://doi.org/10.1093/nar/gkv1364

Dumont, P., Burton, M., Chen, Q. M., Gonos, E. S., Frippiat, C., Mazarati, J.-B., Eliaers, F., Remacle, J., & Toussaint, O. (2000). Induction of replicative senescence biomarkers by sublethal oxidative stresses in normal human fibroblast. *Free Radical Biology and Medicine*, *28*(3), 361–373. https://doi.org/10.1016/S0891-5849(99)00249-X

Edifizi, D., Nolte, H., Babu, V., Castells-Roca, L., Mueller, M.M., Brodesser, S., Krüger, M., Schumacher, B. (2017). Multilayered Reprogramming in Response to Persistent DNA Damage in C. elegans. Cell Reports 20, 2026–2043. https://doi.org/10.1016/j.celrep.2017.08.028

El Ghissassi, F., Baan, R., Straif, K., Grosse, Y., Secretan, B., Bouvard, V., Benbrahim-Tallaa, L., Guha, N., Freeman, C., Galichet, L., Cogliano, V., & WHO International Agency for Research on Cancer Monograph Working Group. (2009). A review of human carcinogens--part D: Radiation. The Lancet. Oncology, 10(8), 751–752. https://doi.org/10.1016/s1470-2045(09)70213-x

Elia, A.E.H., Boardman, A.P., Wang, D.C., Huttlin, E.L., Everley, R.A., Dephoure, N., Zhou, C., Koren, I., Gygi, S.P., Elledge, S.J. (2015). Quantitative Proteomic Atlas of Ubiquitination and Acetylation in the DNA Damage Response. Mol. Cell 59, 867–881. https://doi.org/10.1016/j.molcel.2015.05.006

Eng, J. K., McCormack, A. L., & Yates, J. R. (1994). An approach to correlate tandem mass spectral data of peptides with amino acid sequences in a protein database. Journal of the American Society for Mass Spectrometry, 5(11), 976–989. https://doi.org/10.1016/1044-0305(94)80016-2

Eng, J. K., Searle, B. C., Clauser, K. R., & Tabb, D. L. (2011). A Face in the Crowd: Recognizing Peptides Through Database Search *. Molecular & Cellular Proteomics, 10(11). https://doi.org/10.1074/mcp.R111.009522

Fagot, D., Asselineau, D., & Bernerd, F. (2004). Matrix Metalloproteinase-1 Production Observed After Solar-Simulated Radiation Exposure is Assumed by Dermal Fibroblasts but Involves a Paracrine Activation Through Epidermal Keratinocytes. Photochemistry and Photobiology, 79(6), 499–506. https://doi.org/10.1111/j.1751-1097.2004.tb01266.x

Feoktistova, M., Geserick, P., & Leverkus, M. (2016). Crystal Violet Assay for Determining Viability of Cultured Cells. Cold Spring Harbor Protocols, 2016(4), pdb.prot087379. https://doi.org/10.1101/pdb.prot087379

Fernández-García, E. (2014). Skin protection against UV light by dietary antioxidants. Food & Function, 5(9), 1994–2003. https://doi.org/10.1039/C4FO00280F

Filhol, O., Baudier, J., Delphin, C., Loue-Mackenbach, P., Chambaz, E.M., Cochet, C. (1992). Casein kinase II and the tumor suppressor protein P53 associate in a molecular complex that is negatively regulated upon P53 phosphorylation. J. Biol. Chem. 267, 20577–20583.

Fisher, G. J., Datta, S. C., Talwar, H. S., Wang, Z.-Q., Varani, J., Kang, S., & Voorhees, J. J. (1996). Molecular basis of sun-induced premature skin ageing and retinoid antagonism. Nature, 379(6563), 335–339. https://doi.org/10.1038/379335a0

Fisher, G. J., Wang, Z., Datta, S. C., Varani, J., Kang, S., & Voorhees, J. J. (2009). Pathophysiology of Premature Skin Aging Induced by Ultraviolet Light. Massachusetts Medical Society. https://doi.org/10.1056/NEJM199711133372003

Fitsiou, E., Pulido, T., Campisi, J., Alimirah, F., & Demaria, M. (2020). Cellular Senescence and the Senescence-Associated Secretory Phenotype as Drivers of Skin Photoaging. Journal of Investigative Dermatology, 0(0). https://doi.org/10.1016/j.jid.2020.09.031

Foster, L. J., Hoog, C. L. de, Zhang, Y., Zhang, Y., Xie, X., Mootha, V. K., & Mann, M. (2006). A Mammalian Organelle Map by Protein Correlation Profiling. Cell, 125(1), 187–199. https://doi.org/10.1016/j.cell.2006.03.022

Franz, A., Pirson, P.A., Pilger, D., Halder, S., Achuthankutty, D., Kashkar, H., Ramadan, K., Hoppe, T. (2016). Chromatin-associated degradation is defined by UBXN-3/FAF1 to safeguard DNA replication fork progression. Nat Commun 7. https://doi.org/10.1038/ncomms10612

Friedel, M. G., Gierlich, J., & Carell, T. (2009). Cyclobutane Pyrimidine Dimers as UV-Induced DNA Lesions. In PATAI'S Chemistry of Functional Groups. American Cancer Society. https://doi.org/10.1002/9780470682531.pat0336

Fusenig, N. E., & Boukamp, P. (1998). Multiple stages and genetic alterations in immortalization, malignant transformation, and tumor progression of human skin keratinocytes. Molecular Carcinogenesis, 23(3), 144–158. https://doi.org/10.1002/(SICI)1098-2744(199811)23:3<144::AID-MC3>3.0.CO;2-U

Gatto, L., Breckels, L. M., Burger, T., Nightingale, D. J. H., Groen, A. J., Campbell, C., Nikolovski, N., Mulvey, C. M., Christoforou, A., Ferro, M., & Lilley, K. S. (2014). A Foundation for Reliable Spatial Proteomics Data Analysis. Molecular & Cellular Proteomics : MCP, 13(8), 1937–1952. https://doi.org/10.1074/mcp.M113.036350

Gatto, L., Breckels, L. M., & Lilley, K. S. (2019). Assessing sub-cellular resolution in spatial proteomics experiments. Current Opinion in Chemical Biology, 48, 123–149. https://doi.org/10.1016/j.cbpa.2018.11.015

Gatto, L., Breckels, L.M., Wieczorek, S., Burger, T., Lilley, K.S. (2014b). Mass-spectrometry-based spatial proteomics data analysis using pRoloc and pRolocdata. Bioinformatics 30, 1322–1324. https://doi.org/10.1093/bioinformatics/btu013

Gęgotek, A., Domingues, P., & Skrzydlewska, E. (2018). Proteins involved in the antioxidant and inflammatory response in rutin-treated human skin fibroblasts exposed to UVA or UVB irradiation. Journal of Dermatological Science, 90(3), 241–252. https://doi.org/10.1016/j.jdermsci.2018.02.002

Gęgotek, A., Jarocka-Karpowicz, I., & Skrzydlewska, E. (2019). Synergistic Cytoprotective Effects of Rutin and Ascorbic Acid on the Proteomic Profile of 3D-Cultured Keratinocytes Exposed to UVA or UVB Radiation. Nutrients, 11(11), 2672. https://doi.org/10.3390/nu11112672

Gęgotek, A., Łuczaj, W., & Skrzydlewska, E. (2021). Effects of Natural Antioxidants on Phospholipid and Ceramide Profiles of 3D-Cultured Skin Fibroblasts Exposed to UVA or UVB Radiation. Antioxidants, 10(4), 578. https://doi.org/10.3390/antiox10040578

Geladaki, A., Kočevar Britovšek, N., Breckels, L. M., Smith, T. S., Vennard, O. L., Mulvey, C. M., Crook, O. M., Gatto, L., & Lilley, K. S. (2019). Combining LOPIT with differential ultracentrifugation for high-resolution spatial proteomics. Nature Communications, 10(1), 331. https://doi.org/10.1038/s41467-018-08191-w

Gilhar, A., Ullmann, Y., Karry, R., Shalaginov, R., Assy, B., Serafimovich, S., & Kalish, R. S. (2004). Aging of Human Epidermis: Reversal of Aging Changes Correlates With Reversal of Keratinocyte Fas Expression and Apoptosis. The Journals of Gerontology: Series A, 59(5), B411–B415. https://doi.org/10.1093/gerona/59.5.B411

Gniadecki, R., Thorn, T., Vicanova, J., Petersen, A., & Wulf, H. C. (2001). Role of mitochondria in ultraviolet-induced oxidative stress. Journal of Cellular Biochemistry, 80(2), 216–222. https://doi.org/10.1002/1097-4644(20010201)80:2<216::AID-JCB100>3.0.CO;2-H

Goebel, T., Mausbach, S., Tuermer, A., Eltahir, H., Winter, D., Gieselmann, V., & Thelen, M. (2020). Proteaphagy in Mammalian Cells Can Function Independent of ATG5/ATG7. Molecular & Cellular Proteomics : MCP, 19(7), 1120–1131. https://doi.org/10.1074/mcp.RA120.001983

Gray, G.K., McFarland, B.C., Rowse, A.L., Gibson, S.A., Benveniste, E.N. (2014). Therapeutic CK2 inhibition attenuates diverse prosurvival signaling cascades and

decreases cell viability in human breast cancer cells. Oncotarget 5, 6484–6496. https://doi.org/10.18632/oncotarget.2248

Grecu, D., Assairi, L. (2014). CK2 phosphorylation of human centrins 1 and 2 regulates their binding to the DNA repair protein XPC, the centrosomal protein Sfi1 and the phototransduction protein transducin β. FEBS Open Bio 4, 407–419. https://doi.org/10.1016/j.fob.2014.04.002

Grether-Beck, S., Bonizzi, G., Schmitt-Brenden, H., Felsner, I., Timmer, A., Sies, H., Johnson, J. P., Piette, J., & Krutmann, J. (2000). Non-enzymatic triggering of the ceramide signalling cascade by solar UVA radiation. The EMBO Journal, 19(21), 5793–5800. https://doi.org/10.1093/emboj/19.21.5793

Grether-Beck, S., Olaizola-Horn, S., Schmitt, H., Grewe, M., Jahnke, A., Johnson, J. P., Briviba, K., Sies, H., & Krutmann, J. (1996). Activation of transcription factor AP-2 mediates UVA radiation- and singlet oxygen-induced expression of the human intercellular adhesion molecule 1 gene. Proceedings of the National Academy of Sciences, 93(25), 14586–14591. https://doi.org/10.1073/pnas.93.25.14586

Grether-Beck, S., Salahshour-Fard, M., Timmer, A., Brenden, H., Felsner, I., Walli, R., Füllekrug, J., & Krutmann, J. (2008). Ceramide and raft signaling are linked with each other in UVA radiation-induced gene expression. Oncogene, 27(35), 4768–4778. https://doi.org/10.1038/onc.2008.116

Grether-Beck, S., Timmer, A., Felsner, I., Brenden, H., Brammertz, D., & Krutmann, J. (2005). Ultraviolet A-Induced Signaling Involves a Ceramide-Mediated Autocrine Loop Leading to Ceramide De Novo Synthesis. Journal of Investigative Dermatology, 125(3), 545–553. https://doi.org/10.1111/j.0022-202X.2005.23782.x

Gronemeyer, T., Wiese, S., Ofman, R., Bunse, C., Pawlas, M., Hayen, H., Eisenacher, M., Stephan, C., Meyer, H. E., Waterham, H. R., Erdmann, R., Wanders, R. J., & Warscheid, B. (2013). The proteome of human liver peroxisomes: Identification of five

new peroxisomal constituents by a label-free quantitative proteomics survey. PloS One, 8(2), e57395. https://doi.org/10.1371/journal.pone.0057395

Gruber, F., Mayer, H., Lengauer, B., Mlitz, V., Sanders, J. M., Kadl, A., Bilban, M., de Martin, R., Wagner, O., Kensler, T. W., Yamamoto, M., Leitinger, N., & Tschachler, E. (2010). NF-E2-related factor 2 regulates the stress response to UVA-1-oxidized phospholipids in skin cells. The FASEB Journal, 24(1), 39–48. https://doi.org/10.1096/fj.09-133520

Gruber, F., Oskolkova, O., Leitner, A., Mildner, M., Mlitz, V., Lengauer, B., Kadl, A., Mrass, P., Krönke, G., Binder, B. R., Bochkov, V. N., Leitinger, N., & Tschachler, E. (2007). Photooxidation Generates Biologically Active Phospholipids That Induce Heme Oxygenase-1 in Skin Cells *. Journal of Biological Chemistry, 282(23), 16934–16941. https://doi.org/10.1074/jbc.M702523200

Halliday, G. M., Byrne, S. N., & Damian, D. L. (2011). Ultraviolet A radiation: Its role in immunosuppression and carcinogenesis. Seminars in Cutaneous Medicine and Surgery, 30(4), 214–221. https://doi.org/10.1016/j.sder.2011.08.002

Halliday, G.M., Rana, S. (2008). Waveband and Dose Dependency of Sunlight-induced Immunomodulation and Cellular Changes†. Photochemistry and Photobiology 84, 35–46. https://doi.org/10.1111/j.1751-1097.2007.00212.x

Han, C., Srivastava, A. K., Cui, T., Wang, Q.-E., & Wani, A. A. (2016). Differential DNA lesion formation and repair in heterochromatin and euchromatin. Carcinogenesis, 37(2), 129–138. https://doi.org/10.1093/carcin/bgv247

Hayflick, L., & Moorhead, P. S. (1961). The serial cultivation of human diploid cell strains. Experimental Cell Research, 25(3), 585–621. https://doi.org/10.1016/0014-4827(61)90192-6

He, Y.-Y., Huang, J.-L., Sik, R.H., Chignell, C.F., Liu, J., Waalkes, M.P. (2004). Expression Profiling of Human Keratinocyte Response to Ultraviolet A: Implications in Apoptosis. Journal of Investigative Dermatology 122, 533–543. https://doi.org/10.1046/j.0022-202X.2003.22123.x

He, Y.-Y., Pi, J., Huang, J.-L., Diwan, B. A., Waalkes, M. P., & Chignell, C. F. (2006). Chronic UVA irradiation of human HaCaT keratinocytes induces malignant transformation associated with acquired apoptotic resistance. Oncogene, 25(26), 3680–3688. https://doi.org/10.1038/sj.onc.1209384

Herbig, U., Ferreira, M., Condel, L., Carey, D., & Sedivy, J. M. (2006). Cellular Senescence in Aging Primates. *Science*. https://doi.org/10.1126/science.1122446

Hernandez-Segura, A., Nehme, J., & Demaria, M. (2018). Hallmarks of Cellular Senescence. Trends in Cell Biology, 28(6), 436–453. https://doi.org/10.1016/j.tcb.2018.02.001

Hilario, M., & Kalousis, A. (2008). Approaches to dimensionality reduction in proteomic biomarker studies. Briefings in Bioinformatics, 9(2), 102–118. https://doi.org/10.1093/bib/bbn005

Hildesheim, J., Awwad, R.T., Fornace, A.J. (2004). p38 Mitogen-Activated Protein Kinase Inhibitor Protects the Epidermis Against the Acute Damaging Effects of Ultraviolet Irradiation by Blocking Apoptosis and Inflammatory Responses. Journal of Investigative Dermatology 122, 497–502. https://doi.org/10.1111/j.1523-1747.2004.22229.x

Hintsala, H.-R., Siponen, M., Haapasaari, K.-M., Karihtala, P., Soini, Y. (2013). Claudins 1, 2, 3, 4, 5 and 7 in solar keratosis and squamocellular carcinoma of the skin. Int J Clin Exp Pathol 6, 2855–2863.

Hirst, J., Itzhak, D. N., Antrobus, R., Borner, G. H. H., & Robinson, M. S. (2018). Role of the AP-5 adaptor protein complex in late endosome-to-Golgi retrieval. PLOS Biology, 16(1), e2004411. https://doi.org/10.1371/journal.pbio.2004411

Holick, M. F. (2001). Chapter 2 - A perspective on the beneficial effects of moderate exposure to sunlight: Bone health, cancer prevention, mental health and well being. In P. U. Giacomoni (Org.), Comprehensive Series in Photosciences (Vol. 3, p. 11–37). Elsevier. https://doi.org/10.1016/S1568-461X(01)80037-5

Höhn, A., Weber, D., Jung, T., Ott, C., Hugo, M., Kochlik, B., Kehm, R., König, J., Grune, T., & Castro, J. P. (2017). Happily (n)ever after: Aging in the context of oxidative stress, proteostasis loss and cellular senescence. *Redox Biology*, *11*, 482–501. https://doi.org/10.1016/j.redox.2016.12.001

Ikehata, H. (2018). Mechanistic considerations on the wavelength-dependent variations of UVR genotoxicity and mutagenesis in skin: The discrimination of UVA-signature from UV-signature mutation. Photochemical & Photobiological Sciences, 17(12), 1861–1871. https://doi.org/10.1039/C7PP00360A

Ikehata, H., Kawai, K., Komura, J., Sakatsume, K., Wang, L., Imai, M., Higashi, S., Nikaido, O., Yamamoto, K., Hieda, K., Watanabe, M., Kasai, H., & Ono, T. (2008). UVA1 Genotoxicity Is Mediated Not by Oxidative Damage but by Cyclobutane Pyrimidine Dimers in Normal Mouse Skin. Journal of Investigative Dermatology, 128(9), 2289–2296. https://doi.org/10.1038/jid.2008.61

Ikehata, H., Mori, T., & Yamamoto, M. (2015). In Vivo Spectrum of UVC-induced Mutation in Mouse Skin Epidermis May Reflect the Cytosine Deamination Propensity of Cyclobutane Pyrimidine Dimers. Photochemistry and Photobiology, 91(6), 1488–1496. https://doi.org/10.1111/php.12525

Ikehata, H., & Ono, T. (2011). The Mechanisms of UV Mutagenesis. Journal of Radiation Research, 52(2), 115–125. https://doi.org/10.1269/jrr.10175

Islinger, M., Luöers, G. H., Li, K. W., Loos, M., & Voölkl, A. (2007). Rat Liver Peroxisomes after Fibrate Treatment: A SURVEY USING QUANTITATIVE MASS SPECTROMETRY*. Journal of Biological Chemistry, 282(32), 23055–23069. https://doi.org/10.1074/jbc.M610910200

Itahana, K., Zou, Y., Itahana, Y., Martinez, J.-L., Beausejour, C., Jacobs, J. J. L., Lohuizen, M. van, Band, V., Campisi, J., & Dimri, G. P. (2003). Control of the Replicative Life Span of Human Fibroblasts by p16 and the Polycomb Protein Bmi-1. *Molecular and Cellular Biology*. https://doi.org/10.1128/MCB.23.1.389-401.2003

Ito, S., Tan, L.J., Andoh, D., Narita, T., Seki, M., Hirano, Y., Narita, K., Kuraoka, I., Hiraoka, Y., Tanaka, K. (2010). MMXD, a TFIIH-Independent XPD-MMS19 Protein Complex Involved in Chromosome Segregation. Molecular Cell 39, 632–640. https://doi.org/10.1016/j.molcel.2010.07.029

Itzhak, D. N., Davies, C., Tyanova, S., Mishra, A., Williamson, J., Antrobus, R., Cox, J., Weekes, M. P., & Borner, G. H. H. (2017). A Mass Spectrometry-Based Approach for Mapping Protein Subcellular Localization Reveals the Spatial Proteome of Mouse Primary Neurons. Cell Reports, 20(11), 2706–2718. https://doi.org/10.1016/j.celrep.2017.08.063

Itzhak, D. N., Tyanova, S., Cox, J., & Borner, G. H. (2016). Global, quantitative and dynamic mapping of protein subcellular localization. eLife, 5, e16950. https://doi.org/10.7554/eLife.16950

Iwasa, H., Han, J., & Ishikawa, F. (2003). Mitogen-activated protein kinase p38 defines the common senescence-signalling pathway. *Genes to Cells*, 8(2), 131–144. https://doi.org/10.1046/j.1365-2443.2003.00620.x

Janzen, V., Forkert, R., Fleming, H. E., Saito, Y., Waring, M. T., Dombkowski, D. M., Cheng, T., DePinho, R. A., Sharpless, N. E., & Scadden, D. T. (2006). Stem-cell ageing

modified by the cyclin-dependent kinase inhibitor p16INK4a. *Nature*, *443*(7110), 421–426. https://doi.org/10.1038/nature05159

Jaskelioff, M., Muller, F. L., Paik, J.-H., Thomas, E., Jiang, S., Adams, A. C., Sahin, E., Kost-Alimova, M., Protopopov, A., Cadiñanos, J., Horner, J. W., Maratos-Flier, E., & DePinho, R. A. (2011). Telomerase reactivation reverses tissue degeneration in aged telomerase-deficient mice. *Nature*, *469*(7328), 102–106. https://doi.org/10.1038/nature09603

Jean Beltran, P. M., Mathias, R. A., & Cristea, I. M. (2016). A Portrait of the Human Organelle Proteome In Space and Time during Cytomegalovirus Infection. Cell Systems, 3(4), 361-373.e6. https://doi.org/10.1016/j.cels.2016.08.012

Jethwaney, D., Islam, M. R., Leidal, K. G., de Bernabe, D. B.-V., Campbell, K. P., Nauseef, W. M., & Gibson, B. W. (2007). Proteomic analysis of plasma membrane and secretory vesicles from human neutrophils. Proteome Science, 5(1), 12. https://doi.org/10.1186/1477-5956-5-12

Jiang, Y., Rabbi, M., Kim, M., Ke, C., Lee, W., Clark, R. L., Mieczkowski, P. A., & Marszalek, P. E. (2009). UVA Generates Pyrimidine Dimers in DNA Directly. Biophysical Journal, 96(3), 1151–1158. https://doi.org/10.1016/j.bpj.2008.10.030

Jugé, R., Breugnot, J., Da Silva, C., Bordes, S., Closs, B., Aouacheria, A. (2016). Quantification and Characterization of UVB-Induced Mitochondrial Fragmentation in Normal Primary Human Keratinocytes. Sci Rep 6, 35065. https://doi.org/10.1038/srep35065

Kappes, U. P., Luo, D., Potter, M., Schulmeister, K., & Rünger, T. M. (2006). Short- and Long-Wave UV Light (UVB and UVA) Induce Similar Mutations in Human Skin Cells. Journal of Investigative Dermatology, 126(3), 667–675. https://doi.org/10.1038/sj.jid.5700093

Karran, P., & Brem, R. (2016). Protein oxidation, UVA and human DNA repair. DNA Repair, 44, 178–185. https://doi.org/10.1016/j.dnarep.2016.05.024

Kennedy, M. A., Hofstadter, W. A., & Cristea, I. M. (2020). TRANSPIRE: A Computational Pipeline to Elucidate Intracellular Protein Movements from Spatial Proteomics Data Sets. Journal of the American Society for Mass Spectrometry, 31(7), 1422–1439. https://doi.org/10.1021/jasms.0c00033

Keyse, S. M., & Tyrrell, R. M. (1987). Both near ultraviolet radiation and the oxidizing agent hydrogen peroxide induce a 32-kDa stress protein in normal human skin fibroblasts. Journal of Biological Chemistry, 262(30), 14821–14825. https://doi.org/10.1016/S0021-9258(18)47869-6

Kimura, S., Warabi, E., Yanagawa, T., Ma, D., Itoh, K., Ishii, Y., Kawachi, Y., & Ishii, T. (2009). Essential role of Nrf2 in keratinocyte protection from UVA by quercetin. Biochemical and Biophysical Research Communications, 387(1), 109–114. https://doi.org/10.1016/j.bbrc.2009.06.136

Kiyoshima, T., Enoki, N., Kobayashi, I., Sakai, T., Nagata, K., Wada, H., Fujiwara, H., Ookuma, Y., & Sakai, H. (2012). Oxidative stress caused by a low concentration of hydrogen peroxide induces senescence-like changes in mouse gingival fibroblasts. International Journal of Molecular Medicine, 30(5), 1007–1012. https://doi.org/10.3892/ijmm.2012.1102

Klecak, G., Urbach, F., & Urwyler, H. (1997). Fluoroquinolone antibacterials enhance UVA-induced skin tumors. Journal of Photochemistry and Photobiology B: Biology, 37(3), 174–181. https://doi.org/10.1016/S1011-1344(96)07424-6

Kochevar, I. E. (1983). Basic Concepts in Photobiology. In J. A. Parrish, M. L. Kripke, & W. L. Morison (Orgs.), Photoimmunology (p. 5–21). Springer US. https://doi.org/10.1007/978-1-4613-3670-9_1

Kolarsick, P. A. J., Kolarsick, M. A., & Goodwin, C. (2011). Anatomy and Physiology of the Skin. Journal of the Dermatology Nurses' Association, 3(4), 203–213. https://doi.org/10.1097/JDN.0b013e3182274a98

Koning, T. M. G., Davies, R. J. H., & Kaptein, R. (1990). The solution structure of the intramolecular photoproduct of d(TpA) derived with the use of NMR and a combination of distance geometry and molecular dynamics. Nucleic Acids Research, 18(2), 277–284. https://doi.org/10.1093/nar/18.2.277

Korolchuk, V. I., Miwa, S., Carroll, B., & Zglinicki, T. von. (2017). Mitochondria in Cell Senescence: Is Mitophagy the Weakest Link? EBioMedicine, 21, 7–13. https://doi.org/10.1016/j.ebiom.2017.03.020

Krahmer, N., Hilger, M., Kory, N., Wilfling, F., Stoehr, G., Mann, M., Farese, R. V., & Walther, T. C. (2013). Protein Correlation Profiles Identify Lipid Droplet Proteins with High Confidence. Molecular & Cellular Proteomics: MCP, 12(5), 1115–1126. https://doi.org/10.1074/mcp.M112.020230

Krahmer, N., Najafi, B., Schueder, F., Quagliarini, F., Steger, M., Seitz, S., Kasper, R., Salinas, F., Cox, J., Uhlenhaut, N. H., Walther, T. C., Jungmann, R., Zeigerer, A., Borner, G. H. H., & Mann, M. (2018). Organellar Proteomics and Phospho-Proteomics Reveal Subcellular Reorganization in Diet-Induced Hepatic Steatosis. Developmental Cell, 47(2), 205-221.e7. https://doi.org/10.1016/j.devcel.2018.09.017

Kranen, H. J. van, Laat, A. de, Ven, J. van de, Wester, P. W., Vries, A. de, Berg, R. J. W., Kreijl, C. F. van, & Gruijl, F. R. de. (1997). Low Incidence of p53 Mutations in UVA (365-nm)-induced Skin Tumors in Hairless Mice. Cancer Research, 57(7), 1238–1240.

Krenciute, G., Liu, S., Yucer, N., Shi, Y., Ortiz, P., Liu, Q., Kim, B.-J., Odejimi, A.O., Leng, M., Qin, J., Wang, Y. (2013). Nuclear BAG6-UBL4A-GET4 Complex Mediates DNA Damage Signaling and Cell Death. J. Biol. Chem. 288, 20547–20557. https://doi.org/10.1074/jbc.M112.443416

Krtolica, A., Parrinello, S., Lockett, S., Desprez, P. Y., & Campisi, J. (2001). Senescent fibroblasts promote epithelial cell growth and tumorigenesis: A link between cancer and aging. Proceedings of the National Academy of Sciences of the United States of America, 98(21), 12072–12077. https://doi.org/10.1073/pnas.211053698

Kucera, M., Isserlin, R., Arkhangorodsky, A., & Bader, G. D. (2016). AutoAnnotate: A Cytoscape app for summarizing networks with semantic annotations. F1000Research, 5. https://doi.org/10.12688/f1000research.9090.1

Kuilman, T., Michaloglou, C., Mooi, W. J., & Peeper, D. S. (2010). The essence of senescence. Genes & Development, 24(22), 2463–2479. https://doi.org/10.1101/gad.1971610

Kuluncsics, Z., Perdiz, D., Brulay, E., Muel, B., & Sage, E. (1999). Wavelength dependence of ultraviolet-induced DNA damage distribution: Involvement of direct or indirect mechanisms and possible artefacts. Journal of Photochemistry and Photobiology B: Biology, 49(1), 71–80. https://doi.org/10.1016/S1011-1344(99)00034-2

Kvam, E., Noel, A., Basu-Modak, S., & Tyrrell, R. M. (1999). Cyclooxygenase dependent release of heme from microsomal hemeproteins correlates with induction of heme oxygenase 1 transcription in human fibroblasts. Free Radical Biology and Medicine, 26(5), 511–517. https://doi.org/10.1016/S0891-5849(98)00224-X

Kvam, E., & Tyrrell, R. M. (1997). Induction of oxidative DNA base damage in human skin cells by UV and near visible radiation. Carcinogenesis, 18(12), 2379–2384. https://doi.org/10.1093/carcin/18.12.2379

Lamore, S. D., & Wondrak, G. T. (2011). Autophagic-lysosomal dysregulation downstream of cathepsin B inactivation in human skin fibroblasts exposed to UVA. Photochemical & Photobiological Sciences, 11(1), 163–172. https://doi.org/10.1039/C1PP05131H

Larance, M., Lamond, A.I., 2015. Multidimensional proteomics for cell biology. Nature Reviews Molecular Cell Biology 16, 269–280. https://doi.org/10.1038/nrm3970

Lautier, D., Luscher, P., & Tyrrell, R. M. (1992). Endogenous glutathione levels modulate both constitutive and UVA radiation/hydrogen peroxide inducible expression of the human heme oxygenase gene. Carcinogenesis, 13(2), 227–232. https://doi.org/10.1093/carcin/13.2.227

Lee, D.-H., & Pfeifer, G. P. (2003). Deamination of 5-Methylcytosines within Cyclobutane Pyrimidine Dimers Is an Important Component of UVB Mutagenesis *. Journal of Biological Chemistry, 278(12), 10314–10321. https://doi.org/10.1074/jbc.M212696200

Lee, S., & Schmitt, C. A. (2019). The dynamic nature of senescence in cancer. Nature Cell Biology, 21(1), 94–101. https://doi.org/10.1038/s41556-018-0249-2

Lehman, T. A., Modali, R., Boukamp, P., Stanek, J., Bennett, W. P., Welsh, J. A., Metcalf, R. A., Stampfer, M. R., Fusenig, N., Rogan, E. M., & Harris, C. C. (1993). P53 Mutations in human immortalized epithelial cell lines. Carcinogenesis, 14(5), 833–839. https://doi.org/10.1093/carcin/14.5.833

Leiter, U., Eigentler, T., & Garbe, C. (2014). Epidemiology of skin cancer. Advances in Experimental Medicine and Biology, 810, 120–140. https://doi.org/10.1007/978-1-4939-0437-2_7

Leontieva, O. V., & Blagosklonny, M. V. (2017). While reinforcing cell cycle arrest, rapamycin and Torins suppress senescence in UVA-irradiated fibroblasts. Oncotarget, 8(65), 109848–109856. https://doi.org/10.18632/oncotarget.17827

Liang, W., Gao, R., Yang, M., Wang, X., Cheng, K., Shi, X., He, C., Li, Y., Wu, Y., Shi, L., Chen, J., & Yu, X. (2020). MARCKSL1 promotes the proliferation, migration and invasion of lung adenocarcinoma cells. Oncology Letters, 19(3), 2272–2280. https://doi.org/10.3892/ol.2020.11313

Lippens, S., Denecker, G., Ovaere, P., Vandenabeele, P., & Declercq, W. (2005). Death penalty for keratinocytes: Apoptosis versus cornification. Cell Death & Differentiation, 12(2), 1497–1508. https://doi.org/10.1038/sj.cdd.4401722

Liu, X., Ding, J., & Meng, L. (2018). Oncogene-induced senescence: A double edged sword in cancer. Acta Pharmacologica Sinica, *39*(10), 1553–1558. https://doi.org/10.1038/aps.2017.198

Liu, Y., Xu, G., Sayre, L. M. (2003). Carnosine inhibits (E)-4-hydroxy-2-nonenal-induced protein cross-linking: structural characterization of carnosine-HNE adducts. Chemical Research in Toxicology, 16 (12), 1589–1597. https://doi.org/10.1021/tx034160a

Liu, L., Xie, H., Chen, X., Shi, W., Xiao, X., Lei, D., Li, J. Differential response of normal human epidermal keratinocytes and HaCaT cells to hydrogen peroxide-induced oxidative stress. Clinical and Experimental Dermatology, 37 (7), 772-780. https://doi:10.1111/j.1365-2230.2011.04315.x

López-Otín, C., Blasco, M. A., Partridge, L., Serrano, M., & Kroemer, G. (2013). The Hallmarks of Aging. Cell, 153(6), 1194–1217. https://doi.org/10.1016/j.cell.2013.05.039

Lundberg, E., & Borner, G. H. H. (2019). Spatial proteomics: A powerful discovery tool for cell biology. Nature Reviews Molecular Cell Biology, 20(5), 285–302. https://doi.org/10.1038/s41580-018-0094-y

Maaten, L. van der, & Hinton, G. E. (2008). Visualizing Data using t-SNE. Journal of Machine Learning Research, 9, 2579-2605.

Marshall, A. G. and Hendrickson, C. L. (2008). High-Resolution Mass Spectrometers. Annual Review of Analytical Chemistry, 1, 579-599. https://doi.org/10.1146/annurev.anchem.1.031207.112945

Martinez-Val, A., Bekker-Jensen, D. B., Steigerwald, S., Mehta, A., Tran, T., Sikorski, K., Torres-Vega, E., Kwasniewicz, E., Brynjólfsdóttir, S. H., Frankel, L. B., Kjøbsted, R., Krogh, N., Lundby, A., Bekker-Jensen, S., Lund-Johansen, F., & Olsen, J. V. (2021). Spatial-proteomics reveal in-vivo phospho-signaling dynamics at subcellular resolution, Nature Communications, 12, 7113. https://doi.org/10.1038/s41467-021-27398-y

Marusyk, A., Wheeler, L. J., Mathews, C. K., & DeGregori, J. (2007). P53 Mediates Senescence-Like Arrest Induced by Chronic Replicational Stress. Molecular and Cellular Biology, 27(15), 5336–5351. https://doi.org/10.1128/MCB.01316-06

Matsui, M. S., Hsia, A., Miller, J. D., Hanneman, K., Scull, H., Cooper, K. D., & Baron, E. (2009). Non-Sunscreen Photoprotection: Antioxidants Add Value to a Sunscreen. Journal of Investigative Dermatology Symposium Proceedings, 14(1), 56–59. https://doi.org/10.1038/jidsymp.2009.14

Mattiazzi Usaj, M., Styles, E.B., Verster, A.J., Friesen, H., Boone, C., Andrews, B.J. (2016). High-Content Screening for Quantitative Cell Biology. Trends Cell Biol. 26, 598–611. https://doi.org/10.1016/j.tcb.2016.03.008

Mazière, C., Conte, M.-A., Leborgne, L., Levade, T., Hornebeck, W., Santus, R., & Mazière, J.-C. (2001). UVA Radiation Stimulates Ceramide Production: Relationship to Oxidative Stress and Potential Role in ERK, JNK, and p38 Activation. Biochemical and Biophysical Research Communications, 281(2), 289–294. https://doi.org/10.1006/bbrc.2001.4348

McCulloch, S. D., Kokoska, R. J., Garg, P., Burgers, P. M., & Kunkel, T. A. (2009). The efficiency and fidelity of 8-oxo-guanine bypass by DNA polymerases δ and η. Nucleic Acids Research, 37(9), 2830–2840. https://doi.org/10.1093/nar/gkp103

Meewes, C., Brenneisen, P., Wenk, J., Kuhr, L., Ma, W., Alikoski, J., Poswig, A., Krieg, T., & Scharffetter-Kochanek, K. (2001). Adaptive antioxidant response protects dermal fibroblasts from UVA-induced phototoxicity. Free Radical Biology and Medicine, 30(3), 238–247. https://doi.org/10.1016/S0891-5849(00)00463-9

Meissner, F., & Mann, M. (2014). Quantitative shotgun proteomics: Considerations for a high-quality workflow in immunology. Nature Immunology, 15(2), 112–117. https://doi.org/10.1038/ni.2781

Melnikova, V. O., & Ananthaswamy, H. N. (2005). Cellular and molecular events leading to the development of skin cancer. Mutation Research/Fundamental and Molecular Mechanisms of Mutagenesis, 571(1), 91–106. https://doi.org/10.1016/j.mrfmmm.2004.11.015

Milanovic, M., Fan, D. N. Y., Belenki, D., Däbritz, J. H. M., Zhao, Z., Yu, Y., Dörr, J. R., Dimitrova, L., Lenze, D., Monteiro Barbosa, I. A., Mendoza-Parra, M. A., Kanashova, T., Metzner, M., Pardon, K., Reimann, M., Trumpp, A., Dörken, B., Zuber, J., Gronemeyer, H., … Schmitt, C. A. (2018). Senescence-associated reprogramming promotes cancer stemness. Nature, 553(7686), 96–100. https://doi.org/10.1038/nature25167

Minami, Y., Kawabata, K., Kubo, Y., Arase, S., Hirasaka, K., Nikawa, T., Bando, N., Kawai, Y., & Terao, J. (2009). Peroxidized cholesterol-induced matrix metalloproteinase-9 activation and its suppression by dietary β-carotene in photoaging of hairless mouse skin. The Journal of Nutritional Biochemistry, 20(5), 389–398. https://doi.org/10.1016/j.jnutbio.2008.04.010

Mitchell, D. L., Haipek, C. A., & Clarkson, J. M. (1985). (6–4) Photoproducts are removed from the DNA of UV-irradiated mammalian cells more efficiently than cyclobutane pyrimidine dimers. Mutation Research Letters, 143(3), 109–112. https://doi.org/10.1016/S0165-7992(85)80018-X

Montenarh, M. (2016). Protein kinase CK2 in DNA damage and repair. Translational Cancer Research 5. https://doi.org/10.21037/6469

Moore, D. E. (2002). Drug-Induced Cutaneous Photosensitivity. Drug Safety, 25(5), 345–372. https://doi.org/10.2165/00002018-200225050-00004

Moosa, J. M., Guan, S., Moran, M. F., & Ma, B. (2020). Repeat-Preserving Decoy Database for False Discovery Rate Estimation in Peptide Identification. Journal of Proteome Research, 19(3), 1029–1036. https://doi.org/10.1021/acs.jproteome.9b00555

Moreno, N. C., de Souza, T. A., Garcia, C. C. M., Ruiz, N. Q., Corradi, C., Castro, L. P., Munford, V., Ienne, S., Alexandrov, L. B., & Menck, C. F. M. (2020). Whole-exome sequencing reveals the impact of UVA light mutagenesis in xeroderma pigmentosum variant human cells. Nucleic Acids Research, 48(4), 1941–1953. https://doi.org/10.1093/nar/gkz1182

Mouret, S., Baudouin, C., Charveron, M., Favier, A., Cadet, J., & Douki, T. (2006a). Cyclobutane pyrimidine dimers are predominant DNA lesions in whole human skin exposed to UVA radiation. Proceedings of the National Academy of Sciences of the United States of America, 103(37), 13765–13770. https://doi.org/10.1073/pnas.0604213103

Mouret, S., Baudouin, C., Charveron, M., Favier, A., Cadet, J., & Douki, T. (2006b). Cyclobutane pyrimidine dimers are predominant DNA lesions in whole human skin exposed to UVA radiation. Proceedings of the National Academy of Sciences, 103(37), 13765–13770. https://doi.org/10.1073/pnas.0604213103

Mouret, S., Forestier, A., & Douki, T. (2012). The specificity of UVA-induced DNA damage in human melanocytes. Photochemical & Photobiological Sciences: Official Journal of the European Photochemistry Association and the European Society for Photobiology, 11(1), 155–162. https://doi.org/10.1039/c1pp05185g

Mouret, S., Philippe, C., Gracia-Chantegrel, J., Banyasz, A., Karpati, S., Markovitsi, D., & Douki, T. (2010). UVA-induced cyclobutane pyrimidine dimers in DNA: A direct photochemical mechanism? Organic & Biomolecular Chemistry, 8(7), 1706–1711. https://doi.org/10.1039/B924712B

Mueller, M. M., Peter, W., Mappes, M., Huelsen, A., Steinbauer, H., Boukamp, P., Vaccariello, M., Garlick, J., & Fusenig, N. E. (2001). Tumor Progression of Skin Carcinoma Cells in Vivo Promoted by Clonal Selection, Mutagenesis, and Autocrine Growth Regulation by Granulocyte Colony-Stimulating Factor and Granulocyte-

Macrophage Colony-Stimulating Factor. The American Journal of Pathology, 159(4), 1567–1579.

Mulvey, C. M., Breckels, L. M., Crook, O. M., Sanders, D. J., Ribeiro, A. L. R., Geladaki, A., Christoforou, A., Britovšek, N. K., Hurrell, T., Deery, M. J., Gatto, L., Smith, A. M., & Lilley, K. S. (2021). Spatiotemporal proteomic profiling of the pro-inflammatory response to lipopolysaccharide in the THP-1 human leukaemia cell line. Nature Communications, 12(1), 5773. https://doi.org/10.1038/s41467-021-26000-9

Mulvey, C. M., Breckels, L. M., Geladaki, A., Britovšek, N. K., Nightingale, D. J. H., Christoforou, A., Elzek, M., Deery, M. J., Gatto, L., & Lilley, K. S. (2017). Using hyperLOPIT to perform high-resolution mapping of the spatial proteome. Nature Protocols, 12(6), 1110–1135. https://doi.org/10.1038/nprot.2017.026

Murai, K., Skrupskelyte, G., Piedrafita, G., Hall, M., Kostiou, V., Ong, S. H., Nagy, T., Cagan, A., Goulding, D., Klein, A. M., Hall, B. A., & Jones, P. H. (2018). Epidermal Tissue Adapts to Restrain Progenitors Carrying Clonal p53 Mutations. Cell Stem Cell, 23(5), 687-699.e8. https://doi.org/10.1016/j.stem.2018.08.017

Nacarelli, T., Lau, L., Fukumoto, T., Zundell, J., Fatkhutdinov, N., Wu, S., Aird, K. M., Iwasaki, O., Kossenkov, A. V., Schultz, D., Noma, K., Baur, J. A., Schug, Z., Tang, H.-Y., Speicher, D. W., David, G., & Zhang, R. (2019). NAD + metabolism governs the proinflammatory senescence-associated secretome. Nature Cell Biology, 21(3), 397–407. https://doi.org/10.1038/s41556-019-0287-4

Naidoo, N. (2009). ER and aging—Protein folding and the ER stress response. Ageing Research Reviews, 8(3), 150–159. https://doi.org/10.1016/j.arr.2009.03.001

Narzt, M.-S., Nagelreiter, I.-M., Oskolkova, O., Bochkov, V. N., Latreille, J., Fedorova, M., Ni, Z., Sialana, F. J., Lubec, G., Filzwieser, M., Laggner, M., Bilban, M., Mildner, M., Tschachler, E., Grillari, J., & Gruber, F. (2019). A novel role for NUPR1 in the keratinocyte stress response to UV oxidized phospholipids. Redox Biology, 20, 467–482. https://doi.org/10.1016/j.redox.2018.11.006

Nelson, G., Wordsworth, J., Wang, C., Jurk, D., Lawless, C., Martin-Ruiz, C., & Zglinicki, T. von. (2012). A senescent cell bystander effect: Senescence-induced senescence. Aging Cell, 11(2), 345–349. https://doi.org/10.1111/j.1474-9726.2012.00795.x

Nishi, R., Okuda, Y., Watanabe, E., Mori, T., Iwai, S., Masutani, C., Sugasawa, K., Hanaoka, F. (2005). Centrin 2 Stimulates Nucleotide Excision Repair by Interacting with Xeroderma Pigmentosum Group C Protein. Molecular and Cellular Biology 25, 5664–5674. https://doi.org/10.1128/MCB.25.13.5664-5674.2005

O'Donovan, P., Perrett, C. M., Zhang, X., Montaner, B., Xu, Y.-Z., Harwood, C. A., McGregor, J. M., Walker, S. L., Hanaoka, F., & Karran, P. (2005). Azathioprine and UVA Light Generate Mutagenic Oxidative DNA Damage. Science, 309(5742), 1871–1874. https://doi.org/10.1126/science.1114233

Okada, K., Takahashi, Y., Ohnishi, K., Ishikawa, O., & Miyachi, Y. (1994). Time-dependent effect of chronic UV irradiation on superoxide dismutase and catalase activity in hairless mice skin. Journal of Dermatological Science, 8(3), 183–186. https://doi.org/10.1016/0923-1811(94)90052-3

Orre, L. M., Vesterlund, M., Pan, Y., Arslan, T., Zhu, Y., Woodbridge, A. F., Frings, O., Fredlund, E., & Lehtiö, J. (2019). SubCellBarCode: Proteome-wide Mapping of Protein Localization and Relocalization. Molecular Cell, 73(1), 166-182.e7. https://doi.org/10.1016/j.molcel.2018.11.035

Ouédraogo, G. D., & Redmond, R. W. (2003). Secondary Reactive Oxygen Species Extend the Range of Photosensitization Effects in Cells: DNA Damage Produced Via Initial Membrane Photosensitization¶†. Photochemistry and Photobiology, 77(2), 192–203. https://doi.org/10.1562/0031-8655(2003)0770192SROSET2.0.CO2

Pagliarini, D. J., Calvo, S. E., Chang, B., Sheth, S. A., Vafai, S. B., Ong, S.-E., Walford, G. A., Sugiana, C., Boneh, A., Chen, W. K., Hill, D. E., Vidal, M., Evans, J. G., Thorburn, D. R., Carr, S. A., & Mootha, V. K. (2008). A Mitochondrial Protein Compendium

Elucidates Complex I Disease Biology. Cell, 134(1), 112–123. https://doi.org/10.1016/j.cell.2008.06.016

Parca, L., Beck, M., Bork, P., & Ori, A. (2018). Quantifying compartment-associated variations of protein abundance in proteomics data. Molecular Systems Biology, 14(7). https://doi.org/10.15252/msb.20178131

Parrinello, S., Coppe, J.-P., Krtolica, A., & Campisi, J. (2005). Stromal-epithelial interactions in aging and cancer: Senescent fibroblasts alter epithelial cell differentiation. Journal of Cell Science, 118(3), 485–496. https://doi.org/10.1242/jcs.01635

Passos, J. F., Saretzki, G., Ahmed, S., Nelson, G., Richter, T., Peters, H., Wappler, I., Birket, M. J., Harold, G., Schaeuble, K., Birch-Machin, M. A., Kirkwood, T. B. L., & Zglinicki, T. von. (2007). Mitochondrial Dysfunction Accounts for the Stochastic Heterogeneity in Telomere-Dependent Senescence. PLOS Biology, 5(5), e110. https://doi.org/10.1371/journal.pbio.0050110

Persa, O. D., Koester, J., & Niessen, C. M. (2021). Regulation of Cell Polarity and Tissue Architecture in Epidermal Aging and Cancer. Journal of Investigative Dermatology, 141(4, Supplement), 1017–1023. https://doi.org/10.1016/j.jid.2020.12.012

Perkins, D. N., Pappin, D. J., Creasy, D. M., & Cottrell, J. S. (1999). Probability-based protein identification by searching sequence databases using mass spectrometry data. Electrophoresis, 20(18), 3551–3567. https://doi.org/10.1002/(SICI)1522-2683(19991201)20:18<3551::AID-ELPS3551>3.0.CO;2-2

Perry, R. H., Cooks, R. G., & Noll, R. J. (2008). Orbitrap mass spectrometry: Instrumentation, ion motion and applications. Mass Spectrometry Reviews, 27(6), 661–699. https://doi.org/10.1002/mas.20186

Petersen, M. J., Hansen, C., & Craig, S. (1992). Ultraviolet A irradiation stimulates collagenase production in cultured human fibroblasts. The Journal of Investigative Dermatology, 99(4), 440–444. https://doi.org/10.1111/1523-1747.ep12616142

Pfeifer, G. P. (2020). Mechanisms of UV-induced mutations and skin cancer. Genome Instability & Disease, 1(3), 99–113. https://doi.org/10.1007/s42764-020-00009-8

Pincelli, C., & Marconi, A. (2010). Keratinocyte stem cells: Friends and foes. Journal of Cellular Physiology, 225(2), 310–315. https://doi.org/10.1002/jcp.22275

Plikus, M. V., Wang, X., Sinha, S., Forte, E., Thompson, S. M., Herzog, E. L., Driskell, R. R., Rosenthal, N., Biernaskie, J., & Horsley, V. (2021). Fibroblasts: Origins, definitions, and functions in health and disease. Cell, 184(15), 3852–3872. https://doi.org/10.1016/j.cell.2021.06.024

Pluquet, O., Pourtier, A., & Abbadie, C. (2014). The unfolded protein response and cellular senescence. A Review in the Theme: Cellular Mechanisms of Endoplasmic Reticulum Stress Signaling in Health and Disease. American Journal of Physiology-Cell Physiology, 308(6), C415–C425. https://doi.org/10.1152/ajpcell.00334.2014

Ponomarenko, E. A., Poverennaya, E. V., Ilgisonis, E. V., Pyatnitskiy, M. A., Kopylov, A. T., Zgoda, V. G., Lisitsa, A. V., & Archakov, A. I. (2016). The Size of the Human Proteome: The Width and Depth. International Journal of Analytical Chemistry, 2016, 7436849. https://doi.org/10.1155/2016/7436849

Poswig, A., Wenk, J., Brenneisen, P., Wlaschek, M., Hommel, C., Quel, G., Faisst, K., Dissemond, J., Krieg, T., Scharffetter-Kochanek, K., & Briviba, K. (1999). Adaptive Antioxidant Response of Manganese-Superoxide Dismutase Following Repetitive UVA Irradiation. Journal of Investigative Dermatology, 112(1), 13–18. https://doi.org/10.1046/j.1523-1747.1999.00465.x

Pouget, J.-P., Douki, T., Richard, M.-J., & Cadet, J. (2000). DNA Damage Induced in Cells by γ and UVA Radiation as Measured by HPLC/GC−MS and HPLC−EC and Comet Assay. Chemical Research in Toxicology, 13(7), 541–549. https://doi.org/10.1021/tx000020e

Pourzand, C., Watkin, R. D., Brown, J. E., & Tyrrell, R. M. (1999). Ultraviolet A radiation induces immediate release of iron in human primary skin fibroblasts: The role of ferritin. Proceedings of the National Academy of Sciences, 96(12), 6751–6756. https://doi.org/10.1073/pnas.96.12.6751

Premi, S., Wallisch, S., Mano, C. M., Weiner, A. B., Bacchiocchi, A., Wakamatsu, K., Bechara, E. J. H., Halaban, R., Douki, T., & Brash, D. E. (2015). Chemiexcitation of melanin derivatives induces DNA photoproducts long after UV exposure. Science, 347(6224), 842–847. https://doi.org/10.1126/science.1256022

Pruitt, S. C., Freeland, A., Rusiniak, M. E., Kunnev, D., & Cady, G. K. (2013). Cdkn1b overexpression in adult mice alters the balance between genome and tissue ageing. Nature Communications, 4(1), 2626. https://doi.org/10.1038/ncomms3626

Rakovic, A., Grünewald, A., Kottwitz, J., Brüggemann, N., Pramstaller, P.P., Lohmann, K., Klein, C. (2011). Mutations in PINK1 and Parkin Impair Ubiquitination of Mitofusins in Human Fibroblasts. PLOS ONE 6, e16746. https://doi.org/10.1371/journal.pone.0016746

Ramos, M. C., Steinbrenner, H., Stuhlmann, D., Sies, H., & Brenneisen, P. (2004). Induction of MMP-10 and MMP-1 in a squamous cell carcinoma cell line by ultraviolet radiation. 385(1), 75–86. https://doi.org/10.1515/BC.2004.010

Rappsilber, J., Mann, M., & Ishihama, Y. (2007). Protocol for micro-purification, enrichment, pre-fractionation and storage of peptides for proteomics using StageTips. Nature Protocols, 2(8), 1896–1906. https://doi.org/10.1038/nprot.2007.261

Ray, G. J., Boydston, E. A., Shortt, E., Wyant, G. A., Lourido, S., Chen, W. W., & Sabatini, D. M. (2020). A PEROXO-Tag Enables Rapid Isolation of Peroxisomes from Human Cells. iScience, 23(5). https://doi.org/10.1016/j.isci.2020.101109

Remy, G., Risco, A.M., Iñesta-Vaquera, F.A., González-Terán, B., Sabio, G., Davis, R.J., Cuenda, A. (2010). Differential activation of p38MAPK isoforms by MKK6 and MKK3. Cellular Signalling 22, 660–667. https://doi.org/10.1016/j.cellsig.2009.11.020

Ren, Q., Kari, C., Quadros, M. R. D., Burd, R., McCue, P., Dicker, A. P., & Rodeck, U. (2006). Malignant Transformation of Immortalized HaCaT Keratinocytes through Deregulated Nuclear Factor κB Signaling. Cancer Research, 66(10), 5209–5215. https://doi.org/10.1158/0008-5472.CAN-05-4158

Ridley, A.J., Whiteside, J.R., McMillan, T.J., Allinson, S.L. (2009). Cellular and sub-cellular responses to UVA in relation to carcinogenesis. International Journal of Radiation Biology 85, 177–195. https://doi.org/10.1080/09553000902740150

Rochette, P. J., & Brash, D. E. (2010). Human Telomeres Are Hypersensitive to UV-Induced DNA Damage and Refractory to Repair. PLOS Genetics, 6(4), e1000926. https://doi.org/10.1371/journal.pgen.1000926

Rosen, J. E., Prahalad, A. K., & Williams, G. M. (1996). 8-Oxodeoxyguanosine Formation in the DNA of Cultured Cells After Exposure to H2O2 Alone or with UVB or UVA Irradiation. Photochemistry and Photobiology, 64(1), 117–122. https://doi.org/10.1111/j.1751-1097.1996.tb02430.x

Rozenblatt-Rosen, O., Stubbington, M. J. T., Regev, A., & Teichmann, S. A. (2017). The Human Cell Atlas: From vision to reality. Nature, 550(7677), 451–453. https://doi.org/10.1038/550451a

Rudan, M. V., Mishra, A., Klose, C., Eggert, U. S., & Watt, F. M. (2020). Human epidermal stem cell differentiation is modulated by specific lipid subspecies. Proceedings of the National Academy of Sciences, 117(36), 22173–22182. https://doi.org/10.1073/pnas.2011310117

Ryšavá, A., Čížková, K., Franková, J., Roubalová, L., Ulrichová, J., Vostálová, J., Vrba, J., Zálešák, B., & Rajnochová Svobodová, A. (2020). Effect of UVA radiation on the Nrf2 signalling pathway in human skin cells. Journal of Photochemistry and Photobiology B: Biology, 209, 111948. https://doi.org/10.1016/j.jphotobiol.2020.111948

Sabouny, R., Shutt, T.E. (2020). Reciprocal Regulation of Mitochondrial Fission and Fusion. Trends in Biochemical Sciences 45, 564–577. https://doi.org/10.1016/j.tibs.2020.03.009

Sage, E., Girard, P.-M., & Francesconi, S. (2011). Unravelling UVA-induced mutagenesis. Photochemical & Photobiological Sciences, 11(1), 74–80. https://doi.org/10.1039/C1PP05219E

Saliou, C., Kitazawa, M., McLaughlin, L., Yang, J.-P., Lodge, J.K., Tetsuka, T., Iwasaki, K., Cillard, J., Okamoto, T., Packer, L. (1999). Antioxidants modulate acute solar ultraviolet radiation-induced NF-kappa-B activation in a human keratinocyte cell line. Free Radical Biology and Medicine 26, 174–183. https://doi.org/10.1016/S0891-5849(98)00212-3

Sarkisian, C. J., Keister, B. A., Stairs, D. B., Boxer, R. B., Moody, S. E., & Chodosh, L. A. (2007). Dose-dependent oncogene-induced senescence in vivo and its evasion during mammary tumorigenesis. Nature Cell Biology, 9(5), 493–505. https://doi.org/10.1038/ncb1567

Scharffetter, K., Wlaschek, M., Hogg, A., Bolsen, K., Schothorst, A., Goerz, G., Krieg, T., & Plewig, G. (1991). UVA irradiation induces collagenase in human dermal fibroblasts in vitro and in vivo. Archives of Dermatological Research, 283(8), 506–511. https://doi.org/10.1007/BF00371923

Schirmer, E. C., Florens, L., Guan, T., Yates, J. R., & Gerace, L. (2003). Nuclear Membrane Proteins with Potential Disease Links Found by Subtractive Proteomics. Science, 301(5638), 1380–1382. https://doi.org/10.1126/science.1088176

Schmidtke, C., Tiede, S., Thelen, M., Käkelä, R., Jabs, S., Makrypidi, G., Sylvester, M., Schweizer, M., Braren, I., Brocke-Ahmadinejad, N., Cotman, S. L., Schulz, A., Gieselmann, V., & Braulke, T. (2019). Lysosomal proteome analysis reveals that CLN3-defective cells have multiple enzyme deficiencies associated with changes in intracellular trafficking. Journal of Biological Chemistry, 294(24), 9592–9604. https://doi.org/10.1074/jbc.RA119.008852

Schuch, A. P., Moreno, N. C., Schuch, N. J., Menck, C. F. M., & Garcia, C. C. M. (2017). Sunlight damage to cellular DNA: Focus on oxidatively generated lesions. Free Radical Biology & Medicine, 107, 110–124. https://doi.org/10.1016/j.freeradbiomed.2017.01.029

Sen, P., Shah, P. P., Nativio, R., & Berger, S. L. (2016). Epigenetic mechanisms regulating longevity and aging. *Cell*, *166*(4), 822–839. https://doi.org/10.1016/j.cell.2016.07.050

Senko, M. W., Remes, P. M., Canterbury, J. D., Mathur, R., Song, Q., Eliuk, S. M., Mullen, C., Earley, L., Hardman, M., Blethrow, J. D., Bui, H., Specht, A., Lange, O., Denisov, E., Makarov, A., Horning, S., & Zabrouskov, V. (2013). Novel Parallelized Quadrupole/Linear Ion Trap/Orbitrap Tribrid Mass Spectrometer Improving Proteome Coverage and Peptide Identification Rates. Analytical Chemistry, 85(24), 11710–11714. https://doi.org/10.1021/ac403115c

Setlow, R. B., Grist, E., Thompson, K., & Woodhead, A. D. (1993). Wavelengths effective in induction of malignant melanoma. Proceedings of the National Academy of Sciences, 90(14), 6666–6670. https://doi.org/10.1073/pnas.90.14.6666

Setlow, R. B., & Setlow, J. K. (1962). Evidence That Ultraviolet-Induced Thymine Dimers In Dna Cause Biological Damage. Proceedings of the National Academy of Sciences of the United States of America, 48(7), 1250–1257.

Serrano, M., Lin, A. W., McCurrach, M. E., Beach, D., & Lowe, S. W. (1997). Oncogenic ras Provokes Premature Cell Senescence Associated with Accumulation of p53 and p16INK4a. *Cell*, *88*(5), 593–602. https://doi.org/10.1016/S0092-8674(00)81902-9

Shannon, P., Markiel, A., Ozier, O., Baliga, N. S., Wang, J. T., Ramage, D., Amin, N., Schwikowski, B., & Ideker, T. (2003). Cytoscape: A Software Environment for Integrated Models of Biomolecular Interaction Networks. Genome Research, 13(11), 2498–2504. https://doi.org/10.1101/gr.1239303

Shehadul Islam, M., Aryasomayajula, A., & Selvaganapathy, P. R. (2017). A Review on Macroscale and Microscale Cell Lysis Methods. Micromachines, 8(3), 83. https://doi.org/10.3390/mi8030083

Shindo, Y., & Hashimoto, T. (1997). Time course of changes in antioxidant enzymes in human skin fibroblasts after UVA irradiation. Journal of Dermatological Science, 14(3), 225–232. https://doi.org/10.1016/S0923-1811(96)00578-6

Silverstein, T. D., Jain, R., Johnson, R. E., Prakash, L., Prakash, S., & Aggarwal, A. K. (2010). Structural Basis for Error-free Replication of Oxidatively Damaged DNA by Yeast DNA Polymerase η. Structure, 18(11), 1463–1470. https://doi.org/10.1016/j.str.2010.08.019

Radrezza, S., Carini, M., Baron, G., Aldini, G., Negre-Salvarye, A., & D'Amato, A. (2021). Study of Carnosine's effect on nude mice skin to prevent UV-A damage. Free Radical Biology and Medicine, 173, 97–103. https://doi.org/10.1016/j.freeradbiomed.2021.07.010

Basisty, N., Kale, A., Jean, O., Kuehnemann, C., Payne, T., Rao, C., Holtz, A., Shah, S., Sharma, V., Ferrucci, L, Campisi, J., Schilling, B. (2020) A proteomic atlas of senescence-associated secretomes for aging biomarker development. Plos Biology, 18(1), e3000599, https://doi.org/10.1371/journal.pbio.3000599

Slominski, A. T., Zmijewski, M. A., Plonka, P. M., Szaflarski, J. P., & Paus, R. (2018). How UV Light Touches the Brain and Endocrine System Through Skin, and Why. Endocrinology, 159(5), 1992–2007. https://doi.org/10.1210/en.2017-03230

Song, Q., Cannistraro, V. J., & Taylor, J.-S. (2014). Synergistic modulation of cyclobutane pyrimidine dimer photoproduct formation and deamination at a TmCG site over a full helical DNA turn in a nucleosome core particle. Nucleic Acids Research, 42(21), 13122–13133. https://doi.org/10.1093/nar/gku1049

Su, D. G. T., Fang, H., Gross, M. L., & Taylor, J.-S. A. (2009). Photocrosslinking of human telomeric G-quadruplex loops by anti cyclobutane thymine dimer formation. Proceedings of the National Academy of Sciences, 106(31), 12861–12866. https://doi.org/10.1073/pnas.0902386106

Strober, W. (1997). Trypan Blue Exclusion Test of Cell Viability. Current Protocols in Immunology, 21(1), A.3B.1-A.3B.2. https://doi.org/10.1002/0471142735.ima03bs21

Swiader, A., Camaré, C., Guerby, P., Salvayre, R., & Negre-Salvayre, A. (2021). 4-Hydroxynonenal Contributes to Fibroblast Senescence in Skin Photoaging Evoked by UV-A Radiation. Antioxidants, 10(3), 365. https://doi.org/10.3390/antiox10030365

Szewczyk, G., Zadlo, A., Sarna, M., Ito, S., Wakamatsu, K., & Sarna, T. (2016). Aerobic photoreactivity of synthetic eumelanins and pheomelanins: Generation of singlet oxygen and superoxide anion. Pigment Cell & Melanoma Research, 29(6), 669–678. https://doi.org/10.1111/pcmr.12514

Tebbe, B., Schwarz, C., Ruderisch, H.S., Treudler, R., Orfanos, C.E. (2001). L-Ascorbic Acid Increases NFκB Binding Activity in UVA-Irradiated HaCaT Keratinocytes. J Invest Dermatol 117, 154–156. https://doi.org/10.1046/j.0022-202x.2001.01392.x

Teitz, T., Eli, D., Penner, M., Bakhanashvili, M., Naiman, T., Timme, T.L., Wood, C.M., Moses, R.E., Canaani, D. (1990). Expression of the cDNA for the beta subunit of human casein kinase II confers partial UV resistance on xeroderma pigmentosum cells. Mutation Research/DNA Repair 236, 85–97. https://doi.org/10.1016/0921-8777(90)90036-5

The UniProt Consortium. (2017). UniProt: The universal protein knowledgebase. Nucleic Acids Research, 45(D1), D158–D169. https://doi.org/10.1093/nar/gkw1099

Thul, P.J., Åkesson, L., Wiking, M., Mahdessian, D., Geladaki, A., Ait Blal, H., Alm, T., Asplund, A., Björk, L., Breckels, L.M., Bäckström, A., Danielsson, F., Fagerberg, L., Fall, J., Gatto, L., Gnann, C., Hober, S., Hjelmare, M., Johansson, F., Lee, S., Lindskog, C., Mulder, J., Mulvey, C.M., Nilsson, P., Oksvold, P., Rockberg, J., Schutten, R., Schwenk, J.M., Sivertsson, Å., Sjöstedt, E., Skogs, M., Stadler, C., Sullivan, D.P., Tegel, H., Winsnes, C., Zhang, C., Zwahlen, M., Mardinoglu, A., Pontén, F., von Feilitzen, K., Lilley, K.S., Uhlén, M., Lundberg, E. (2017). A subcellular map of the human proteome. Science 356. https://doi.org/10.1126/science.aal3321

Ting, W., Schultz, K., Cac, N. N., Peterson, M., & Walling, H. W. (2007). Tanning bed exposure increases the risk of malignant melanoma. International Journal of Dermatology, 46(12), 1253–1257. https://doi.org/10.1111/j.1365-4632.2007.03408.x

Tommasi, S., Denissenko, M. F., & Pfeifer, G. P. (1997). Sunlight Induces Pyrimidine Dimers Preferentially at 5-Methylcytosine Bases. Cancer Research, 57(21), 4727–4730.

Tondera, D., Grandemange, S., Jourdain, A., Karbowski, M., Mattenberger, Y., Herzig, S., Da Cruz, S., Clerc, P., Raschke, I., Merkwirth, C., Ehses, S., Krause, F., Chan, D.C., Alexander, C., Bauer, C., Youle, R., Langer, T., Martinou, J.-C. (2009). SLP-2 is required for stress-induced mitochondrial hyperfusion. The EMBO Journal 28, 1589–1600. https://doi.org/10.1038/emboj.2009.89

Trojan, P., Rausch, S., Gießl, A., Klemm, C., Krause, E., Pulvermüller, A., Wolfrum, U. (2008). Light-dependent CK2-mediated phosphorylation of centrins regulates complex formation with visual G-protein. Biochimica et Biophysica Acta (BBA) - Molecular Cell Research 1783, 1248–1260. https://doi.org/10.1016/j.bbamcr.2008.01.006

Tyanova, S., Temu, T., Sinitcyn, P., Carlson, A., Hein, M. Y., Geiger, T., Mann, M., & Cox, J. (2016). The Perseus computational platform for comprehensive analysis of (prote)omics data. Nature Methods, 13(9), 731–740. https://doi.org/10.1038/nmeth.3901

Tyrrell, R. M. (2000). [27] Role for singlet oxygen in biological effects of ultraviolet a radiation. In Methods in Enzymology (Vol. 319, p. 290–296). Academic Press. https://doi.org/10.1016/S0076-6879(00)19029-9

Tyrrell, R. M. (2011). Modulation of gene expression by the oxidative stress generated in human skin cells by UVA radiation and the restoration of redox homeostasis. Photochemical & Photobiological Sciences, 11(1), 135–147. https://doi.org/10.1039/C1PP05222E

Twig, G., Shirihai, O.S. (2011). The Interplay Between Mitochondrial Dynamics and Mitophagy. Antioxid Redox Signal 14, 1939–1951. https://doi.org/10.1089/ars.2010.3779

Valerio, H. P., Ravagnani, F. G., Candela, A. P. Y., Costa, B. D. C. da, Ronsein, G. E., & Mascio, P. D. (2021). Spatial proteomics reveals profound subcellular reorganization in human keratinocytes exposed to UVA light (p. 2021.09.01.458617). https://doi.org/10.1101/2021.09.01.458617

Valencia, A., & Kochevar, I. E. (2008). Nox1-Based NADPH Oxidase Is the Major Source of UVA-Induced Reactive Oxygen Species in Human Keratinocytes. Journal of Investigative Dermatology, 128(1), 214–222. https://doi.org/10.1038/sj.jid.5700960

Verger, A., Quinlan, K.G.R., Crofts, L.A., Spanò, S., Corda, D., Kable, E.P.W., Braet, F., Crossley, M. (2006). Mechanisms Directing the Nuclear Localization of the CtBP Family Proteins. Molecular and Cellular Biology 26, 4882–4894. https://doi.org/10.1128/MCB.02402-05

Victorelli, S., Lagnado, A., Halim, J., Moore, W., Talbot, D., Barrett, K., Chapman, J., Birch, J., Ogrodnik, M., Meves, A., Pawlikowski, J. S., Jurk, D., Adams, P. D., van Heemst, D., Beekman, M., Slagboom, P. E., Gunn, D. A., & Passos, J. F. (2019).

Senescent human melanocytes drive skin ageing via paracrine telomere dysfunction. The EMBO Journal, 38(23), e101982. https://doi.org/10.15252/embj.2019101982

Vile, G.F., Tanew-Ilitschew, A., Tyrrell, R.M. (1995). Activation of NF-kappa B in human skin fibroblasts by the oxidative stress generated by UVA radiation. Photochem Photobiol 62, 463–468. https://doi.org/10.1111/j.1751-1097.1995.tb02369.x

Vono, R., Jover Garcia, E., Spinetti, G., & Madeddu, P. (2017). Oxidative Stress in Mesenchymal Stem Cell Senescence: Regulation by Coding and Noncoding RNAs. Antioxidants & Redox Signaling, 29(9), 864–879. https://doi.org/10.1089/ars.2017.7294

Wan, F., Lenardo, M.J. (2010). The Nuclear Signaling of NF-κB – Current Knowledge, New Insights, and Future Perspectives. Cell Res 20, 24–33. https://doi.org/10.1038/cr.2009.137

Wang, G., Shang, L., Burgett, A.W.G., Harran, P.G., Wang, X. (2007). Diazonamide toxins reveal an unexpected function for ornithine δ-amino transferase in mitotic cell division. Proc Natl Acad Sci U S A 104, 2068–2073. https://doi.org/10.1073/pnas.0610832104

Wang, Ping, Wang, Peiguo, Liu, B., Zhao, J., Pang, Q., Agrawal, S.G., Jia, L., Liu, F.-T. (2015). Dynamin-related protein Drp1 is required for Bax translocation to mitochondria in response to irradiation-induced apoptosis. Oncotarget 6, 22598–22612. https://doi.org/10.18632/oncotarget.4200

Warner, W. G., & Wei, R. R. (1997). In vitro Photooxidation of Nucleic Acids by Ultraviolet A Radiation. Photochemistry and Photobiology, 65(3), 560–563. https://doi.org/10.1111/j.1751-1097.1997.tb08605.x

Watanabe, H., Shimizu, T., Nishihira, J., Abe, R., Nakayama, T., Taniguchi, M., Sabe, H., Ishibashi, T., & Shimizu, H. (2004). Ultraviolet A-induced Production of Matrix Metalloproteinase-1 Is Mediated by Macrophage Migration Inhibitory Factor (MIF) in

Human Dermal Fibroblasts *. Journal of Biological Chemistry, 279(3), 1676–1683. https://doi.org/10.1074/jbc.M303650200

Wenczl, E., Smit, N. P. M., Pavel, S., Schothorst, A. A., Schans, G. P. V. der, Timmerman, A. J., Roza, L., & Kolb, R. M. (1998). (Pheo)Melanin Photosensitizes UVA-Induced DNA Damage in Cultured Human Melanocytes1. Journal of Investigative Dermatology, 111(4), 678–682. https://doi.org/10.1046/j.1523-1747.1998.00357.x

Wenk, J., Schüller, J., Hinrichs, C., Syrovets, T., Azoitei, N., Podda, M., Wlaschek, M., Brenneisen, P., Schneider, L.-A., Sabiwalsky, A., Peters, T., Sulyok, S., Dissemond, J., Schauen, M., Krieg, T., Wirth, T., Simmet, T., & Scharffetter-Kochanek, K. (2004). Overexpression of Phospholipid-hydroperoxide Glutathione Peroxidase in Human Dermal Fibroblasts Abrogates UVA Irradiation-induced Expression of Interstitial Collagenase/Matrix Metalloproteinase-1 by Suppression of Phosphatidylcholine Hydroperoxide-mediated NFκB Activation and Interleukin-6 Release *. Journal of Biological Chemistry, 279(44), 45634–45642. https://doi.org/10.1074/jbc.M408893200

Wertz, K., Hunziker, P. B., Seifert, N., Riss, G., Neeb, M., Steiner, G., Hunziker, W., & Goralczyk, R. (2005). β-Carotene Interferes with Ultraviolet Light A-Induced Gene Expression by Multiple Pathways. Journal of Investigative Dermatology, 124(2), 428–434. https://doi.org/10.1111/j.0022-202X.2004.23593.x

Wertz, K., Seifert, N., Hunziker, P. B., Riss, G., Wyss, A., Lankin, C., & Goralczyk, R. (2004). β-carotene inhibits UVA-induced matrix metalloprotease 1 and 10 expression in keratinocytes by a singlet oxygen-dependent mechanism. Free Radical Biology and Medicine, 37(5), 654–670. https://doi.org/10.1016/j.freeradbiomed.2004.05.018

Willems, P.H.G.M., Rossignol, R., Dieteren, C.E.J., Murphy, M.P., Koopman, W.J.H. (2015). Redox Homeostasis and Mitochondrial Dynamics. Cell Metabolism 22, 207–218. https://doi.org/10.1016/j.cmet.2015.06.006

Wiley, C. D., Liu, S., Limbad, C., Zawadzka, A. M., Beck, J., Demaria, M., Artwood, R., Alimirah, F., Lopez-Dominguez, J.-A., Kuehnemann, C., Danielson, S. R., Basisty, N., Kasler, H. G., Oron, T. R., Desprez, P.-Y., Mooney, S. D., Gibson, B. W., Schilling, B., Campisi, J., & Kapahi, P. (2019). SILAC Analysis Reveals Increased Secretion of Hemostasis-Related Factors by Senescent Cells. Cell Reports, 28(13), 3329-3337.e5. https://doi.org/10.1016/j.celrep.2019.08.049

Wiley, C. D., Velarde, M. C., Lecot, P., Liu, S., Sarnoski, E. A., Freund, A., Shirakawa, K., Lim, H. W., Davis, S. S., Ramanathan, A., Gerencser, A. A., Verdin, E., & Campisi, J. (2016). Mitochondrial Dysfunction Induces Senescence with a Distinct Secretory Phenotype. Cell Metabolism, 23(2), 303–314. https://doi.org/10.1016/j.cmet.2015.11.011

Winkler, J., Abisoye-Ogunniyan, A., Metcalf, K. J., & Werb, Z. (2020). Concepts of extracellular matrix remodelling in tumour progression and metastasis. Nature Communications, 11(1), 5120. https://doi.org/10.1038/s41467-020-18794-x

Wlaschek, M., Briviba, K., Stricklin, G. P., Sies, H., & Scharffetter-Kochanek, K. (1995). Singlet Oxygen May Mediate the Ultraviolet A-Induced Synthesis of Interstitial Collagenase. Journal of Investigative Dermatology, 104(2), 194–198. https://doi.org/10.1111/1523-1747.ep12612751

Wlaschek, M., Heinen, G., Poswig, A., Schwarz, A., Krieg, T., & Scharffetter-Kochanek, K. (1994). Uva-Induced Autocrine Stimulation Of Fibroblast-Derived Collagenase/Mmp-1 By Interrelated Loops Of Interleukin–1 Andinterleukin–6. Photochemistry and Photobiology, 59(5), 550–556. https://doi.org/10.1111/j.1751-1097.1994.tb02982.x

Wlaschek, M., Maity, P., Makrantonaki, E., & Scharffetter-Kochanek, K. (2021). Connective Tissue and Fibroblast Senescence in Skin Aging. Journal of Investigative Dermatology. https://doi.org/10.1016/j.jid.2020.11.010

Wondrak, G. T., Jacobson, M. K., & Jacobson, E. L. (2006). Endogenous UVA-photosensitizers: Mediators of skin photodamage and novel targets for skin

photoprotection. Photochemical & Photobiological Sciences, 5(2), 215–237. https://doi.org/10.1039/B504573H

Yang, Y., Sharma, A., Sharma, R., Patrick, B., Singhal, S. S., Zimniak, P., Awasthi, S., & Awasthi, Y. C. (2003). Cells Preconditioned with Mild, Transient UVA Irradiation Acquire Resistance to Oxidative Stress and UVA-induced Apoptosis: ROLE OF 4-HYDROXYNONENAL IN UVA-MEDIATED SIGNALING FOR APOPTOSIS *. Journal of Biological Chemistry, 278(42), 41380–41388. https://doi.org/10.1074/jbc.M305766200

Yefi, R., Ponce, D.P., Niechi, I., Silva, E., Cabello, P., Rodriguez, D.A., Marcelain, K., Armisen, R., Quest, A.F.G., Tapia, J.C. (2011). Protein kinase CK2 promotes cancer cell viability via up-regulation of cyclooxygenase-2 expression and enhanced prostaglandin E2 production. Journal of Cellular Biochemistry 112, 3167–3175. https://doi.org/10.1002/jcb.23247

Yi, Y., Xie, H., Xiao, X., Wang, B., Du, R., Liu, Y., Li, Z., Wang, J., Sun, L., Deng, Z., & Li, J. (2018). Ultraviolet A irradiation induces senescence in human dermal fibroblasts by down-regulating DNMT1 via ZEB1. Aging, 10(2), 212–228. https://doi.org/10.18632/aging.101383

Yogev, Ohad, Yogev, Orli, Singer, E., Shaulian, E., Goldberg, M., Fox, T.D., Pines, O. (2010). Fumarase: A Mitochondrial Metabolic Enzyme and a Cytosolic/Nuclear Component of the DNA Damage Response. PLoS Biol 8. https://doi.org/10.1371/journal.pbio.1000328

You, Y.-H., Szabó, P. E., & Pfeifer, G. P. (2000). Cyclobutane pyrimidine dimers form preferentially at the major p53 mutational hotspot in UVB-induced mouse skin tumors. Carcinogenesis, 21(11), 2113–2117. https://doi.org/10.1093/carcin/21.11.2113

Zhang, T., Dutton-Regester, K., Brown, K. M., & Hayward, N. K. (2016). The genomic landscape of cutaneous melanoma. Pigment Cell & Melanoma Research, 29(3), 266–283. https://doi.org/10.1111/pcmr.12459

Zhang, X., Rosenstein, B. S., Wang, Y., Lebwohl, M., Mitchell, D. M., & Wei, H. (1997). Induction of 8-Oxo-7,8-Dihydro-2'-Deoxyguanosine by Ultraviolet Radiation in Calf Thymus DNA and HeLa Cells. Photochemistry and Photobiology, 65(1), 119–124. https://doi.org/10.1111/j.1751-1097.1997.tb01886.x

Zhang, Y., Fonslow, B. R., Shan, B., Baek, M.-C., & Yates, J. R. (2013). Protein Analysis by Shotgun/Bottom-up Proteomics. Chemical Reviews, 113(4), 2343–2394. https://doi.org/10.1021/cr3003533

Zhang, Z., Liu, L., Wu, S., Xing, D. (2016). Drp1, Mff, Fis1, and MiD51 are coordinated to mediate mitochondrial fission during UV irradiation-induced apoptosis. The FASEB Journal 30, 466–476. https://doi.org/10.1096/fj.15-274258

Zhao, X., Nadji, S., Kao, J. L.-F., & Taylor, J.-S. (1996). The Structure of d(TpA)*, the Major Photoproduct of Thymidylyl-(3'–5')-Deoxyadenosine. Nucleic Acids Research, 24(8), 1554–1560. https://doi.org/10.1093/nar/24.8.1554

Zhong, J. L., Yiakouvaki, A., Holley, P., Tyrrell, R. M., & Pourzand, C. (2004). Susceptibility of Skin Cells to UVA-induced Necrotic Cell Death Reflects the Intracellular Level of Labile Iron. Journal of Investigative Dermatology, 123(4), 771–780. https://doi.org/10.1111/j.0022-202X.2004.23419.x

Zhou, C., Elia, A.E.H., Naylor, M.L., Dephoure, N., Ballif, B.A., Goel, G., Xu, Q., Ng, A., Chou, D.M., Xavier, R.J., Gygi, S.P., Elledge, S.J. (2016). Profiling DNA damage-induced phosphorylation in budding yeast reveals diverse signaling networks. Proc Natl Acad Sci USA 113, E3667–E3675. https://doi.org/10.1073/pnas.1602827113

Zhu, J.-W., Wu, X.-J., Lu, Z.-F., Luo, D., Cai, S.-Q., & Zheng, M. (2013). Role of VEGF Receptors in Normal and Psoriatic Human Keratinocytes: Evidence from Irradiation with Different UV Sources. PLOS ONE, 8(1), e55463. https://doi.org/10.1371/journal.pone.0055463

Zubarev, R. A., & Makarov, A. (2013). Orbitrap mass spectrometry. Analytical Chemistry, 85(11), 5288–5296. https://doi.org/10.1021/ac4001223